# CONVECTIVE HEAT TRANSFER AND FLOW PERFORMANCE ANALYSIS FOR A NON-HOMOGENEOUS NANOFLUID IN A CIRCULAR MINICHANNEL

by

Siamak Vajdi Hokmabad

B.S., Mechanical Engineering, University of Tabriz, 2015

Submitted to the Institute for Graduate Studies in
Science and Engineering in partial fulfillment of
the requirements for the degree of
Master of Science

Graduate Program in Mechanical Engineering

Boğaziçi University

2019

# ACKNOWLEDGEMENTS

This thesis is dedicated to my parents, Aliasghar and Afsaneh, and to my brother Babak for providing me with unfailing support and continuous encouragement throughout my years of study and through the process of researching and writing this thesis. This accomplishment would not have been possible without them.

# ABSTRACT


## CONVECTIVE HEAT TRANSFER AND FLOW PERFORMANCE ANALYSIS FOR A NON-HOMOGENEOUS NANOFLUID IN A CIRCULAR MINICHANNEL

This study investigates convective laminar flow and heat transfer of alumina-water nanofluid inside a circular minichannel subjected to constant heat flux and wall temperature. The results of numerical studies on non-homogeneous two-component and single phase homogeneous methods revealed that the non-homogeneous model provides more accurate results, while homogeneous model highly underestimates the experimental data available in literature. The nanofluid showed higher performance and efficiency rates at lower Pe number, although decrease in particle size raised the friction factor and pressure drop. The comparison of numerical results between non-homogeneous and homogeneous methods, applying the Ryzhkov and Minakov thermophoresis coefficient [68] showed higher performance and efficiency rates compared to the McNab and Meisen thermophoresis coefficient [90]. The results on the effect of thermophoresis strength showed higher heat transfer coefficient, Nusselt number, and lower wall shear stress. The performance results show higher values at low Pe numbers. The results of numerical studies on non-homogeneous model presented higher performance compared to the base fluid with increasing the particle size and decreasing the Pe number. The results obtained via nanofluid properties dependent on additional parameters such as particle size and temperature have higher accuracy compared to applying only particle concentration dependent nanofluid properties. Further experimental and numerical studies on mechanisms of heat transfer, and thermophoresis effect in nanofluids are strongly recommended.

# ÖZET


## SILINDIRIK MINIKANALDA HOMOJEN OLMAYAN NANOAKIŞAN IÇIN KONVEKTIF ISI TRANSFERI VE AKIŞ PERFORMANS ANALIZI

Bu çalışma, sabit ısı akışına ve duvar sıcaklığına maruz kalan dairesel bir minikanal içindeki alüminyum oksit-su konvektif laminer akışını ve ısı transferini araştırmaktadır. İki bileşenli homojen olmayan ve tek fazlı homojen yöntemler sayısal çalışmaların sonuçları homojen olmayan modeline göre daha doğru sonuçlar verdiği, homojen modelin ise literatürdeki deneysel verilerden daha düşük sonuç verdiğini ortaya koydu. Nanoakışkan, düşük Pe sayısında yüksek performans ve verim oranları göstermiştir, ancak partikül boyutundaki düşüş sürtünme faktörünü ve basınç düşüşünü arttırmıştır. Homojen olmayan ve homojen olmayan yöntemler arasındaki sayısal sonuçların Ryzhkov ve Minakov termoforez katsayısı [68] kullanılarak karşılaştırılması, McNab ve Meisen termoforez katsayısına [90] göre daha yüksek performans ve verim oranları göstermiştir. Termoforez kuvvetinin ısı transfer katsayısını düşürdüğünü gözlemlenmiştir, Nusselt sayısı ve daha düşük duvar kayma gerilimi göstermiştir. Homojen olmayan model üzerinde yapılan sayısal çalışmaların sonuçları, partikül boyutunu artıran ve Pe sayısını azaltan suya kıyasla daha yüksek performans gözlemlenmiştir. Performans sonuçları düşük Pe sayılarında daha yüksek değerler göstermektedir. Partikül büyüklüğü ve sıcaklık gibi ek parametrelere bağlı olarak nanoakışkan özellikleri vasıtasıyla elde edilen sonuçlar, yalnızca parçacık konsantrasyonuna bağlı nanoakışkan özelliklerinin uygulanmasına kıyasla daha yüksek bir hassasiyete sahiptir. Isı transfer mekanizmaları ve nano-akışkanlarda termoforez etkisi üzerine ileri deneysel ve sayısal çalışmalar şiddetle tavsiye edilir.

# TABLE OF CONTENTS

# LIST OF FIGURES

# LIST OF TABLES

# LIST OF SYMBOLS

| | |
|---|---|
| C | correction factor |
| $C_m$ | particle mass fraction |
| $C_p$ | specific heat capacity, J/kgK |
| $C_v$ | particle volume fraction |
| $D$ | tube diameter, m |
| $D_B$ | Brownian motion coefficient, $m^2/s$ |
| $D_h$ | hydraulic diameter, m |
| $D_T$ | thermophoresis coefficient, $m^2/sK$ |
| $d_p$ | nanoparticle diameter, m |
| ER | efficiency ratio |
| h | local heat transfer coefficient, $W/m^2K$ |
| $k$ | thermal conductivity, W/mK |
| $L$ | tube length, m |
| $m_p$ | mass of a single particle |
| $m_f$ | mass of base fluid |
| $Nu$ | local Nusselt number |
| $Nu_T$ | local Nusselt number of two-component non-homogeneous model |
| $Nu_H$ | local Nusselt number of homogeneous modeling |
| $Nu_\alpha$ | local Nusselt number with considering thermophoresis effect |
| $Nu_0$ | local Nusselt number without considering thermophoresis effect |
| P | pressure, Pa |
| Pe | Peclet number |
| PEC | Performance evaluation criteria |

| | |
|---|---|
| $Pr$ | Prandtl number |
| $q$ | heat flux, $\mathrm{W/m^2}$ |
| $R$ | tube radius, m |
| $r$ | radius, m |
| $r_p$ | radius of particle, m |
| Re | Reynolds number |
| T | temperature, K |
| $t_v$ | nanolayers thickness, m |
| $u$ | velocity in radial direction, $\mathrm{m/s}$ |
| $v$ | velocity in axial direction, $\mathrm{m/s}$ |
| $v_0$ | mean velocity in axial direction, $\mathrm{m/s}$ |
| $V$ | velocity, $\mathrm{m/s}$ |
| $V_f$ | Fluid volume, $\mathrm{m^3}$ |
| $V_p$ | Particle volume, $\mathrm{m^3}$ |
| $V_{void}$ | void volume, $\mathrm{m^3}$ |
| $V_\mathrm{b}$ | Brownian velocity |

| | |
|---|---|
| $a$ | proportionality coefficient, $\mathrm{Kgm/s^2}$ |
| $\beta_T$ | thermal expansion, $\mathrm{K^{-1}}$ |
| $k_B$ | Boltzmann constant, $1.3807 \times 10^{-23}$ J/K |
| μ | dynamic viscosity, Pa.s |
| $k$ | kinematic viscosity, $\mathrm{m^2/s}$ |
| $\rho$ | density, $\mathrm{Kg/m^3}$ |
| $\tau_w$ | wall shear stress, Pa |
| $f$ | friction factor |
| $\delta$ | distance between the nanoparticles |

| | |
|---|---|
| 0 | (subscript) result without considering thermophoresis effect |
| $\alpha$ | (subscript) result with considering thermophoresis effect |
| $b$ | (subscript) bulk mean |
| $bf$ | (subscript) base fluid |
| $eff$ | (subscript) Effective |
| $f$ | (subscript) Fluid |
| $H$ | (subscript) homogeneous single phase |
| $m$ | (subscript) Mean |
| $nf$ | (subscript) Nanofluid |
| $p$ | (subscript) Particle |
| $T$ | (subscript) non-homogeneous two-component |
| $w$ | (subscript) water |

# 1. INTRODUCTION

Heat transfer augmentation methods can be categorized into two main groups, active and passive methods. Heat transfer augmentation in active methods, is achieved by applying external energy like magnetic or electric field [1] [2]. This aim can be attained by change in the geometry in the passive methods such as miniaturization of channel, with the intention of increasing the heat transfer area [3]. One other passive method is enhancing heat transfer by modifying the fluid properties by dispersing fine solid particles in a base fluid like nanofluids [4] [5]. Utilization of heat transfer enhancement methods combined with more advanced heat transfer fluids (improving thermal characteristics of conventional heat transfer fluids), can help to increase efficiency of thermal systems.

## 1.1. Nanofluid

Conventional heat transfer fluids, like water, ethylene-glycols (EGs) and oils have poor heat transfer characteristics compared to solids, which have higher thermal conductivity [6] Therefore, adding solid particles to the base fluid with the intention of improving heat transfer characteristics appears to be reasonable. The idea was foundation of many experiments and studies. Maxwell [7] was the first in presenting the basic concept of adding micro sized particles to the fluids. This method was not applicable because of some problems such as agglomeration, rapid sedimentation, high pressure drop, erosion, and clogging [8]. However, not only dispersing stably a very small amount of nanoparticles in a base fluid obviated the abovementioned impediments but also significantly enhanced heat transfer properties of the fluid. The nanofluid term was first introduced by Choi *et al*. [9] referring to dispersing solid particles in scale of 1-100 nanometers within a fluid. Experiment by Choi *et al*. [10] revealed that thermal conductivity of base fluid increased 2.5 times with dispersing a small amount of nanoparticles (1% particle volume fraction).

## 1.2. Thermal Conductivity of Nanofluids

The early measurements of the thermal conductivity of nanofluids were done using oxide nanoparticles since they could be stabilized easier than metal particles. Experimental works have shown intensity of the thermal conductivity rises by increasing the nanoparticle volume fraction [11]. In experiments conducted by Wang *et al*. [12], thermal conductivity increased for all nanofluids prepared by dispersing $Al_2O_3$ and CuO nanoparticles in water, Ethylene Glycol, engine oil and vacuum pump oil. Lee *et al*. [13] observed higher thermal conductivities for nanofluids compared to their base fluids. They performed experiments on CuO and $Al_2O_3$ nanoparticles dispersed in water and ethylene glycol and reported 20% higher thermal conductivity for ethylene glycol by adding 4% CuO nanoparticle volume fraction.

Das *et al*. [14] reported intense dependency of nanofluids thermal conductivity on the temperature. They performed experiments on the thermal conductivity of nanofluids including $Al_2O_3$ and CuO nanoparticles with 1% and 4% nanoparticle volume fractions in temperature range 21°C and 55°C. The measured enhancement in thermal conductivity grows from 9.4% at 21°C up to 24.3% at 51°C for 4% nanoparticle volume fraction of alumina water nanofluid.

## 1.3. Heat Transfer Coefficient of Nanofluids

Works done on nanofluids show that convective heat transfer coefficient of fluids increases by adding nanoparticles to base fluid. Jung *et al*. [15] experimentally investigated the convective heat transfer of $Al_2O_3$ water nanofluid in a rectangular microchannel. They observed 32% improvement in convective heat transfer coefficient for 1.8% fraction of nanoparticles.

Anoop *et al*. [16] experimentally investigated the heat transfer enhancement in the thermally developing region of channel with water containing alumina nanoparticles subjected to uniform heat flux. They performed the studies with 45 nm and 150 nm particle diameters. Nanofluids showed higher heat transfer coefficient compared to the base fluid in all experiments. They observed 25% increase in heat transfer coefficient with 45 nm particles and

11% increase with 150 nm particles for 4% particle volume fraction. They concluded that increasing in volume fraction of nanoparticles and Reynolds number, and decreasing the particle size led to higher heat transfer coefficient.

Experimental results of Wen and Ding [17] showed the heat transfer enhancement of laminar flow regime in the entrance region with γ- $Al_2O_3$ nanoparticles and deionized water, flowing within a copper tube. 41% enhancement in heat transfer for 1.6% of particle volume concentration was reported. The results showed the main significant improvement in the entrance zone. They also mentioned the classical Shah correlation could not predict the behavior of nanofluid well.

## 1.4. Nanofluid Viscosity

Studies have shown the viscosity of a nanofluid is severely dependent on both temperature and particle volume fraction. In order to estimate the particle suspension viscosity, some theoretical approaches have been proposed. All such equations have been derived from Einstein equation [18] which can be labeled as the pioneer one. Einstein considered a linear viscous fluid containing dilute, suspended, spherical particles with low volume fraction of nanoparticles to obtain a correlation as follow,

$$\mu_{nf} = \mu_{bf}(1 + 2.5C_v) \tag{1.1}$$

where, $\mu_{nf}$ is the viscosity of suspension, $\mu_{bf}$ is the viscosity of base fluid and $C_v$ is the volume fraction of particle in base fluid. The Einstein model is valid for very low particle volume fractions ($C_v \leq 0.02$). Therefore, Brinkman [19] in 1952 modified the Einstein correlation considering the effect of addition of solute molecule to an existing continuous medium of particle concentrations, valid for higher concentrations ($C_v \leq 0.04$) as,

$$\mu_{\mathrm{nf}} = \mu_{\mathrm{f}}/(1 - C_v)^{2.5} \tag{1.2}$$

Krieger and Dougherty [20] in 1959 proposed a semi-empirical model for nanofluids shear viscosity as follow,

$$\frac{\mu_{nf}}{\mu_{\mathrm{f}}} = \left[1 - \frac{C_v}{C_{v_{\mathrm{m}}}}\right]^{-\eta C_{v_{\mathrm{m}}}} \tag{1.3}$$

where $C_{v_{\mathrm{m}}}$ is the maximum particle fraction, varies from 0.495 to 0.54 and at higher shear rates is around 0.605. The intrinsic viscosity constant, η is 2.5 for monodispersed suspensions of hard spheres.

Lundgren [21] in 1972 proposed a version of the Einstein formula under the form of Taylor series. It is obvious that if the second and higher order terms of $C_v$ are neglected, the above formula reduces to that of Einstein [18].

$$\mu_{nf} = \mu_{bf}(1 + 2.5C_v + \frac{25}{4}{C_v}^2 + O({C_v}^3)) \tag{1.4}$$

Batchelor [22] in 1977, proposed another equation by considering the Brownian motion effect of particles and the expressed the formula as

$$\mu_{nf} = \mu_{bf}(1 + 2.5C_v + 6.5{C_v}^2) \tag{1.5}$$

Since none of the aforementioned models can predict the viscosity of nanofluids in a wide range of nanoparticle volume fraction, Graham [23] in 1981, proposed a generalized version as

$$\mu_{nf} = \mu_{bf}(1 + 2.5C_v + 4.5[1/(\frac{h}{d_p} \cdot (2 + \frac{h}{d_p}) \cdot (1 + \frac{h}{d_p})^2]) \tag{1.6}$$

where, $d_p$ is the particle diameter and $h$ is the inter-particle spacing.

Nguyen *et al*. [24] in 2007 presented that even for low fraction of the particles, the Einstein's formula and all other ones (i.e. Lundgren [21] and Batchelor [22]) have severely underestimated the viscosity of the nanofluids. They proposed modified correlations for nanofluids prepared by two different sizes of $Al_2O_3$ (47 nm and 36) nanoparticles and water, respectively, as presented in Equation 1.7 and Equation 1.8. Both models just consider the viscosity of the base fluid and the volume fraction of particle. The results showed that for volume fraction under 4% the viscosities are near same value, while for higher volume fractions, nanofluid with 47 nm particles show higher viscosities compared to nanofluid with 36 nm particles.

$$\mu_{nf} = \mu_{bf} \times 0.904e^{0.1482C_v} \tag{1.7}$$

$$\mu_{nf} = \mu_{bf}(1 + 0.025C_v + 0.904{C_v}^2) \tag{1.8}$$

Some other models have been proposed by Kitano *et al*. [25] and Bicerano *et al*. [26] for prediction of the two phase mixtures viscosity, and a correlation for volumetric effect of viscosity in Equations 1.9 and 1.10, respectively.

$$\mu_{nf} = \mu_{bf}(1 - (\frac{C_v}{C_{v_m}}))^{-2} \tag{1.9}$$

$$\mu_{nf} = \mu_{bf}(1 + \eta C_v + k_H{C_v}^2) \tag{1.10}$$

where $\eta$ is a virtual coefficient and $k_H$ is Hugins coefficient which contains important information about particle shape and interparticle interactions. Moreover, Bicerano *et al*. [26] summarized many reliable experimental data and theoretical derivations available for η as a function of the particle shape and Hugins coefficient.

In fact, most formulas have been developed to relate viscosity as a function of volume fraction of nanoparticles, but temperature is an important factor affecting the viscosity of nanofluids.

Abu-Nada [27] in 2009 used experimental data reported by Nguyen *et al*. [28] in order to derive a model (Equation 1.11) for predicting nanofluid viscosity as a function of nanoparticle concentration and temperature. The results had an acceptable agreement with Nguyen *et al*. experimental data. However, comparison of obtained model and Brinkman model revealed that these two models give different results.

$$\mu_{Al_2O_3} = -0.155 - \frac{19.582}{T} + 0.794C_v + \frac{2094.47}{f^2} - .192{C_v}^2 - 8.11\frac{C_v}{T} - \frac{27463.863}{T^3} + .0127{C_v}^3 + 1.6044\frac{{C_v}^2}{T} + 2.1754\frac{C_v}{T^2} \quad (1.1)$$

There are some correlations which simultaneously consider the influences of temperature, volume fraction of nanoparticles or other effective factors such as nanoparticle density and base fluid physical properties to have higher accuracy in the prediction of nanofluid viscosity. Masoumi *et al*. [29] proposed a new theoretical model for predicting viscosity of nanofluids, considering Brownian motion effect, particle diameter, particle volume fraction, particle density, etc. This model will be discussed more in next chapter as the model of nanofluids viscosity.

$$\mu_{nf} = \mu_f\left(1 + \frac{\rho_N V_b d_p^2}{72C\delta\mu_f}\right) \quad (1.2)$$

where $\rho_N$ is the density, $d_p$ is the particle diameter, $\delta$ is the distance between the nanoparticles and $C$ and $V_b$ are functions of particle diameter, volume fraction and temperature.

Table 1.1 lists some of various models proposed for predicting viscosity of nanofluids available in the literature.

Table 1.1. Various models proposed for calculating viscosity of nanofluids.

| **Model** | **Year** | **Equation** |
|---|---|---|
| Einstein [18] | 1906 | $\mu_{nf}= (2.5C_v + 1)\,\mu_f\,, C_v < 0.02$ |
| Brinkman [19] | 1952 | $\mu_{nf} = (1 - C_v)^{2.5}\mu_f, C_v < 0.04$ |
| Kriger and Dougherty [20] | 1959 | $\mu_{nf} = \mu_{bf}(1 - C_{v_\mathrm{p}}/C_{v_\mathrm{m}})^{-[\eta]C_{v_\mathrm{m}}}$ |
| Lundgren [21] | 1972 | $\mu_{nf} = \mu_{bf}(1 + 2.5C_v + \frac{25}{4}{C_v}^2 + \mathrm{O}({C_v}^3))$ |
| Batchelor [22] | 1977 | $\mu_{nf} = \mu_{bf}(1 + 2.5C_v + 6.5{C_v}^2)$ |
| Graham [23] | 1981 | $\mu_{nf} = \mu_{bf}(1 + 2.5C_v + 4.5[1/(\frac{h}{\mathrm{d_p}}\cdot(2 + \frac{h}{\mathrm{d_p}})\cdot(1 + \frac{h}{\mathrm{d_p}})^2])$ |
| Kitano *et al*. [25] | 1981 | $\mu_{nf} = \mu_{bf}(1 - (\frac{C_v}{C_{v_m}}))^{-2}$ |
| Bicerano *et al*. [26] | 1999 | $\mu_{nf} = \mu_{bf}(1 + \eta C_v + k_H{C_v}^2)$ |
| Nguyen [24] | 2007 | $\mu_{nf} = \mu_{bf} \times 0.904e^{0.1482C_v}$<br>$\mu_{nf}= \mu_f\,(1 + 0.025C_v + 0.015{C_v}^2)$ |
| Abu-Nada [27] | 2009 | $\mu_{\mathrm{Al_2O_3}} = -0.155 - \frac{19.582}{\mathrm{T}} + 0.794C_v + \frac{2094.47}{f^2} - .192{C_v}^2 - 8.11\frac{C_v}{\mathrm{T}} - \frac{27463.863}{\mathrm{T}^3} + .0127{C_v}^3 + 1.6044\frac{{C_v}^2}{\mathrm{T}} + 2.1754\frac{C_v}{\mathrm{T}^2}$ |
| Masoumi *et al*. [29] | 2009 | $\mu_{\mathrm{nf}} = \mu_{\mathrm{f}}\,(1 + \frac{\rho_{\mathrm{N}}V_{\mathrm{b}}d_{\mathrm{p}}^2}{72\mathrm{C}\delta\mu_{\mathrm{f}}})$ |

## 1.5. Nanofluid Flow in Micro-channels and Mini-channels

Miniaturization of a channel is a passive method in which decreasing the hydraulic diameter, increases the ratio of heat transfer surface area to its volume and leads to higher heat transfer [30]. Bearing this idea in mind, Tuckerman and Pease [31] experiment the first made microchannel heat sink, capable of absorbing 790 W/cm$^2$ heat flux. Development of miniaturized heat exchangers stems from their advantages, where can be mentioned as [31] [32]

- Light weight,
- Smaller in size, and space savings,
- Material savings,
- Energy savings with higher need for heat transfer with increasing energy usage,
- Need for cooling in micro and mini scale devices,
- Ease of handling smaller units,

Experimental studies by Wang *et al*. [33] on friction factor coefficient of circular and rectangular minichannels, $D_h = 0.198 - 2.01$ mm with water and lubricant oil have shown that the conventional correlations for both laminar and turbulent flow conditions are still valid in minichannels. Kandlikar *et al*. [30] widely studied the pressure drop and heat transfer in microchannels and minichannel, and also categorized the channels considering the hydraulic diameter of channels as given in Table 1.2.

Table 1.2. Channel classification scheme by Kandlikar *et al*. [30].

| | |
|---|---|
| Conventional channels | $D_h > 3$mm |
| Minichannels | $200\mu m < D_h \leq 3$mm |
| Microchannels | $10\mu m < D_h \leq 200\mu m$ |
| Transitional channels | $0.1\mu m < D_h \leq 10\mu m$ |
| Molecular nano-channels | $D_h \leq 0.1\mu m$ |

Obtained experimental data presented by Pak and Cho [34] and Li and Xuan [35] for nanofluids pressure drop was in good agreement with both classical correlations.

A slightly more pressure drop in nanofluid compared to base fluid was reported in experimental results conducted by Duangthongsuk and Wongwises [36]. In addition, higher pressure drop was observed by increasing nanoparticle concentration, as well. Lee and Choi [37] used nanofluid for cooling purpose in the microchannel and mentioned intensification of

turbulence, effect on boundary layer and increment of thermal conductivity as the main reasons of heat transfer enhancement by nanofluids.

Lai *et al*. [38] investigated heat transfer enhancement of nanofluids in millimeter sized tube (a single $1.02\ mm$ diameter stainless steel tube) exposed to constant heat flux on the walls obtained by electrical heating. A maximum of 8% enhancement in Nusselt number was reported at 1% nanoparticle volume fraction.

Junmei, *et al*. [39] in 2016, numerically studied the effect of alumina-water nanofluid on improving the performance of rectangular microchannels. The aim was to investigate the suitability of alumina-water nanofluids in microchannel and their performance on cooling. They compared the thermophysical properties of nanofluid, obtained by numerical results, with base fluid water. Single phase governing equations in simulations was used. An empirical correlation proposed by Corcione [40] for predicting the thermal conductivity was used while a polynomial correlation proposed by Nguyen *et al*. [41], was applied to predict the viscosity of the nanofluid. They reported that high nanoparticle concentrations (volume concentration 4.5%) and high viscosity of alumina-water nanofluid resulted in much higher pumping power. Thus, it was concluded that alumina-water nanofluid was not suitable for microchannels.

Considering the presented studies, it is important to perform more studies on nanofluids, miniaturized channels and the parameters affecting the flow and heat transfer to have a better understanding and optimization of the systems. In addition, combination of passive methods like using nanofluids in miniaturized and grooved channels, leads to high heat transfer augmentation. By combining passive methods and active methods such as applying magnetic or electric field, it is possible to achieve higher heat transfer increment. [3]

Table 1.3 shows a summary of nanofluids studies on forced convection in microchannels and minichannels.

Table 1.3. Studies on convection in minichannels and microchannel with nanofluids as working fluid.

| **Authors** | **Channel geometry** | **Nature of the work** | **Flow condition** | **Coolant types** | **Materials** | **Analysis methods** | **Results** |
|---|---|---|---|---|---|---|---|
| Kosar [42] | Rectangular (200mm * 200 mm, 5 cm long) 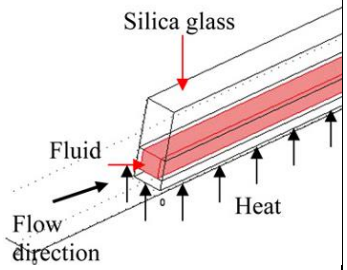  | Numerical | Laminar<br>Re < 2000<br>q" = 50,000-250,000 W/m$^2$ | Water | Cu, Al, Si<br>Steel, silica glass | 3D Numerical<br>COMSOL | Developed a general Nu correlation for fully developed laminar flow as a function of Bi number and relative conductivity k, to take into account the solid substrate conduction effects on heat transfer.<br>$Nu = 4.516 - 0.2551\frac{Bi^{0.04}}{k^{*0.24}}$<br>The Nu is lower for low thermal conductivity materials than the Nu obtained from high conductivity materials. |
| Lee *et al*. [43] | Rectangular 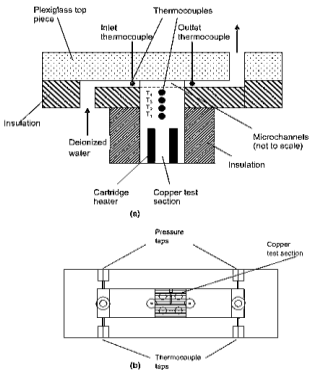  | Experimental<br>Numerical | Laminar<br>Turbulent<br>Re < 4000 | Deionized water | Copper<br>Silicon | Numerical<br>FLUENT | The simplified thin wall analysis can be used as a computationally economical alternative to a full 3D conjugate analysis. |

Table 1.3. Studies on convection in minichannels and microchannel with nanofluids as working fluid. (cont.)

| **Authors** | **Channel geometry** | **Nature of the work** | **Flow condition** | **Coolant types** | **Materials** | **Analysis methods** | **Results** |
|---|---|---|---|---|---|---|---|
| Koo and Kleinstreuer [44] | Rectangular 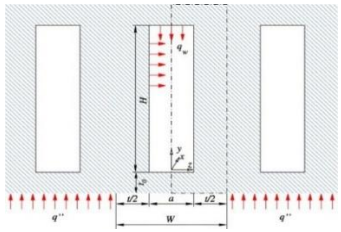 | Analytical<br>Numerical | Laminar<br>low volume fractions<br>$1 \leq C_v \leq 4\%$ | CuO in Water and Ethylene glycol | - | Numerical | Provided recommendations on performance improvements in micro heat sinks: Use of high Prandtl numbers, high nanoparticle volume concentrations (about 4%), and Microchannels with high aspect ratios. |
| Jang *et al*. [45] | Rectangular 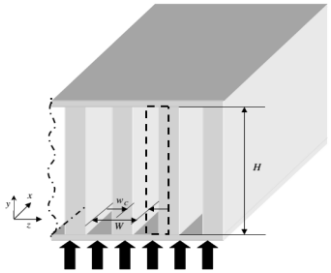 | Numerical | Laminar<br>Re < 100 | Copper-in-water and diamond-in-water | silicon | Numerical code<br>Thermal resistance model | Reported 10% enhancement in cooling performance, and nanofluids reduced thermal resistance and temperature difference between the heated microchannel wall and the coolant. |
| Escher *et al.* [46] | Rectangular (microchannel) 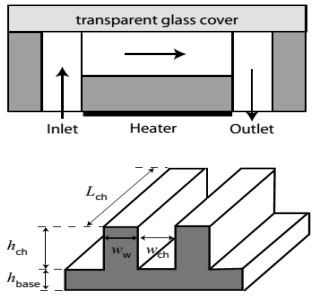  | Experimental<br>Analytical | Laminar<br>$0 < C_v < 31\%$ | $SiO_2$–water | Silicon | Thermal resistance model | Relative thermal conductivity enhancement must be larger than the relative viscosity increase in order to gain a sizeable performance benefit. |

Table 1.3. Studies on convection in minichannels and microchannel with nanofluids as working fluid. (cont.)

| **Authors** | **Channel geometry** | **Nature of the work** | **Flow condition** | **Coolant types** | **Materials** | **Analysis methods** | **Results** |
|---|---|---|---|---|---|---|---|
| Ijam and Saidur [47] | Rectangular (minichannel) (20*20cm) 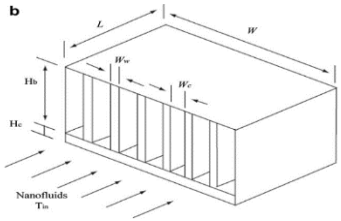  | Analytical | Turbulent $V_m$=2,6 m/s $0.8 < C_v < 4\%$ | SiC–water<br>$TiO_2$–water | Copper | Thermal resistance model | 12.44% and 9.99% enhancement in thermal conductivity reported for 4% SiC and TiO2 in water base fluid, respectively. |
| Mohammed *et al*. [48] | Triangular (microchannel) 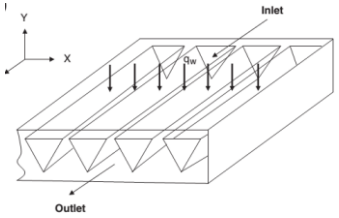  | Numerical | Laminar 100<Re<1000 $C_v$=2% | $Al_2O_3$, Ag, CuO, diamond, $SiO_2$, $TiO_2$ | Aluminum | 3D Numerical [Finite volume] | Slight increase in pressure drop and friction factor observed for all nanofluids comparing to pure water.<br>SiO2–H2O nanofluid had the highest pressure drop while Ag-H2O had the lowest pressure drop among other nanofluid types.<br>Presence of nanoparticles increased the wall shear stress compared to pure water except for Ag–H2O nanofluid. |
| Lelea [49] | Rectangular (microchannel) 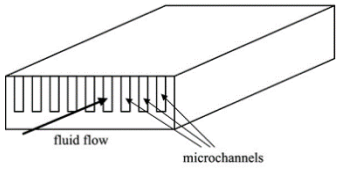  | Numerical | Laminar 107<Re<1760 $1 < C_v < 9\%$ | Alumina–water | Copper | 3D Numerical [Finite volume] | Heat transfer augmentation increased with increasing the particle concentration and decreasing the particle size. |

Table 1.3. Studies on convection in minichannels and microchannel with nanofluids as working fluid. (cont.)

| **Authors** | **Channel geometry** | **Nature of the work** | **Flow condition** | **Coolant types** | **Materials** | **Analysis methods** | **Results** |
|---|---|---|---|---|---|---|---|
| Xia *et al*. [50] | Rectangular (microchannel) (triangular cavities) 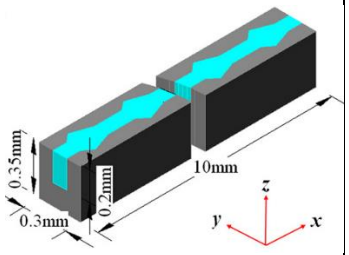  | Numerical | Laminar 201<Re<1016 | Water | Silicon | 3D Numerical FLUENT | Triangular reentrant cavities led to chaotic advection and greatly enhanced the convective fluid mixing. With increasing the Reynolds number, a larger pressure drop penalty was required to improve the heat transfer performance. |
| Ijam *et al*. [51] | Rectangular (minichannel) *20mm*20mm* 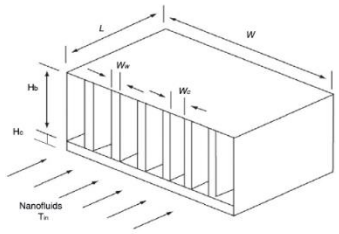  | Analytical | Laminar 0 < V<1.5 m/s 0 < $C_v$ < 4% | $Al_2O_3$–water $TiO_2$–water | Copper | Thermal resistance model | Cooling improved in the ranges 2.95% to 17.32% for $Al_2O_3$–water nanofluid 1.88% to 16.53% for $TiO_2$–water nanofluid |
| Zhang *et al*. [52] 2013 | Circular (microchannel) 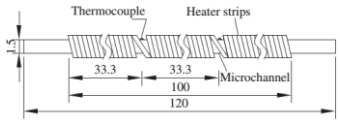  | Experimental | Laminar 500<Re<2000 $C_v$= 0, 0.25, 0.51, 0.77 Heat flux= 69.9 and 108.9 kW.m2 | Al2O3-water | | | A maximum 10.6% Heat transfer enhancement achieved and enhancement was more apparent at higher Re numbers. 7.9% increase in friction factor of the nanofluids was reported. |

Table 1.3. Studies on convection in minichannels and microchannel with nanofluids as working fluid. (cont.)

| **Authors** | **Channel geometry** | **Nature of the work** | **Flow condition** | **Coolant types** | **Materials** | **Analysis methods** | **Results** |
|---|---|---|---|---|---|---|---|
| Sohel *et al*. [53] 2012 | Circular (microchannel) 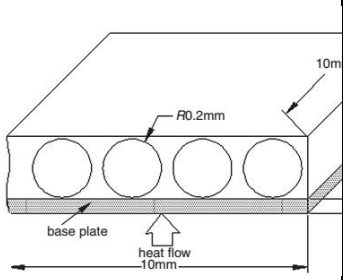  Hydraulic diameter 400 μm block dimension 10 mm×10 mm×4 mm | analytically | steady, laminar, incompressible constant heat flux volume fractions ranging= 0.5% to 4% | $Al_2O_3$-Water, $TiO_2$–water, CuO–water | | | Significant increase in Reynolds number for CuO–water nanofluid due to the higher density compared to other two nanofluids. A maximum 10.35% increase in Reynolds number reported for CuO–water.<br><br>CuO–water had better performance in reducing the friction factor and the thermal resistance compared to other two nanofluids. |

## 1.6. Theoretical and Numerical Methods for Flow and Heat Transfer of Nanofluids

There are different CFD approaches utilized in numerical simulations of nanofluids flow in heat exchangers to obtain the nearest results to experimental results. Vanaki *et al*. [54] comprehensively reviewed and summarized numerical studies on nanofluids. They have categorized the numerical methods (Figure 1.1) mentioning the pros and cons of each approach to find the most suitable method that gives more reliable and realistic results compared to experimental results. They categorized the numerical approaches as single phase, two phase and two other approaches which will be more discussed.

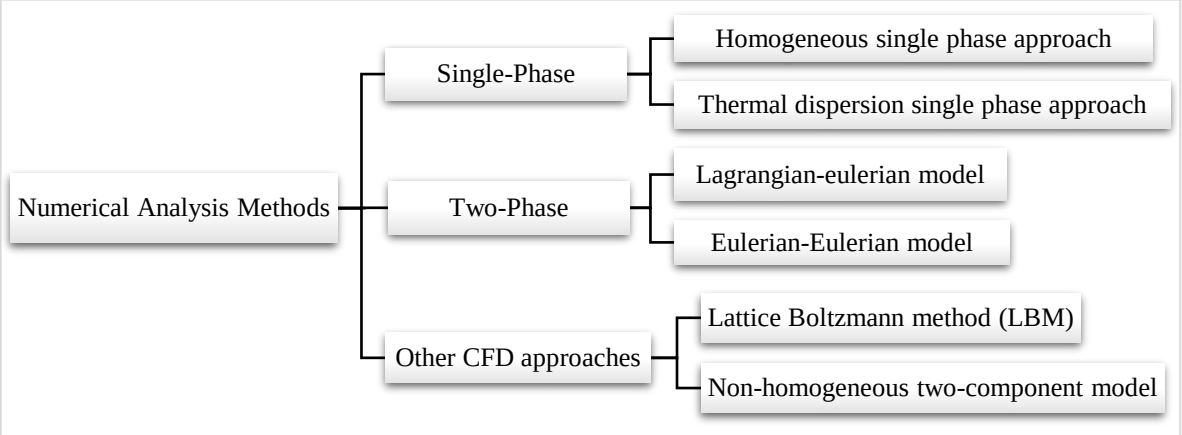


Figure 1.1. Categorized theoretical and numerical methods for flow and heat transfer of nanofluids [54].

This study has employed conventional single phase approach (homogeneous) and non-homogeneous two-component model to compare the results obtained by them and observe the heat transfer of Alumina-water nanofluid.

### 1.6.1. Homogeneous Single Phase Approach

There are assumptions to make studies simpler and computationally efficient. Although nanofluid due to the existence of nanoparticles in base fluid, is multiphase problem, it can be

considered as a homogeneous single phase fluid with average physical properties of phases [54]. In this approach, ultra-fine particles and fluid are in a thermal equilibrium that move with same velocity [54]. In this model governing equations for a forced convection steady state laminar flow in general form are

Mass conservation

$$\nabla \cdot (\rho_{nf} \vec{V}) = 0 \tag{1.3}$$

Momentum conservation

$$\nabla \cdot (\rho_{nf} \vec{V}\vec{V}) = -\nabla P + \mu_{nf} \nabla^2 \vec{V} \tag{1.4}$$

Energy conservation

$$\nabla \cdot ((\rho C_P)_{nf} \vec{V} \mathrm{T}) = \nabla \cdot (k_{nf} \nabla \mathrm{T}) \tag{1.5}$$

where the $\vec{V}$ is velocity, T is temperature and the $\rho_{nf}$, $\mu_{nf}$, $k_{nf}$ and $C_P$ are density, viscosity, thermal conductivity and specific heat of nanofluid, respectively.

Thermophysical property correlations used in homogeneous model have a significant effect on the obtained results. Moreover, choosing the most suitable correlations are considered as an important factor. Need for more studies on this subject is obvious since there are no correlations available in the literature that claim giving the most credible results for all problems, yet. Thus, this model may not have good agreement with experimental results due to the fact aforementioned as well as the model fails in considering chaotic movements of the particles.

### 1.6.2. Non-Homogeneous Two-Component Model

This model was proposed by Buongiorno [55] considering seven different slip mechanisms in nanofluid flow which are inertia, Brownian diffusion, thermophoresis, diffusiophoresis, Magnus effect, fluid drainage, and gravity. He described Brownian diffusion and thermophoresis as more important and effective mechanisms that enforce particles movements. Assuming negligible energy transfer by nanoparticle dispersion, four coupled equations was proposed as described below

Mass conservation,

$$\nabla \cdot (\rho_{nf} \vec{V}) = 0 \tag{1.6}$$

Momentum conservation,

$$\rho_{nf}(\vec{V} \cdot \nabla \vec{V}) = -\nabla \mathrm{P} - \nabla \cdot (-\mu_{nf}[\nabla \vec{V} + \left(\nabla \vec{V}\right)^{t}]) \tag{1.7}$$

Energy conservation,

$$\rho_{nf} \mathrm{C_{nf}}[\vec{V} \cdot \nabla \mathrm{T}] = \nabla \cdot k_{nf} \nabla \mathrm{T} + \rho_{\mathrm{p}} \mathrm{C_{p}}_{p}[\mathrm{D_B} \nabla C_v \cdot \nabla \mathrm{T} + \mathrm{D_T} \frac{\nabla \mathrm{T} \cdot \nabla \mathrm{T}}{\mathrm{T}}] \tag{1.8}$$

and, particle transfer equation,

$$\vec{V} \cdot \nabla C_v = \nabla \cdot [\mathrm{D_B} \nabla C_v + \mathrm{D_T} \frac{\nabla \mathrm{T}}{\mathrm{T}}] \tag{1.9}$$

where $C_v$ is particle concentration, $\mathrm{D_B}$ is Brownian motion coefficient and $\mathrm{D_T}$ is thermophoresis coefficient. The scale analysis by Hwang *et al*. [56] revealed that the Brownian diffusion and

thermophoresis terms in energy equation (second and third terms on right side of Equation 1.18) are negligible, and confirmed that the energy transfer by nanoparticle distribution can be disregarded. They concluded by considering the conduction term in left side of Equation 1.18 as order of one, the Brownian and thermophoresis terms on the right side were in order of $10^{-6}$.

The Buongiorno model has received considerable attention in recent years [57]–[75]. Although there have been studies that their results did not agree with the model [65] and claimed inadequacy of the terms in the model for good prediction of the experimental results [69], there are many studies that could explain the heat transfer trend in nanofluids utilizing the Buongiorno model.

Yu *et al*. [70] performed an experimental study on silicon carbide/water nanofluid with 3.7% particle concentration and 170 nm in particle size. They reported 50-60% increase in heat transfer coefficient compared to the base fluid. Experimental results had a 14-32% higher deviation from the single-phase study and did not support the Brownian and thermophoresis mechanisms. In another study, Moreira *et al*. [66] reported high difference between obtained experimental and numerical data and concluded that the thermophoresis and Buongiorno model is not adequate for explaining the differences between numerical and experimental results. Therefore, there may be an existing mechanism/s not presented yet, that can explain heat transfer enhancement.

Malvandi *et al*. [59], [60], [71]–[75] have divided great attention toward nanofluids. They have also modified the Buongiorno model [71] and discussed the effect of thermophoresis, Brownian motion and particle migration on heat transfer enhancement. Their reported results on nanoparticles move from wall boundaries toward the central region of the channel [60], more uniform velocity profile with rising the slip parameter [71] and also the effect of magnetic field on particle migration [73] is based on utilizing the Buongiorno model. Although in single phase homogeneous studies, the temperature dependency of thermophysical properties can improve the accuracy of results considerably, they investigated this issue in Buongiorno model and stated that the model does not affect the nanofluid heat transfer and flow significantly. Hedayati *et al*.

[57], [58], [69] also considered slip velocity at the wall boundaries in convective heat transfer of alumina-water and $TiO_2$–water in microchannels. They explained that the Brownian motion effect forces the nanofluid to have a more homogeneous and uniform particle concentration whereas the thermophoresis forces particles to move in opposite direction of temperature gradient and have a tendency to gather the particles to the region with lowest temperature gradient.

Heyhat and Kowsary [76] numerically studied the heat transfer of alumina-water nanofluid laminar flow subjected to constant wall temperature utilizing the Buongiorno model. The study revealed that the particle migration has an important role in nanofluids heat transfer augmentation. In addition, increase in bulk thermal conductivity by adding nanoparticles, cannot be the only reason for the increase in heat transfer. The particle migration from walls to the core region and forming a non-homogeneous fluid decreases shear stress and also increases the heat transfer coefficient.

Yang *et al*. [65] [66] modified the Buongiorno model by importing the nanofluid density changes in conventional continuity, momentum, and energy equations, and reported the high temperature gradient and velocity near the walls is a result of particle concentration drop at wall boundaries.

Incompatibility of some results obtained from experimental results with classical theories, significant increase in heat transfer at very low volume fractions and dramatic dependency of thermal conductivity to particle size which were not in decent agreement with classical theories, opened the way to consider new mechanisms and methods such as Thermal dispersion, Particle migration and Brownian diffusion [55], [77], [78]. Sheikholeslami *et al*. [79] in 2016 comprehensively reviewed the nanofluid flow and heat transfer using analytical and numerical approaches. They have mentioned both single phase and two phase models as common methods of simulating nanofluids. They have reviewed thermal conductivity and viscosity models used in literature and summarized the nanofluid viscosity and application of various analytical

methods used by authors as well as introducing novel numerical methods (e.g. finite element method, control-volume finite-element method, lattice boltzmann method).

# 2. THERMOPHYSICAL PROPERTIES OF NANOFLUIDS

## 2.1. Literature Review on Thermophysical Properties of Base Fluid and Particles

### 2.1.1. Thermophysical Properties of Base Fluid (Water)

Thermophysical properties of nanofluids depend on the properties of the base fluid, the particles and the volume fraction of particles. Water properties, density $\rho_w$ , dynamic viscosity $\mu_w$, thermal conductivity $K_w$ and specific heat $C_{p_w}$, are considered dependent on temperature for increasing the accuracy of the simulation as a polynomial interpolation of experimental data as below [80],

$$\rho_w = 999.86 + 6.1238 \cdot 10^{-2} \cdot \mathrm{T} - 8.3131 \cdot 10^{-3}\mathrm{T}^2 + 6.4236 \cdot 10^{-5}\mathrm{T}^3 - 3.9530 \cdot 10^{-7}\mathrm{T}^4 + 1.0808 \cdot 10^{-9}\mathrm{T}^5 \quad (2.1)$$

$$\mu_w = 1.7825 \cdot 10^{-3} - 5.8439 \cdot 10^{-5}\mathrm{T} + 1.2592 \cdot 10^{-6}\mathrm{T}^2 - 1.6986 \cdot 10^{-8}\mathrm{T}^3 + 1.248 \cdot 10^{-10}\mathrm{T}^4 - 3.7458 \cdot 10^{-13}\mathrm{T}^5 \quad (2.2)$$

$$k_w = 0.5609 + 1.9488 \cdot 10^{-3}\mathrm{T} - 1.0133 \cdot 10^{-6}\mathrm{T}^2 - 1.2840 \cdot 10^{-7}\mathrm{T}^3 + 6.2118 \cdot 10^{-10}\mathrm{T}^4 \quad (2.3)$$

$$C_{p_w} = 4218.79 - 3.1667\mathrm{T} + 9.5040 \cdot 10^{-2}\mathrm{T}^2 - 1.3890 \cdot 10^{-3}\mathrm{T}^3 + 1.0722 \cdot 10^{-5}\mathrm{T}^4 - 3.2042 \cdot 10^{-8}\mathrm{T}^5 \quad (2.4)$$

where the temperature, T, is in Celsius degrees.

Thermal expansion of water, $\beta_T$, is defined as below [80],

$$\beta_T = -\frac{1}{\rho_w}\frac{\partial \rho_w}{\partial \mathrm{T}} \quad (2.5)$$

and as a polynomial correlation, $\beta_T$ can be written as,

$$\beta_T = -6.2516 \cdot 10^{-5} + 1.6839 \cdot 10^{-5}\mathrm{T} - 1.9824 \cdot 10^{-7}\mathrm{T}^2 + 1.6867 \cdot 10^{-9}\mathrm{T}^3 - 5.7744 \cdot 10^{-12}\mathrm{T}^4 \ [1/\mathrm{K}] \quad (2.6)$$

### 2.1.2. Thermophysical properties of $Al_2O_3$ Nanoparticles

Same as water (base fluid), properties of nanoparticles, Alumina $Al_2O_3$, has been considered dependent on temperature. Density $\rho_p$, thermal conductivity $K_p$ and specific heat capacity $C_{p_p}$ as a polynomial interpolation of experimental measurements are extracted from literature [81].

$$\rho_p = 3921.71 - 8.5625 \cdot 10^{-2}\mathrm{T}, \qquad 0 \leq \mathrm{T} \leq 100°\mathrm{C} \quad (2.7)$$

$$k_p = 5.5 + 34.5\exp(-0.0033\mathrm{T}), \qquad 0 \leq \mathrm{T} \leq 1300°\mathrm{C} \quad (2.8)$$

$$C_{p_p} = 1044.60 + 0.1742 \cdot (273.15 + \mathrm{T}) - \frac{2.796 \cdot 10^7}{(273.15 + \mathrm{T})^2}, \qquad \mathrm{T} \leq 1500°\mathrm{C} \quad (2.9)$$

## 2.2. Alumina-Water Nanofluid Density

Density of a nanofluid can be simply predicted using mixing theory as [55]

$$\rho_{nf} = C_v\rho_p + (1 - C_v)\rho_w \quad (2.10)$$

where $C_V$ is particle volume fraction, $\rho_{nf}$, $\rho_p$ and $\rho_w$ are density of nanofluid, particle and water.

Mohsen Sharifpur *et al*. (2016) developed a new density model for nanofluids considering nanolayers, which is a layer between base fluid and within nanoparticles [82]. They

demonstrated a mixture model (typical approach for density prediction), which overestimates the nanofluid density (where this can be higher in high particle volume fractions) is due to the lack of considering nanolayers and void volume. They considered a volume as the void, $V_{void}$, which involves the nanolayers, and presented density of nanofluid as

$$\rho_{nf-new} = \frac{m_p + m_f}{V_p + V_f + V_{void}} \tag{2.11}$$

where $m_p$ is mass of a single particle, $m_f$ is mass of base fluid and $V_p$, $V_f$ and $V_{void}$ respectively show volumes of particle, base fluid and Void.

Volume of spherical nanoparticle with radius of $r_p$ is:

$$V_p = \frac{4}{3}\pi {r_p}^3 \tag{2.12}$$

and considering $t_v$ as nanolayers thickness volume of nanoparticle and nanolayers is:

$$V_p + V_{void} = \frac{4}{3}\pi (r_p + t_v)^3 \tag{2.13}$$

where $t_v$ is sensitive to, and a function of particle size, and can be calculated by:

$$t_v = -0.0002833{r_p}^2 + 0.0475 r_p - 0.1417 \tag{2.14}$$

Having same approach, a new model for volume fraction can be presented:

$$C_{v_{new}} = \frac{1}{\frac{1}{C_{v_{old}}} - 1 + \frac{\left(r_p + t_v\right)^3}{r_p^3}} \tag{2.15}$$

where $C_{v_{old}}$is the volume fraction without considering the nanolayers.

Density equation can be rewritten as below,

$$\rho_{nf_{new}} = \frac{\rho_{nf_{old}}}{(1 - C_{v_{new}}) + C_{v_{new}} \frac{\left(r_p + t_v\right)^3}{r_p^3}} \tag{2.16}$$

where considers base fluid and particles densities, size and volume fraction of particles and nanolayers, and old nanofluid density can be simply calculating using correlation below,

$$\rho_{nf_{old}} = C_{v_{old}}\rho_p + (1 - C_{v_{old}})\rho_f \tag{2.17}$$

### 2.3. Alumina-Water Nanofluid Specific Heat Capacity at Constant Pressure

Specific heat capacity at constant pressure of nanofluid can be calculated by thermal equilibrium model as [83]

$$C_{p_{nf}} = \frac{C_v\rho_p C_{p_p} + (1 - C_v)\rho_w C_{p_w}}{\rho_{nf}} \tag{2.18}$$

where density of nanofluid, $\rho_{nf}$ is calculated using the Equation 2.17.

## 2.4. Alumina-Water Nanofluid Viscosity

W. Williams and J. Buongiorno in 2008 [84] conducted experiments on water based Alumina and Zirconia nanofluids, and presented correlations for predicting the viscosity of nanofluids as given by,

Alumina-water nanofluid with particle diameter $d_p$=46 nm

$$\mu_{nf} = \mu_w \exp\left(\frac{4.91C_v}{0.2092 - C_v}\right), \quad 20°C \leq \mathrm{T} \leq 80°\mathrm{C}, \qquad 0 \leq C_v \leq 0.06 \tag{2.19}$$

Masoumi *et al*. [29] studied the viscosity of nanofluids by considering the Brownian motion of the nanoparticles. They proposed a new analytical model and showed its applicability for prediction of viscosity of nanofluids as well as non-Newtonian nanofluids. Their model is not the exact theoretical solution, but the proposed model, in general, has higher accuracy and precision compared to other previous models due to the terms (i.e. temperature, particle diameter, nanoparticle density, nanoparticle volume fraction and physical properties of base fluid) considered in proposed correlation (Equation 2.20). Theoretical and experimental procedures were employed and the results were compared to justify the high accuracy of the model for prediction of viscosity of nanofluids. They considered the effective viscosity as the sum of base fluid viscosity and the apparent viscosity $\mu_{app}$ (Equation 2.20b). In order to investigate the effects of nanoparticles on nanofluid viscosity, they proposed the viscosity ass

$$\mu_{nf} = \mu_{bf} + \mu_{app} \tag{2.20a}$$

$$\mu_{app} = \frac{\rho_p V_B {d_p}^2}{72C\delta} \tag{2.20b}$$

$$V_B = \frac{1}{d_p}\sqrt{\frac{18k_b\mathrm{T}}{\pi\rho_p d_p}} \tag{2.20c}$$

$$\delta = \sqrt[3]{\frac{\pi}{6C_v}}\, d_p \tag{2.20d}$$

$$C = \mu_{bf}^{-1}\left[\left(c_1 d_p + c_2\right)C_v + \left(c_3 d_p + c_4\right)\right] \tag{2.20e}$$

$$c_1 = -1.133 \times 10^{-6}$$

$$c_2 = -2.771 \times 10^{-6}$$

$$c_3 = +9 \times 10^{-8}$$

$$c_4 = -3.93 \times 10^{-7}$$

where $V_B$ is Brownian velocity, $\rho_p$ is density, $d_p$ is the diameter of the nanoparticles, $C$ correction factor and δ is the distance between the centers of the particles.

Further, they have also checked the empirical results of nanofluids with different nanoparticles and base fluids (i.e. CuO-$H_2O$, CuO-EG, $TiO_2$-EG, $Al_2O_3$- $H_2O$, and CuO-EG-$H_2O$) with theoretical results obtained by their proposed model. The comparison of the experimental results and the ones obtained by the introduced model showed that the model could well predict the experimental results.

## 2.5. Alumina-Water Nanofluid Thermal Conductivity

W. Williams and J. Buongiorno in 2008 [84] performed experimental measurements on water based Alumina and Zirconia nanofluids, and proposed correlations for predicting the thermal conductivity of nanofluids as

Alumina-water Nanofluid with particle diameter, $d_p = 46nm$ :

$$k = k_w(1 + 4.5503C_v), \qquad 20°\text{C} \le \text{T} \le 80°C, \quad 0 \le C_v \le 0.06 \tag{2.21}$$

Koo & Kleinstreuer in 2004 [85] proposed KK model by defining the effective thermal conductivity of nanofluid as a combination of particle's conventional static part and a Brownian motion part.

$$k_{eff} = k_{\text{static}} + k_{\text{Browmian}} \tag{2.22}$$

where $k_{\text{static}}$ can be calculated by:

$$\frac{k_{\text{static}}}{k_f} = 1 + \frac{3(\frac{k_p}{k_f} - 1)C_v}{(\frac{k_p}{k_f} + 2) - (\frac{k_p}{k_f} - 1)C_v} \tag{2.23}$$

and $k_{\text{Browmian}}$, Brownian thermal conductivity was proposed by Koo in 2004 [86], analyzing the effect of Brownian motion on the fluid volume and the translational time averaged speed.

$$k_{Bowmian} = 5 \times 10^4 \beta C_V \rho_f c_{p,f} \sqrt{\frac{K_b \mathrm{T}}{\rho_p d_p}} f(\mathrm{T}, C_v) \tag{2.24}$$

where $\rho_f$ and $c_{p,f}$ are the density and specific heat capacity of the fluid, $K_b$ is the Boltzmann constant ($K_b = 1.3807 \times 10^{-23}\, J/K$), T is the temperature, $\rho_p$ is the particle density, $d_p$ is diameter of particles. The $\beta$ and $f(\mathrm{T}, C_v)$ functions are determined semi-empirically. The correlation proposed, is valid for concentration range $1\% < C_v < 4\%$ and temperature range $293\ \mathrm{K} < \mathrm{T} < 325\ \mathrm{K}$. Knowing the limited data ranges of KK model, modifications have been carried out [87] [88] to improve the precision and applicability for wider ranges of particle concentration, size and temperature.

Li in 2008 [87] proposed KKL model for thermal conductivity of nanofluids modifying the KK model considering the types of particle and base fluid combinations, effects of particle

size, particle volume fraction and temperature dependence. He combined $\beta$ and $f(\mathrm{T}, C_v)$ functions to a new $g$ function with coefficients available in the Table 2.1, where for $Al_2O_3$-water and CuO-water nanofluids which is given by

$$g = (a + b\ln(d_p) + c\ln(C_v) + d\ln(C_v)\ln(d_p) + e\ln(d_p)^2)\ln(\mathrm{T}) \\ +(g + h\ln(d_p) + i\ln(C_v) + j\ln(C_V)\ln(d_p) + k\ln(d_p)^2) \tag{2.25}$$

Table 2.1. KKL model coefficients [87]

| Coefficient values | $\mathbf{Al_2O_3}$-water | **CuO**-water |
|---|---|---|
| ***a*** | 52.813488759 | -26.593310846 |
| ***b*** | 6.115637295 | -0.403818333 |
| ***c*** | 0.6955745084 | -33.3516805 |
| ***d*** | 4.17455552786E-02 | -1.915825591 |
| ***e*** | 0.176919300241 | 6.42185846658E-02 |
| ***g*** | -298.19819084 | 48.40336955 |
| ***h*** | -34.532716906 | -9.787756683 |
| ***i*** | -3.9225289283 | 190.245610009 |
| ***j*** | -0.2354329626 | 10.9285386565 |
| ***k*** | -0.999063481 | -0.72009983664 |

Vajjha and Das in 2009 [88] carried out an experimental investigation on the thermal conductivity of three different nanofluids. They developed the Koo and Kleinstreuer [85] thermal conductivity model by refining the $\beta$ and $f(\mathrm{T}, C_v)$ empirical functions of correlation with collecting more and wider range of experimental data sets.

$$k_{nf} = \frac{k_p + 2k_{bf} - 2(k_{bf} - k_p)\phi}{k_p + 2k_{bf} + (k_{bf} - k_p)\phi} k_{bf} + 5 \times 10^4 \beta C_V \rho_{bf} C_{pbf} \sqrt{\frac{\kappa \mathrm{T}}{\rho_p d_p}} f(\mathrm{T}, C_v) \tag{2.26}$$

$$f(T, C_v) = (2.8217 \times 10^{-2} C_V + 3.917 \times 10^{-3})(\frac{T}{T_0}) + (-3.0669 \times 10^{-2} C_V - 3.91123 \times 10^{-3}) \quad (2.27)$$

| | | | | |
|---|---|---|---|---|
| for $Al_2O_3$ | $\beta = 8.4407(100C_V)^{-1.07304}$ | $1\% \leqslant C_v \leqslant 10\%$ | $298K \leqslant T \leqslant 363K$ | (2.28) |
| for ZnO | $\beta = 8.4407(100C_V)^{-1.07304}$ | $1\% \leqslant C_v \leqslant 7\%$ | $298K \leqslant T \leqslant 363K$ | |
| for CuO | $\beta = 9.881(100C_V)^{-0.9446}$ | $1\% \leqslant C_v \leqslant 6\%$ | $298K \leqslant T \leqslant 363K$ | |

The above correlations are valid for particle size range 29-77 nm.

## 2.6. Main Objectives

The main aims of this study are investigating the convective heat transfer and flow performance analysis of alumina-water nanofluid inside a minichannel, comparing the results of non-homogeneous two-component and single phase homogeneous numerical methods and investigating the effect of strength of thermophoresis and particle size on heat transfer. The temperature dependent particle and base fluid properties have been applied, as well as nanofluid viscosity and thermal conductivity models which take into account the parameters, such as particle size, temperature and particle concentration, affecting the flow and heat transfer of nanofluid to observe the effect of applying nanofluid properties with higher accuracy within the governing equations.

This thesis is organized as defining the governing equations for single phase homogeneous and non-homogeneous two-component models, geometry, boundary conditions and mathematical formulations in Section 3. Validating and reproducing the work by Ryzhkov and Minakov [68] in Section 4. Investigating the numerical results, studying the thermophoresis effect and particle size for $Al_2O_3$-water nanofluid, applying the nanofluid properties as only dependent on particle concentration in Section 5.1 and dependent on additional parameters such as particle size and temperature in Section 5.2 and the effect of thermophoresis strength on CuO-water nanofluid in Section 5.3.

# 3. MATHEMATICAL FORMULATION

## 3.1. Governing Equations

In this study, a non-homogenous two-component model has been used for a compressible nanofluid flow case where physical properties of nanofluids are dependent on particle concentration, nanoparticles and base fluid properties are dependent on temperature, and all are expressions taken from experimental measurements. Convection, Brownian diffusion, and thermophoresis are the key terms of nanoparticle transport equation of this modeling. New thermophoresis model used to study the significance of the thermophoresis effect on the nanofluid flow and particle distribution. Single phase homogenous model is utilized for comparisons, as well.

### 3.1.1. Governing Equations of Fluid Dynamics (Continuity, Momentum, and Energy)

Conventional governing equations of mass conservation, momentum, and energy for a compressible single phase homogeneous flow from literature are [68]

$$\nabla \cdot \left(\rho_{nf} \vec{V}\right) = 0 \tag{3.1}$$

$$\rho_{nf} \left(\vec{V} \cdot \nabla\right) \vec{V} = -\nabla \cdot [\, -pI + \mu_{nf}(\nabla \vec{V} + \nabla \vec{V}^{T}) - \frac{2}{3}\mu_{nf}(\nabla \cdot \vec{V})I] \tag{3.2}$$

$$\rho_{nf} C_P \vec{V} \cdot \nabla \mathrm{T} = \nabla \cdot (k_{nf} \nabla \mathrm{T}) \tag{3.3}$$

where Brownian diffusion and thermophoresis terms of energy equation have been disregarded, as a result of scale analysis conducted by Hwang *et al*. [56], which revealed the energy transfer by nanoparticle distribution is negligible.

### 3.1.2. Nanoparticle Transfer Equation

Nanoparticle transfer equation proposed by Buongiorno in 2006 [55] coupled with the governing Equations 3.1-3.3 provides the equations required for non-homogeneous two-component modeling. In this study, the convection, Brownian diffusion, and thermophoresis terms are taken considered. [68]

$$\vec{V} \cdot \nabla C_m = \nabla \cdot (\mathrm{D_B} \nabla C_m + \mathrm{D_T} C_m \nabla \mathrm{T}) \tag{3.4}$$

where $C_m$ is particle mass conservation, $\mathrm{D_B}$ is Brownian motion coefficient and $\mathrm{D_T}$ is Thermophoresis coefficient.

For convenient in calculations mass fraction, $C_m$ is used in nanoparticle transfer equation. Volume fraction of particles and mass fraction are related to each other. Where can be easily calculated by correlation below:

$$\rho_{nf} C_m = \rho_p C_v \tag{3.5a}$$

$$C_v = \frac{\rho_w C_m}{\rho_w C_m + (1 - C_m)\rho_a} \tag{3.5b}$$

$$C_m = \frac{\rho_p C_v}{\rho_p C_v + (1 - C_m)\rho_w} \tag{3.5c}$$

3.1.2.1. Brownian Motion Coefficient is not dependent on volume fraction of particles and is defined from the Einstein-Stokes formula as [89]

$$\mathrm{D_B} = \frac{K_b \mathrm{T}}{3\pi \mu_w d_p} \tag{3.6}$$

where Boltzmann constant is $K_b = 1.3807 \times 10^{-23}$J/K.

3.1.2.2. Thermophoresis Coefficient

G.S. McNab and A. Meisen [90] in 1973 proposed a model for thermophoretic mobility, Equation 3.7. The formula was obtained from experimental data with micro sized particles in water and n-hexane as base fluid. The formula has been used in many works done on modeling of nanofluids.

$$D_T = 0.26 \frac{\kappa_{bf}}{2\kappa_{bf} + \kappa_p} \frac{\mu_{bf}}{\rho_{bf} T} \tag{3.7}$$

The formula shows the thermophoresis coefficient is proportional to viscosity of base fluid and inversely proportional to temperature, and it should decrease with temperature. Nevertheless, the formula fails in matching many experimental results obtained [91]–[93]. The thermophoresis coefficient highly increases with temperature increment as revealed in [94]. Also, the thermophoresis coefficient is proportional to the base fluid viscosity asserted in theoretical studies [91] and molecular dynamics simulations [93]. Many works have been done to understand the complexity of this phenomena and its dependence on the effects of mechanisms such as the Thermal diffusion and particle size effect, the Dispersion forces and temperature dependent density gradient, the Thermoelectric and particle movement directions, the Thermoosmosis, particles electric charges and ion concentration spatial non-homogeneity and etc. [68]. Piazza and Parola [95] critically reviewed the investigations on thermophoresis, theoretical and experimental tools for thermophoresis manipulation, and discussed some of results and novel studies that may bring forward new aspects of thermophoresis.

Thermophoresis coefficient proposed by Ryzhkov and Minakov [68] in 2014 has been used in this study as well. They have shown the significant effect of thermophoresis on reduction of volume fraction of particles near the walls leads to increase in velocity near walls and flattening of velocity profile in channel axis. Affirming the Equation 3.7 contradictions between theoretical studies and experimental results, and mentioning the disadvantage of it as incapable of taking particle size effect, taking base fluid viscosity $\mu_f$ in reverse proportion and solvent

thermal expansion coefficient $\beta_T$ in direct proportion, a new empirical thermophoresis coefficient proposed as

$$\mathrm{D_T} = \alpha \frac{\beta_T}{\mu_f} \frac{k_f}{2k_f + k_p} \tag{3.8}$$

where $\alpha$ is proportionality coefficient and should be extracted from experimental data. Considering the alumina water nanofluid, values of $0.5 \cdot 10^{-9}$, $10^{-9}$ and $2 \cdot 10^{-9}$ used for $\alpha$ by [68] to demonstrate the effect of thermophoresis on mass and heat transfer. In the simulations $\mu_f = \mu_w$, $K_f = K_w$ and $K_a = K_p$. The $\beta_T$ is the thermal expansion of base fluid, water (see Equation 2.6).

In this study, both thermophoresis coefficients have been used to investigate the effect of the thermophoresis on the heat transfer and flow on nanofluids in a minichannel.

### 3.2. Geometry and Boundary Conditions

Figure 3.1 demonstrates geometry of the circular minichannel similar to I. Ryzhkov and A. Minakov [68], with radius of $R = 1\mathrm{mm}$ and two meters in length ($2L = 2m$) in z direction. Nanofluid axisymmetric laminar flow passes through the minichannel with constant temperature $T_0$=20℃ and constant parabolic velocity profile at the inlet of channel as

$$v(r) = 2v_0\left(1 - \left(\frac{r}{R}\right)^2\right) \tag{3.9}$$

where $v_0$ is average velocity and flow exits the channel at zero pressure at the outlet.

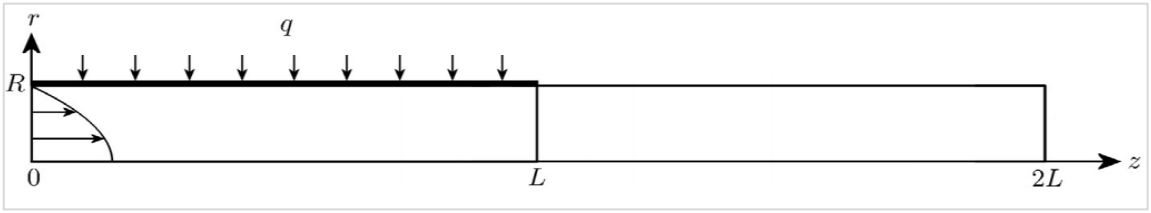


Figure 3.1. The geometry of the circular minichannel. $R = 1\text{mm}$, $2L = 2m$ and parabolic inlet velocity; subjected to constant heat flux from $0 \le z \le L$ [68].

### 3.2.1. Boundary conditions on the walls of channel

The wall $0 \le z \le L$ is subjected to constant heat flux $q = 2000\ W/m^2$ and thermally insulated on $L \le z \le 2L$. There are no slip boundary condition and zero flux particle transfer boundary condition on the walls ($r = R$), and Symmetry boundary condition on axis ($r = 0$).

$$r = 0 : \frac{\partial u}{\partial r} = \frac{\partial v}{\partial r} = \frac{\partial \mathrm{T}}{\partial r} = \frac{\partial C_m}{\partial r} = 0$$
$$r = R : u = v = 0 \tag{3.10}$$

$$k\frac{\partial \mathrm{T}}{\partial r} = \begin{cases} q, & 0 \le z \le L, \\ 0, & L \le z \le 2L, \end{cases} \quad D\frac{\partial C_m}{\partial r} + D_T C_m \frac{\partial \mathrm{T}}{\partial r} = 0 \tag{3.11}$$

$$z = 0 : \quad u = 0, \qquad v = v(r), \quad \mathrm{T} = \mathrm{T}_0, \qquad C_m = C_{m_0}$$
$$z = 2L : \quad \frac{\partial u}{\partial z} = \frac{\partial v}{\partial z} = \frac{\partial \mathrm{T}}{\partial z} = \frac{\partial C_m}{\partial z} = 0 \tag{3.12}$$

## 3.3. Dimensionless Numbers and Output Parameters

The dimensionless Reynolds and thermal Peclet numbers are defined as

$$\mathrm{Re} = \frac{\rho v_0 2R}{\mu_{nf}} \tag{3.13}$$

$$\mathrm{Pe} = \frac{\rho C_p v_0 2R}{k} \tag{3.14}$$

Heat transfer coefficient in the channel subjected to constant heat flux can be calculated by

$$\mathrm{h} = \frac{q}{\mathrm{T}(R,z) - \mathrm{T}_b(z)} \tag{3.15}$$

where constant heat flux is $q = 20000\ W/m^2$, $T(R,z)$ is local temperature of the wall ($r = R$) and $T_b(z)$ is the Bulk temperature of the nanofluid flow in the channel, where can be estimated simply by: [96]

$$\mathrm{T}_b(z) = \mathrm{T}_0 + \frac{2q}{Rv_0\rho C_p} z \tag{3.16}$$

where density $\rho$ and specific heat capacity $C_p$ in analytical solution are equal to the constant values with the inlet temperature and nanofluid volume fraction. In addition, the bulk temperature can be calculated using the definition below as [67]

$$\mathrm{T}_b(z) = \frac{1}{v_0 A_c} \int u \mathrm{T} dA_c \tag{3.17}$$

Heat transfer coefficient in a channel subjected to constant wall temperature can be calculated by [67]

$$\mathrm{h} = \frac{-k \left.\frac{\partial T}{\partial r}\right|_{wall}}{(\mathrm{T_w} - \mathrm{T}_b)} \tag{3.18}$$

the average heat transfer coefficient can be calculated by

$$\overline{\mathrm{h}} = \frac{1}{2\pi RL}\int_0^L \int_0^{2\pi} hRd\varphi dz \tag{3.19}$$

local Nusselt number, Nu and average Nusselt number, $\overline{\mathrm{Nu}}$ have been considered as

$$\mathrm{Nu} = \frac{h2R}{k_b(z)} \tag{3.20}$$

$$\overline{\mathrm{Nu}} = \frac{1}{2\pi RL}\int_0^L \int_0^{2\pi} \mathrm{Nu}Rd\varphi dz \tag{3.21}$$

$$k_b(z) = \frac{1}{v_0 A_c}\int ukdA_c \tag{3.22}$$

A good approximation of analytical expression for Nu is provided by the Shah correlation. [97] Local Nusselt number is a function of the $\xi = z(2RPe)^{-1}$ considering all physical properties as constant.

$$\mathrm{Nu} = \begin{cases} 1.302\xi^{-1/3} - 1, & \xi < 0.00005 \\ 1.302\xi^{-1/3} - 0.5, & 0.00005 < \xi < 0.0015 \\ 4.364 + 0.263\xi^{-0.506}e^{-41\xi} & \xi > 0.0015 \end{cases} \tag{3.23}$$

Shear stress can be calculated with the conventional correlation as below

$$\tau_{wall} = -\mu\frac{\partial u}{\partial r} \tag{3.24}$$

Friction factor can be calculated as a term of wall shear stress (Equation 3.24), and pressure loss between the inlet and outlet using Equations 3.25 and 3.26 respectively. [98] [99]

$$f = -\frac{8\tau}{\rho {v_0}^2} \tag{3.25}$$

$$f = 2\Delta P \frac{D}{L} \frac{1}{\rho {v_0}^2} \tag{3.26}$$

where $D$ is circular channel diameter, $L$, length of channel, $\rho$, density at tube inlet.

The ratio of favorable heat transfer improvement to relative unfavorable pressure loss has been defined as the Performance Evaluation Criteria (PEC). [100] The values higher than one specifies improvement in performance, and lower than one means lower performance. There have been studies such as, Karwa *et al.* [101], Manca *et al*. [102], Chai *et al*. [103], Sayyar and Saghafian [104], Behnampour *et al*. [105], Khoshvaght-aliabadi *et al*. [106], Zhang *et al*. [107] that have used the PEC definitions as

$$\text{PEC} = \frac{\overline{Nu_T}/\overline{Nu_H}}{(\overline{f_T}/\overline{f_H})^{\frac{1}{3}}} \tag{3.27a}$$

$$\text{PEC} = \frac{\overline{Nu_T}/\overline{Nu_H}}{(\overline{\Delta P_T}/\overline{\Delta P_H})^{\frac{1}{3}}} \tag{3.27b}$$

where T and H stand for non-homogeneous two-component model and homogeneous single phase approach results, respectively.

The Efficiency Ratio (ER) has been used for performance studies as below

$$ER = \frac{\overline{Nu_T}/\overline{Nu_H}}{\overline{\Delta P_T}/\overline{\Delta P_H}} \tag{3.28}$$

# 4. NUMERICAL METHOD AND VALIDATION

## 4.1. Numerical Method of Modeling Nanofluid in a Circular Minichannel

In this study convective heat transfer of $Al_2O_3$-water nanofluid in a circular channel, subjected to constant heat flux has been studied. For the initial step, the work published by I. Ryzhkov and A. Minakov in 2014 [68] validated. A non-homogenous two-component model has been used for a compressible nanofluid flow case where physical properties of nanofluids are dependent on particle concentration. Nanoparticles and base fluid properties are dependent on temperature, and all are expressions taken from experimental measurements. Convection, Brownian diffusion and thermophoresis are the key terms of nanoparticle transport equation of this modeling. New thermophoresis model used to study the significance of thermophoresis effect on the nanofluid flow and particle distribution. Single phase homogenous model is utilized in comparisons, as well.

COMSOL Multiphysics version 5.4 utilized for the simulations. The laminar flow, heat transfer in fluid and coefficient form PDE modules selected for a 2D axisymmetric geometry. The geometry was drawn by the tools provided in the program. In the material section, the correlations for the properties of base fluid and particles entered as analytic functions.

In the laminar flow module settings, the stationary equation and weakly compressible flow in the physical model section selected. Discretization of fluid selected as P1+P1 elements, which solves velocity and pressure of fluid with first order discretization. It is important to note that the P2+P1 elements are recommended to be selected for flows with very low Reynolds number. The nanofluid viscosity model entered in the fluid properties section of the module. The wall boundary condition added in the module with no slip wall condition. For the inlet boundary condition the constant parabolic velocity profile correlation entered in normal inflow velocity and zero pressure selected for outlet boundary condition.

In the heat transfer in flow module, the correlations for nanofluid thermal conductivity, density and heat capacity entered in fluid section. Temperature and heat flux boundary conditions added within the module to enter the constant temperature at inlet and uniform heat flux for heated section of channel.

Particle transfer equation entered in the coefficient form PDE module. The zero flux boundary condition added by default in the program, provides the zero particle transfer flux. The Dirichlet boundary condition added within the module for entering the inlet particle volume fraction, and two constraint boundary conditions added, to enter the symmetry on axis and outlet boundary conditions.

The Nonisothermal flow should be added to the Multiphysics section to couple the laminar flow and heat transfer modules. The stationary solver selected in the Study section of the program. By opening the solver configurations, additional settings are visible for the stationary solver. The relative tolerance entered as $10^{-7}$. Fully coupled solver was enabled to solve all four equations simultaneously, and the Direct linear solver used a MUMPS solver with 1.2 memory allocation factor. For the Method and Termination section of fully coupled solver, the initial damping factor and minimum damping factor entered as 0.001 and 1E-4 in the Automatic (Newton) nonlinear method respectively, with 5000 maximum number of iteration

Different Pe numbers and particle concentrations have been studied. The values of calculated nanofluid properties and velocities at inlet are given in Table 4.1 and Table 4.2 respectively, for different Peclet numbers and nanoparticle volume fractions.

Table 4.1. Nanofluid properties of alumina-water nanofluid with $T_0 = 20℃$ at the inlet

| $C_{v0}$ | $C_{m0}$ | $\mu$ [Pa.s] | $\rho$ [Kg/m$^3$] | $C_p$ [J/kgK] | $k$ [W/mK] |
|---|---|---|---|---|---|
| 0.05 | 0.1713 | 0.004675 | 1144.303 | 3599.27 | 0.734720 |
| 0.03 | 0.1083 | 0.002275 | 1085.867 | 3814.272 | 0.680249 |
| 0.01 | 0.0382 | 0.001279 | 1027.431 | 4053.73 | 0.625778 |
| Water | 0 | 0.0010002 | 998.2136 | 4183.973 | 0.598543 |

Table 4.2. Nanofluid velocities at the circular minichannel inlet

| Pe | $C_{v0} = 0$ $C_{m0} = 0$ | $C_{v0} = 0.01$ $C_{m0} = 0.0381$ | $C_{v0} = 0.03$ $C_{m0} = 0.1083$ | $C_{v0} = 0.05$ $C_{m0} = 0.1713$ |
|---|---|---|---|---|
| | $v_0$ [m/s] | $v_0$ [m/s] | $v_0$ [m/s] | $v_0$ [m/s] |
| **2000** | 0.1433 | 0.1502 | 0.1642 | 0.1784 |
| **2500** | 0.1791 | 0.1878 | 0.2053 | 0.2230 |
| **3000** | 0.2150 | 0.2254 | 0.2464 | 0.2676 |
| **4000** | 0.2866 | 0.3005 | 0.3285 | 0.3568 |
| **6000** | 0.4299 | 0.4507 | 0.4927 | 0.5352 |
| **8000** | 0.5732 | 0.6010 | 0.6570 | 0.7136 |
| **10000** | 0.7166 | 0.7512 | 0.8212 | 0.8919 |
| **12000** | 0.8599 | 0.9015 | 0.9854 | 1.0703 |

### 4.1.1. Mesh Dependency Analysis

To obtain accurate results in numerical investigations, verification and mesh dependency checks are necessary. Low number of mesh elements leads to inaccurate results, and having high number of mesh elements may cause long computation time. Therefore, obtaining an optimum mesh node numbers can have a significant role in time efficiency and results accuracy. In this study, four different mesh node numbers are investigated in order to obtain more applicable mesh for numerical analysis.

The Table 4.3. Mesh independency check shows the meshes used, optimum one in bold. Figure 4.1a demonstrates the average velocity at outlet of channel related to each mesh number. At a point increasing number of mesh elements (Mesh No.3) does not change the results accuracy. Figure 4.1b represents the percent increase in average velocity at outlet compared to previous mesh, which for Mesh No.4 this values is 8.6E-04. Therefore Mesh No.3 was selected in this study.

Table 4.3. Mesh independency check

| Mesh node numbers and Ratio | Mesh No. 1 | Mesh No. 2 | Mesh No. 3 | Mesh No. 4 |
|---|---|---|---|---|
| Number of mesh nodes on radial direction | 50 | 100 | 150 | 180 |
| Number of mesh nodes on axial direction for each section (heated and insulated) | 1200 | 1500 | 2000 | 3000 |

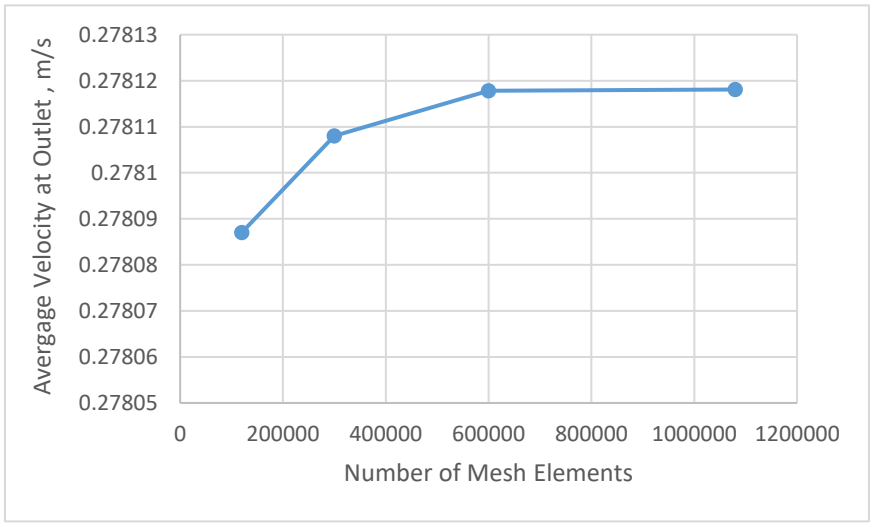


a

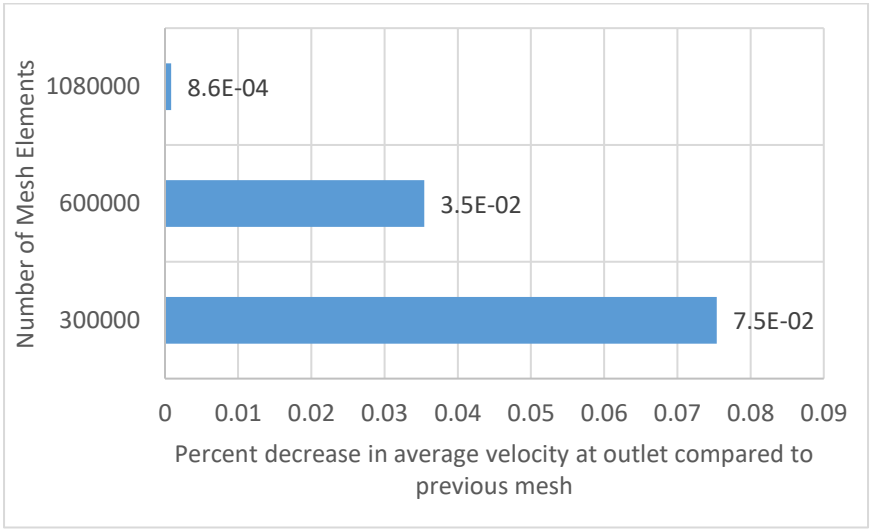


b

Figure 4.1. Mesh independency check. (a) increase in average velocity at outlet related to number of mesh elements. (b) percent increase in average velocity at outlet compared to previous mesh related to number of mesh elements.

## 4.2. Validation

The following simulations are made to reproduce and validate the results with existing numerical results in the literature [68]. The study investigates alumina-water nanofluid laminar flow in a circular minichannel heated via constant heat flux on the first half and isolated on the second half. Three different values of nanoparticle volume fraction $C_{v_0}$ $(0.01, 0.03$ and $0.05)$ and proportionality coefficient $\alpha$ $(0.05 \times 10^{-9}, 10^{-9}$ and $2 \times 10^{-9}$ [Kgm/s$^2$]).The nanofluid viscosity and thermal conductivity are calculated by Equations 2.19 and 2.21, respectively.

Figure 4.2 demonstrates temperature profile in axial and radial coordination. The temperature rises passing through the channel in the axial direction. Temperature gradient increase in the radial direction is obviously visible in the heated section of the channel, after passing this area temperature gradient slowly disappears and reaches a constant temperature. The results of one component model show higher temperature gradient near the walls compared to the non-homogeneous two-component model. The temperature gradient near the walls in the heated section increases thermophoresis effect and forces particles to move away from walls. Reduction of nanoparticles near the wall decreases the thermal conductivity near the wall.

Figure 4.3 demonstrates nanoparticles move toward the low temperature parts, due to the thermophoresis effect. The thermophoresis effect forces nanoparticles to move from walls to center of channel due to the temperature gradient in the heated section. The change in nanoparticle volume fraction in core region of channel is low, but near the walls is significant (see Figure 4.3a and Figure 4.3c). A very slight decrease of particles fraction in middle of channels is corresponding to the temperature rise passing through the channel, decrease in density and increase in specific volume. The highest thermophoresis effect is at the end of heated section, where nanoparticles volume fraction decreases to lowest value (see Figure 4.3c). After passing the heated section Brownian diffusion effect slowly increases and nanoparticle volume fraction gradually increases (see Figure 4.3c). The significant decrease of nanoparticles fraction in wall boundary can only be observed utilizing the non-homogeneous two-component

model. Figure 4.3d shows the numerical solution results utilizing a single phase homogeneous approach considering nanoparticles mass fraction as constant. A very slight decrease in volume fraction is due to the temperature dependency of physical properties.

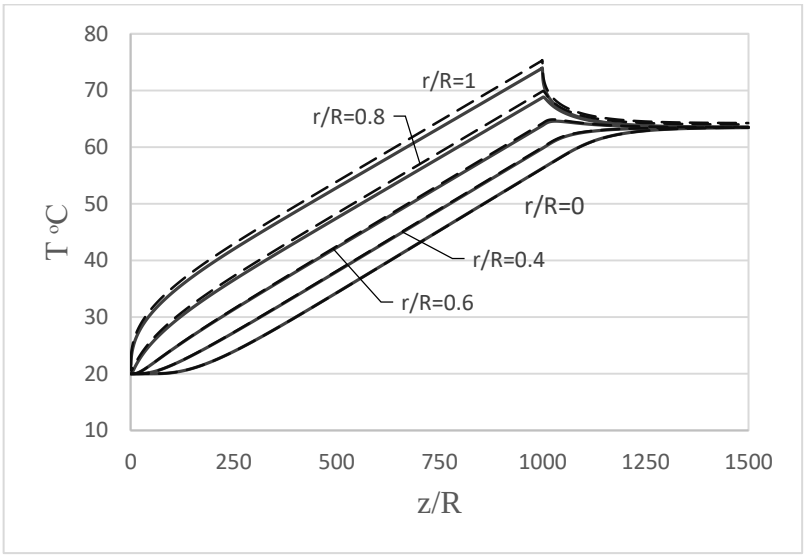


a

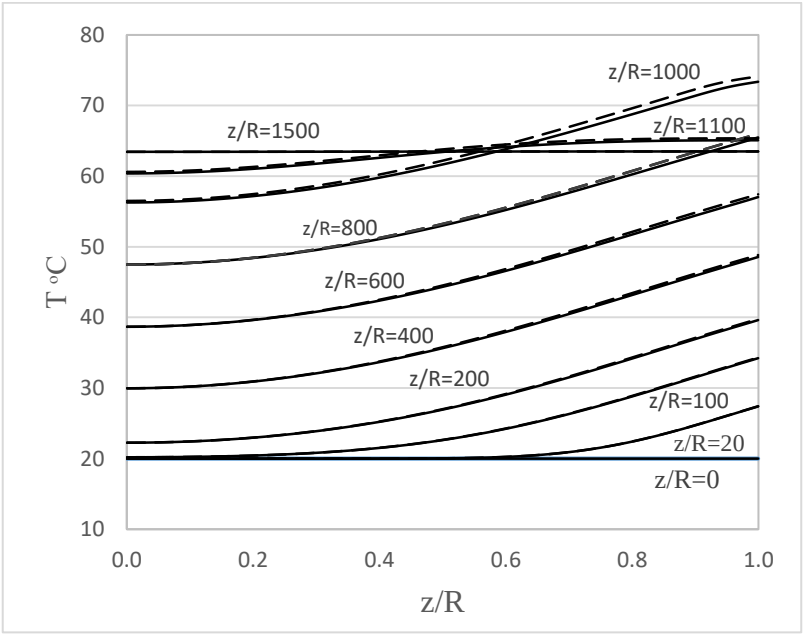


b

Figure 4.2. Temperature profile in radial (a) and axial (b) directions for $C_{v_0}$=0.05 and Pe=2500. The numerical solution for variable physical properties are shown as solid lines and dashed lines are for constant physical properties (constant $C_m$).

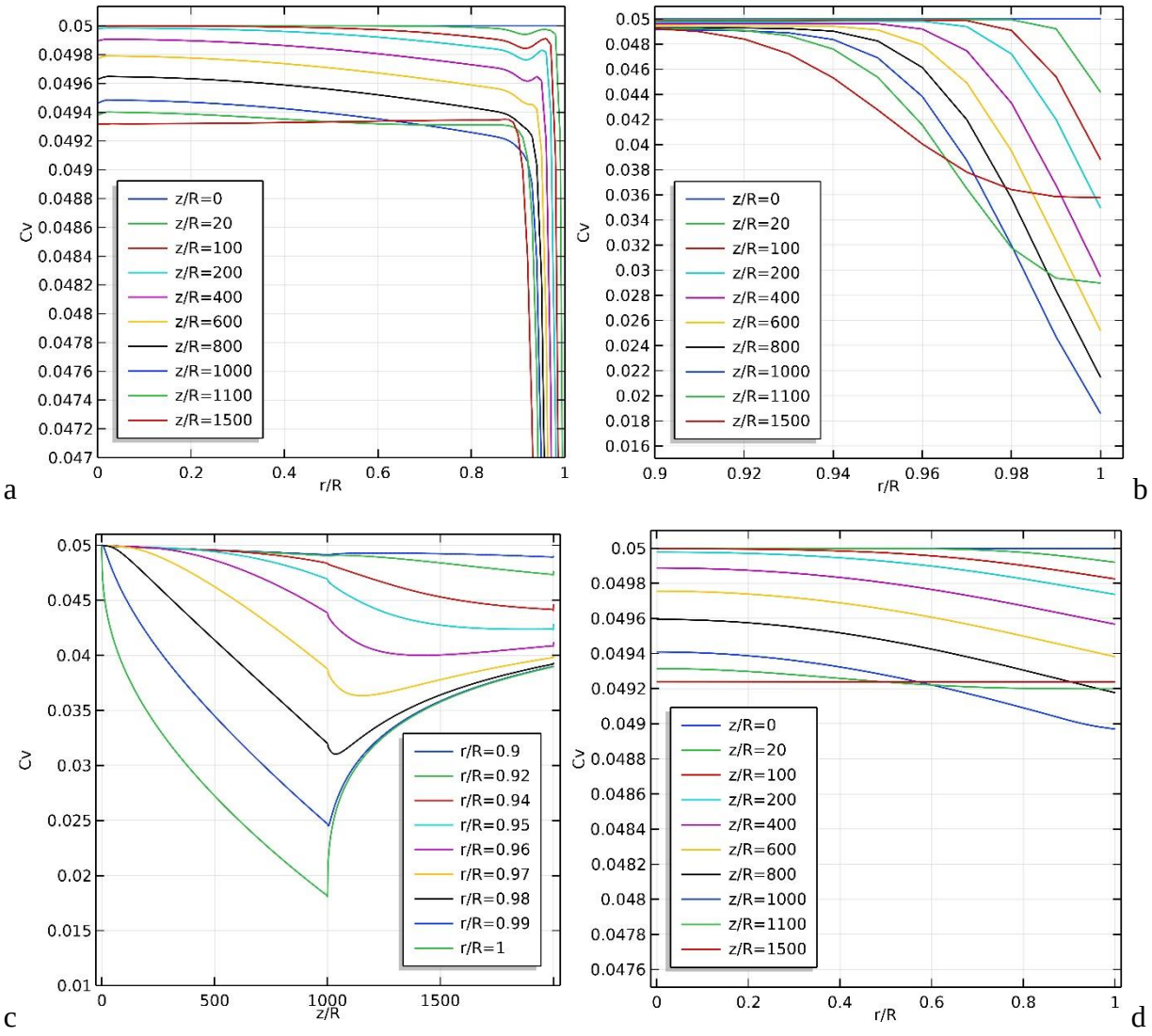


Figure 4.3. Nanoparticle volume fraction $C_v$ in axial and radial directions for $C_{v_0}$=0.05 and Pe=2500. (a) $C_v$ profile in radial directions. (b) $C_v$ profile near the wall ($0.9 \leq r/R \leq 1$). (c) $C_v$ profile in axial direction (two-component model), (d) $C_v$ profile homogenous model.

Figure 4.4 shows the increase in thermal conductivity and decrease in viscosity, which is due to increase in temperature of nanofluid, passing through the channel in axial direction, and from the center of tube to the tube walls, in radial direction (see temperature profiles in Figure

4.2). In addition, significant decrease of nanoparticles volume fraction near walls (see Figure 4.3) decreases the viscosity and thermal conductivity drastically, which can only be explained in non-homogeneous two-component model. High decrease in viscosity near the walls leads to the velocity increase in the wall boundary layer and flattening velocity profile in center of channel, to keep the mass flow rate constant (see Figure 4.5). This effect is more visible by increasing the thermophoresis effect with higher $\alpha$.

Figure 4.6 demonstrates the local heat transfer coefficient h and Figure 4.7 shows the local Nusselt number for different inlet nanoparticle volume fractions, where after a significant decrease at the inlet show a slightly increase, due to the increase in temperature of nanofluid passing through the channel, decrease in viscosity and increase of thermal conductivity (see Figure 4.4). Increasing particle volume fraction leads to increase in local heat transfer coefficient. Two-component non-homogeneous model shows higher values for local heat transfer coefficient compared to single phase homogeneous model which is due to significant decrease of particles volume fraction and viscosity in the wall boundary layer, leading to higher velocity and heat transfer at the channel walls.

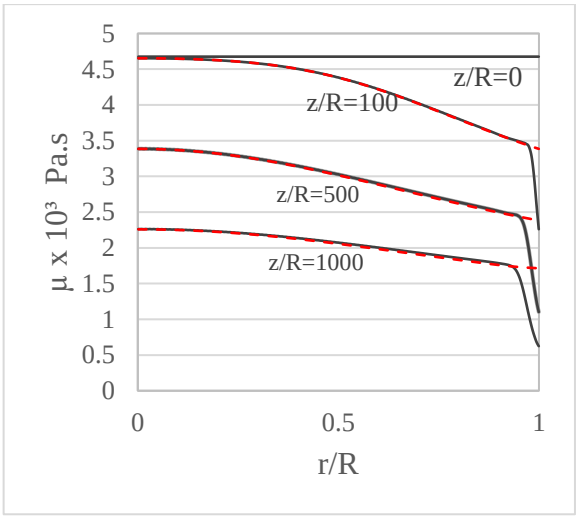


a

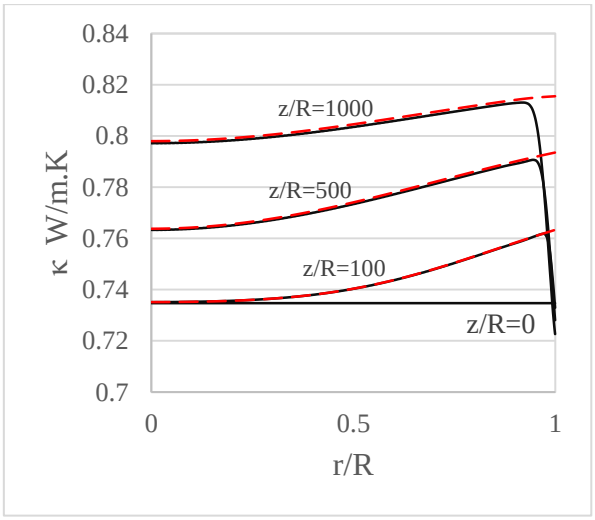


b

Figure 4.4. Profiles of viscosity (a) and thermal conductivity (b) in radial direction of channel for $C_{v_0}$=0.05 and Pe=2500, solid lines are for non-homogeneous two-component model and red dashed lines are for homogeneous single phase model.

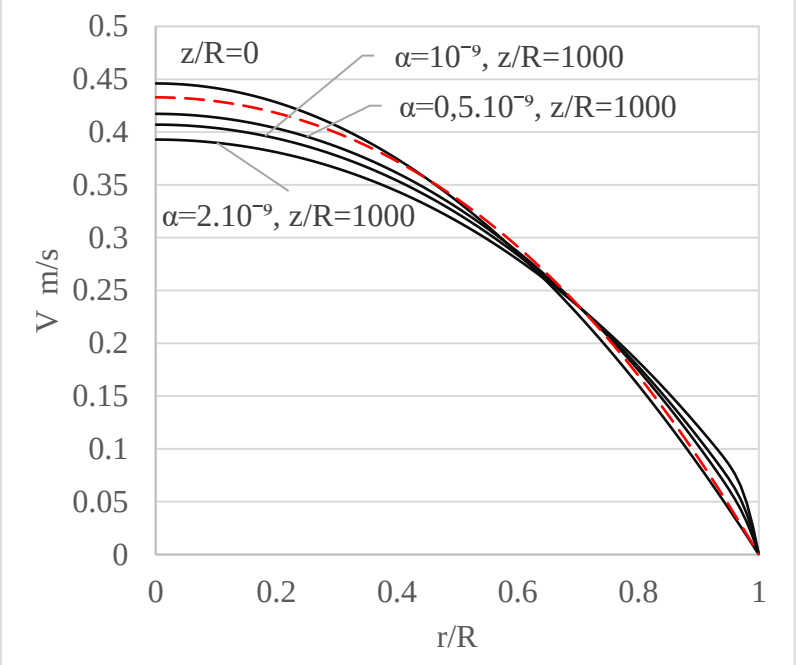


Figure 4.5. The velocity profile in the inlet and outlet of heated section changing thermophoresis effect with different α. results of non-homogeneous two-component model are shown as solid lines and for homogeneous single phase model is dashed line (constant $C_m$).

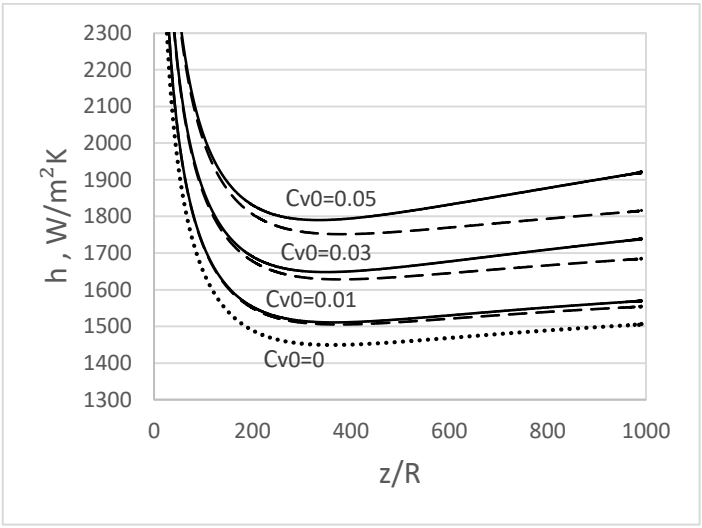


Figure 4.6. The heat transfer coefficient for different values of nanoparticle volume fractions, for Pe=2500. Where solid lines represent non-homogeneous two-component model and dashed lines are for one-component homogenous model results.

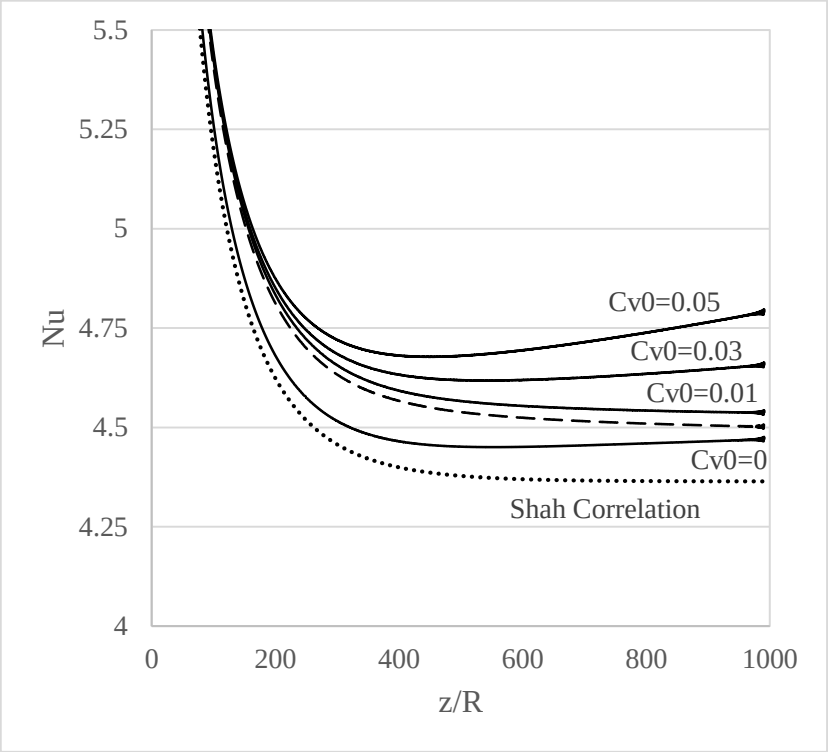


Figure 4.7. The local Nusselt number for different values of nanoparticle volume fractions, for Pe=2500. Where solid lines represent non-homogeneous two-component model and the dashed line is for one-component homogenous model and the dotted line is Shah correlation.

Heat transfer increases with increasing the inlet volume fraction of particles (see Figure 4.8 and Figure 4.9). The results of two-component non-homogeneous model show higher result compared to single phase homogeneous model like local values, due to the decrease of particle concentration near the walls, leading to lower viscosity and higher velocity and higher heat transfer in wall boundaries.

The average heat transfer coefficients ratio of non-homogeneous two-component and single phase homogeneous models (Figure 4.10) show higher increase in heat transfer at lower Pe numbers and higher particle concentrations.

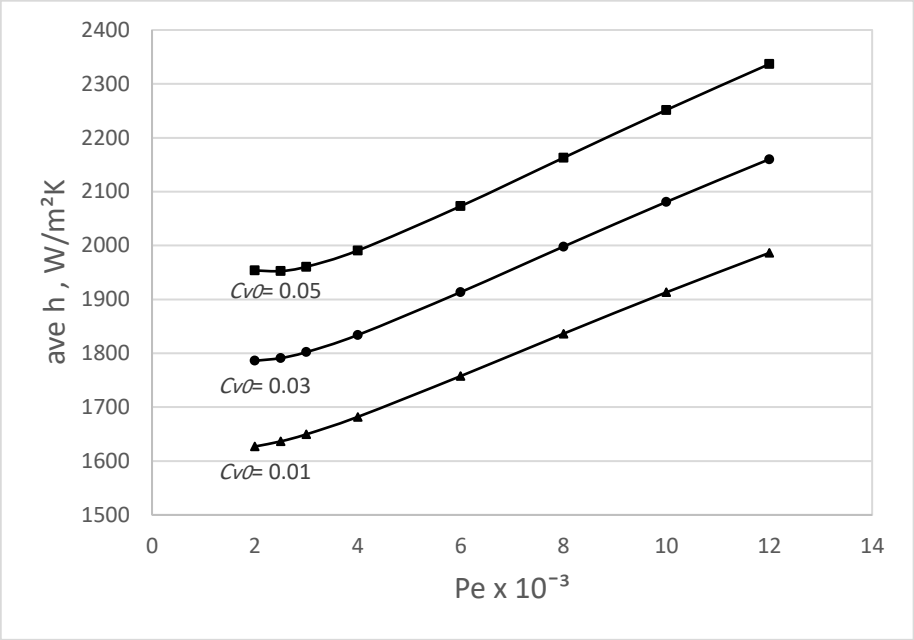


Figure 4.8. The average heat transfer for different values of inlet nanoparticle volume fraction and velocities using non-homogeneous two-component model.

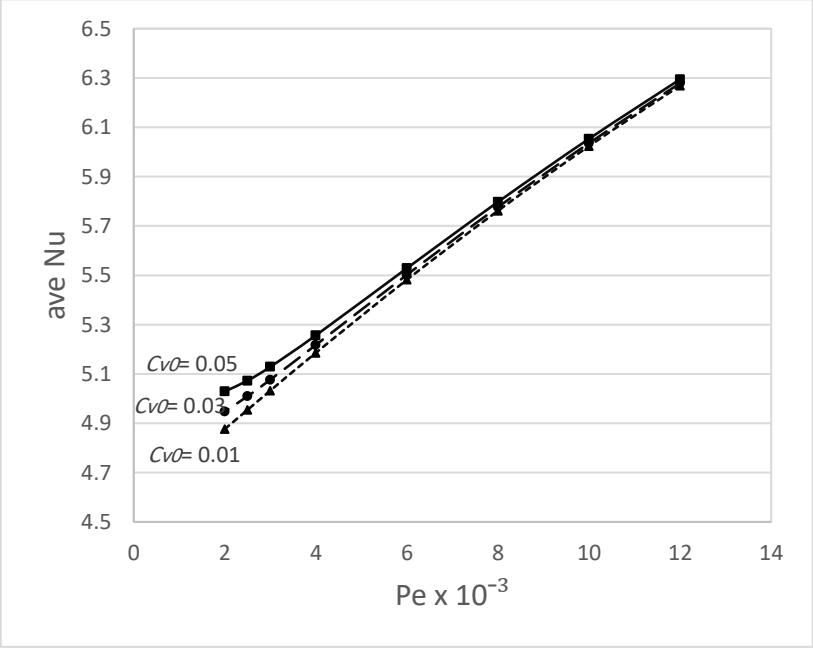


Figure 4.9. The average Nusselt number for different values of inlet nanoparticle volume fraction and velocities using non-homogeneous two-component model.

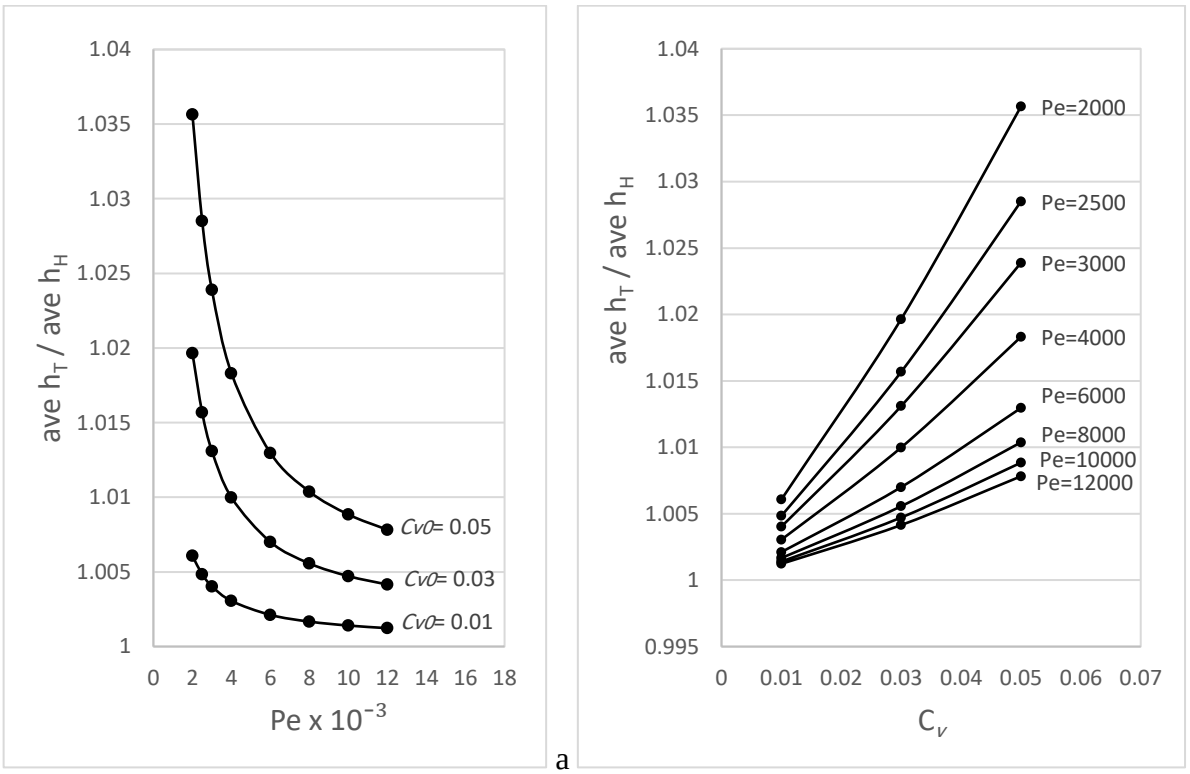


Figure 4.10. The ratio of average heat transfer coefficient between non-homogeneous two-component and single phase homogeneous models, for different values of inlet nanoparticle volume fractions (a) and velocities (b).

Local wall shear stress (Figure 4.11) and friction factor (Figure 4.12) in the heated section of channel for Pe=2500 show decrease, passing through the channel. The higher inlet particle concentration produces higher shear stress and friction factor, which has been observed in numerous experimental [33] [51] [52], numerical [55] [75] and analytical [48] [53] studies.

In addition, lower values of shear stress and friction factor in non-homogeneous two-component model results compared to homogeneous ones is due to the particle reduction by thermophoresis effect near the walls and reduction in viscosity at wall boundaries.

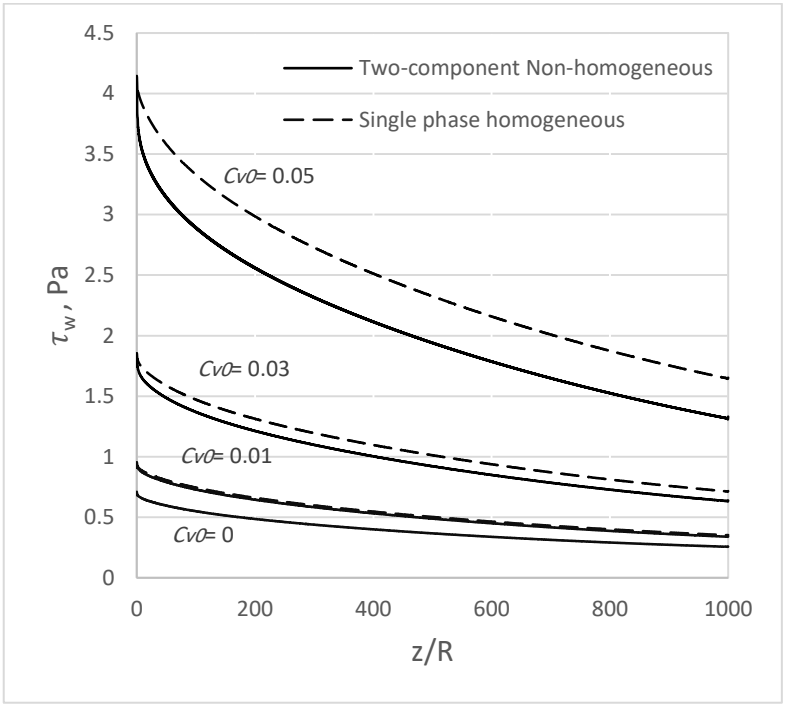


Figure 4.11. The shear stress in the heated section of channel for different values of inlet nanoparticle volume fraction for Pe=2500.

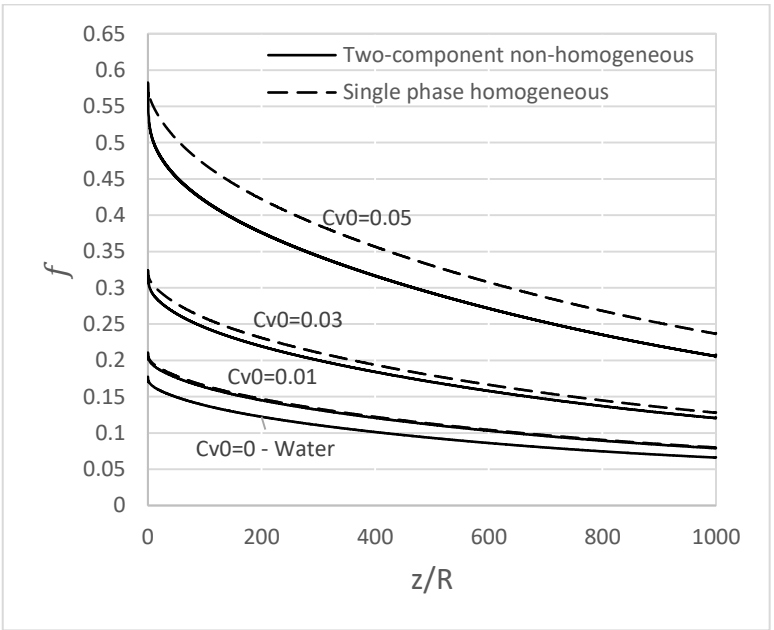


Figure 4.12. The Friction factor in heated section of channel for different values of nanoparticle concentration for Pe=2500.

# 5. RESULTS AND DISCUSSION

## 5.1. Alumina-Water Nanofluid Flow and Heat Transfer with Properties Dependent only on Particle Concentration

This section studies the flow and heat transfer of $Al_2O_3$-water nanofluid with nanofluid properties dependent on the particle concentration. The nanofluid viscosity and thermal conductivity are calculated via proposed models by W. Williams and J. Buongiorno in 2008 [84] (see Equations 2.19 and 2.21) and the inlet temperature is $T_0$=20℃.

### 5.1.1. Alumina-Water Nanofluid Non-Homogenous Two-Component and Single Phase Homogeneous Flow Subjected to Constant Heat Flux

The average Nusselt number ratio results of non-homogeneous two-component and single phase homogeneous models are presented in Figure 5.1 shows higher heat transfer increment at lower Pe numbers and higher particle concentrations. In addition, the ratios of average heat transfer coefficients, and average Nusselt numbers, for non-homogeneous two-component model and base fluid (water) (Figure 5.2 and Figure 5.3) show higher increase in heat transfer at lower Pe numbers as well as higher particle concentrations.

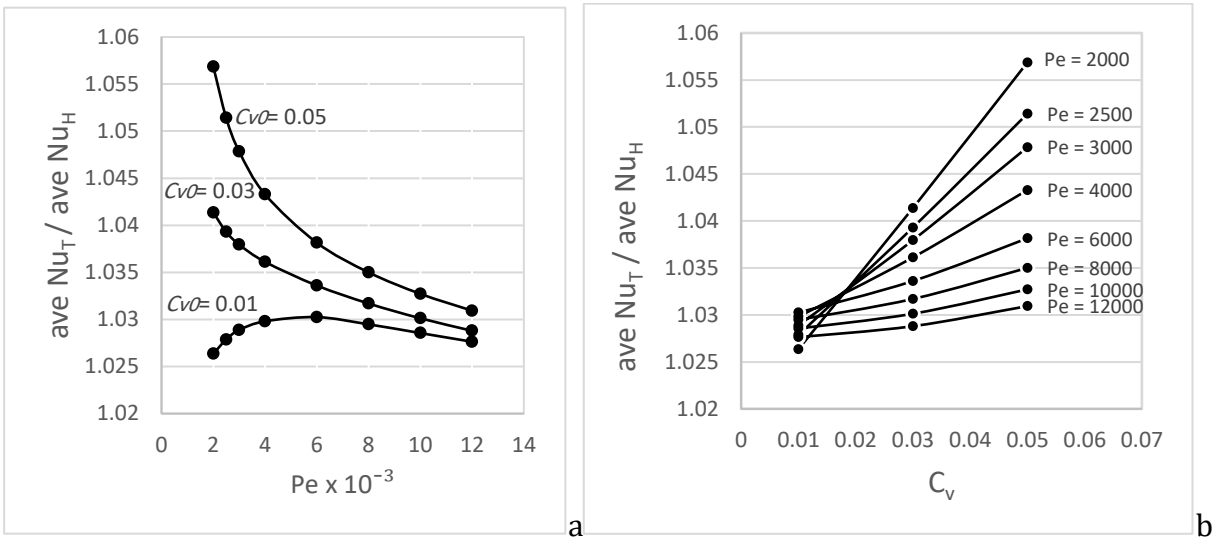


Figure 5.1. The ratio of average Nusselt number between two-component non-homogeneous and single phase homogeneous models, for different values of inlet nanoparticle volume fraction (a) and Pe numbers (b).

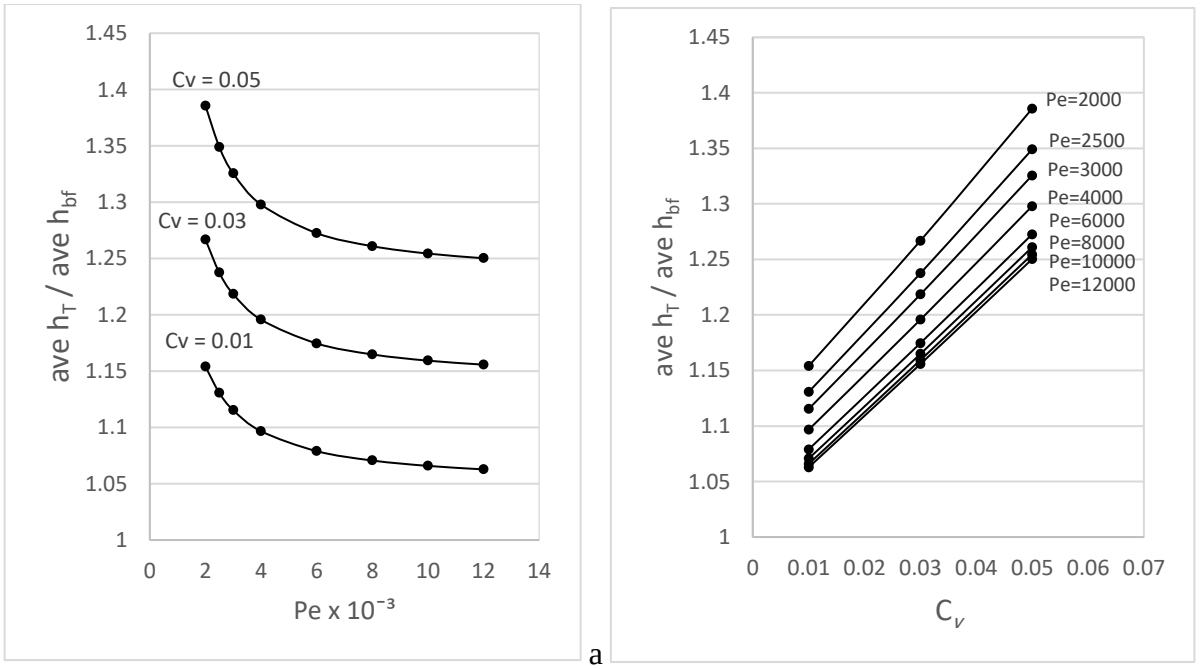


Figure 5.2. The ratio of average heat transfer coefficient between two-component non-homogeneous model and base fluid, for different values of inlet nanoparticle volume fractions (a) and Pe numbers (b).

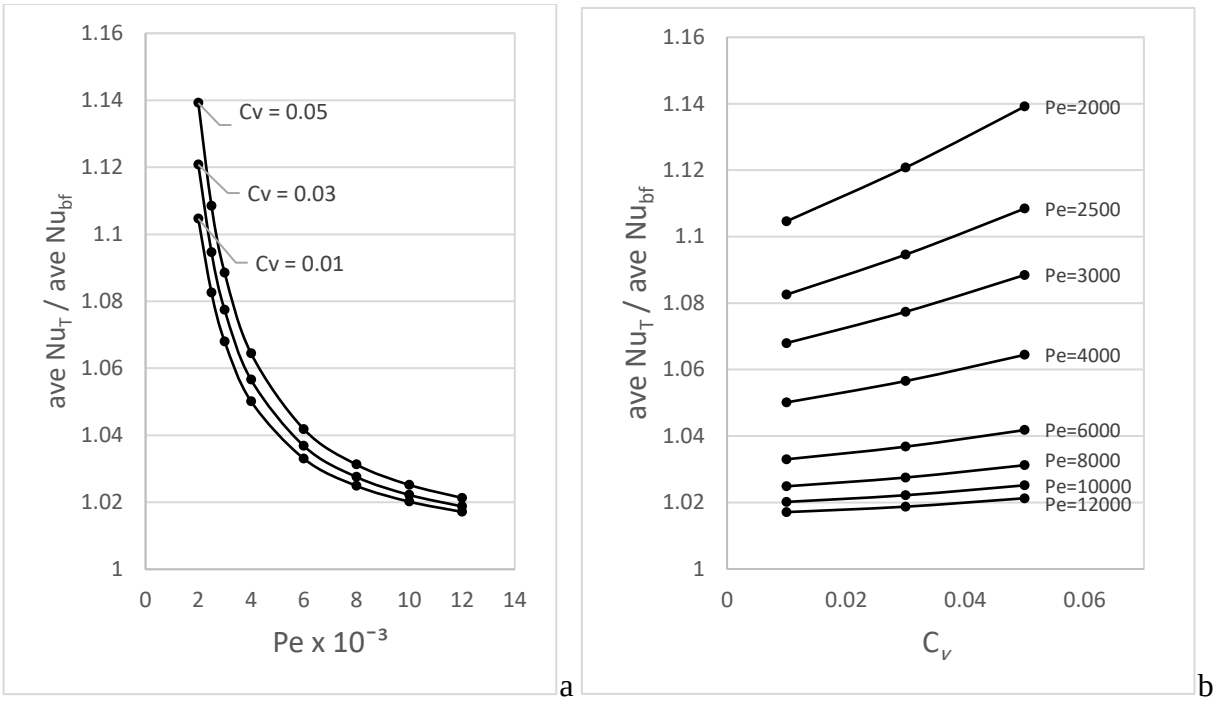


Figure 5.3. The ratio of average Nusselt number between two-component non-homogeneous model and base fluid, for different values of inlet nanoparticle volume fraction (a) and Pe numbers (b).

### 5.1.2. Effect of Thermophoresis Strength on Alumina-Water Nanofluid

Local heat transfer coefficient and Nusselt number results are shown in Figure 5.4 and Figure 5.6 for Pe=2500 and $T_0$=293.15K. Average heat transfer coefficient and average Nusselt number are shown in Figure 5.5 and Figure 5.7 for $2000 \leq \mathrm{Pe} \leq 12000$ for different α proportionality coefficient values. The results show higher heat transfer coefficient and Nusselt number at higher α values. Increasing α intensifies thermophoresis effect leading to higher particle migration from the walls to the central region of tube and heat transfer augmentation. The deviation of results gets larger at higher particle concentrations and lower Pe numbers.

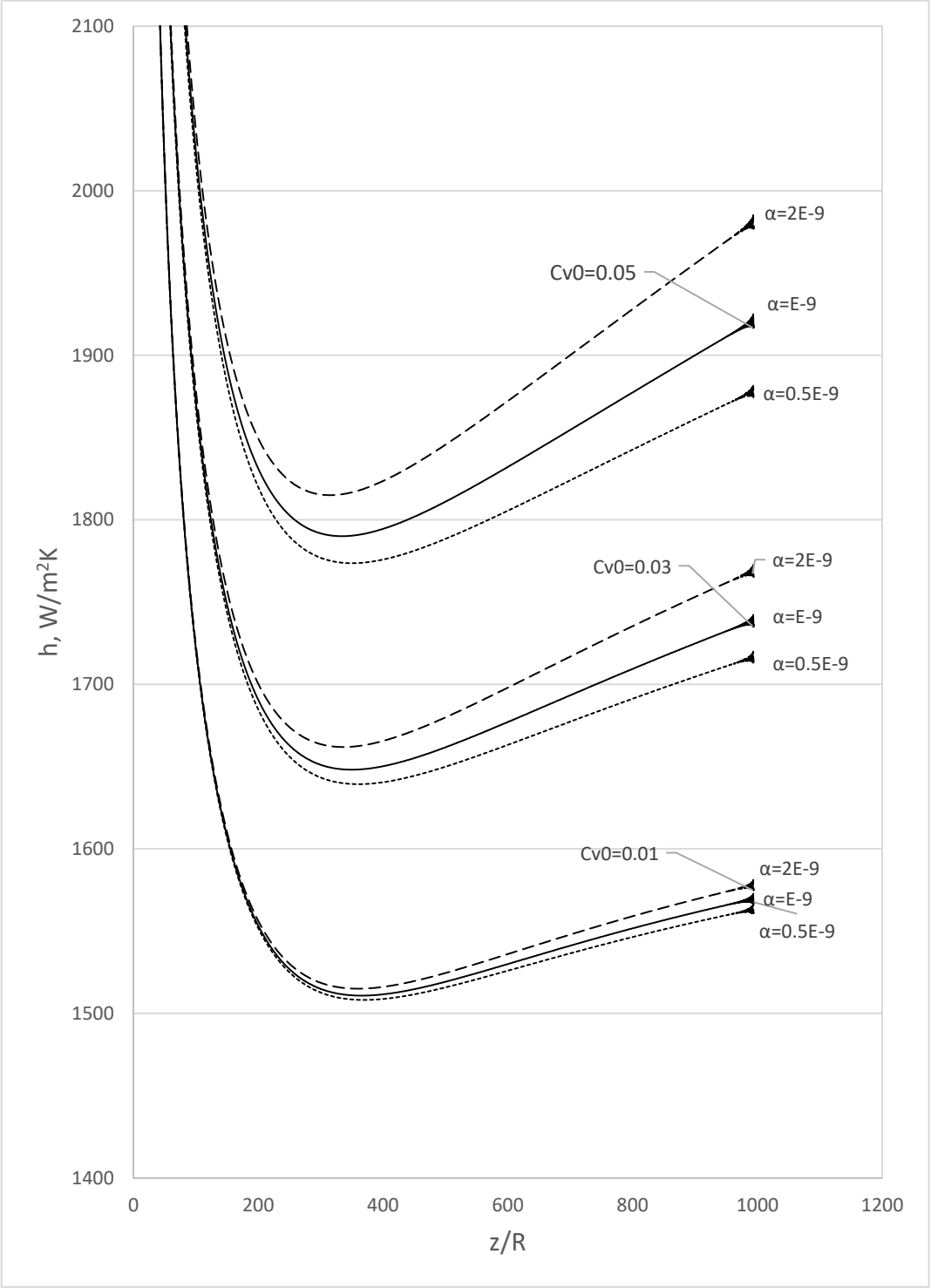


Figure 5.4. Local heat transfer coefficient in the heated section with different particle concentration and α values for Pe=2500 and $T_0$=293.15K.

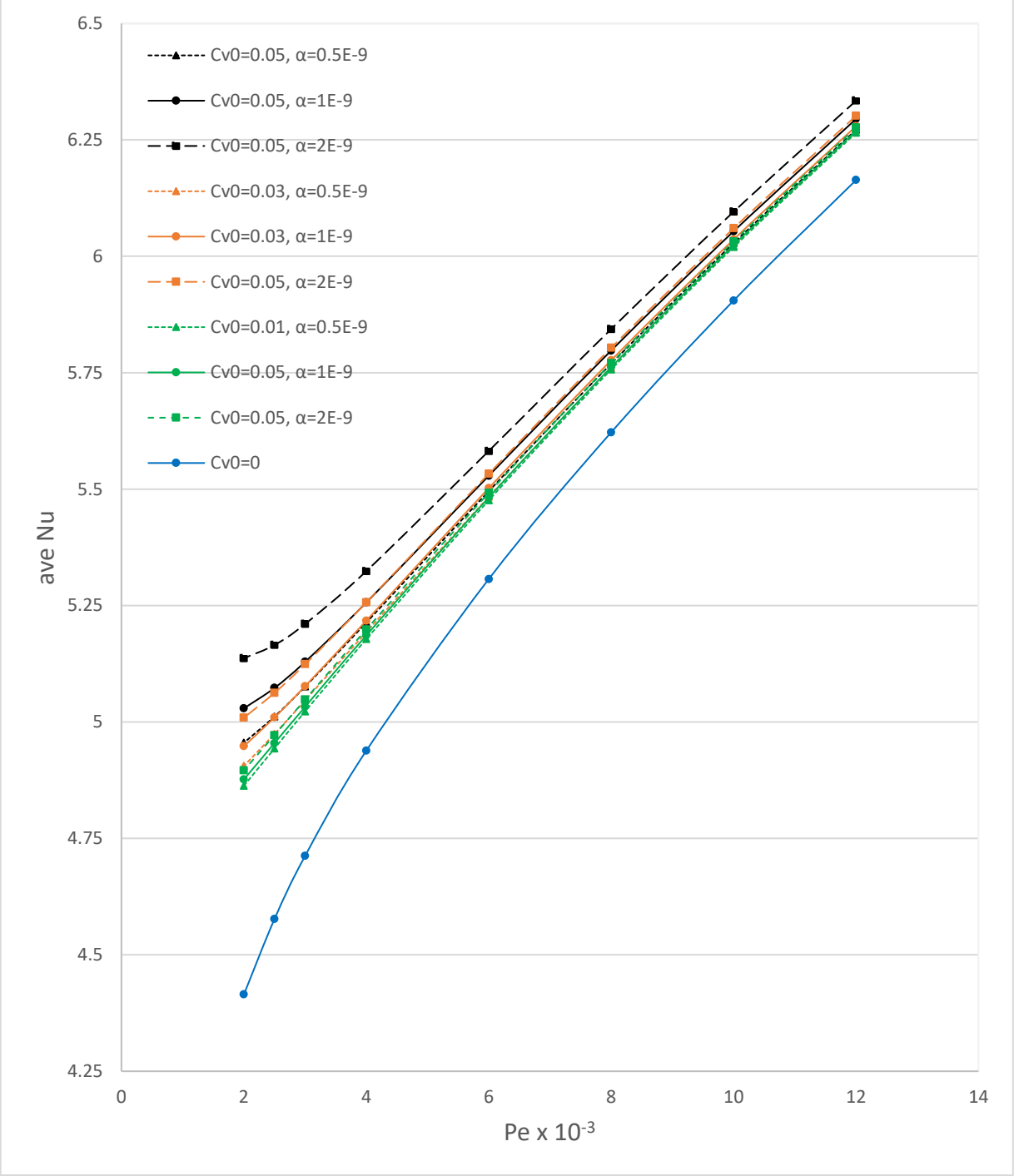


Figure 5.5. Average heat transfer coefficient dependence on Pe number and α in heated section with different particle concentration and $T_0$=293.15K.

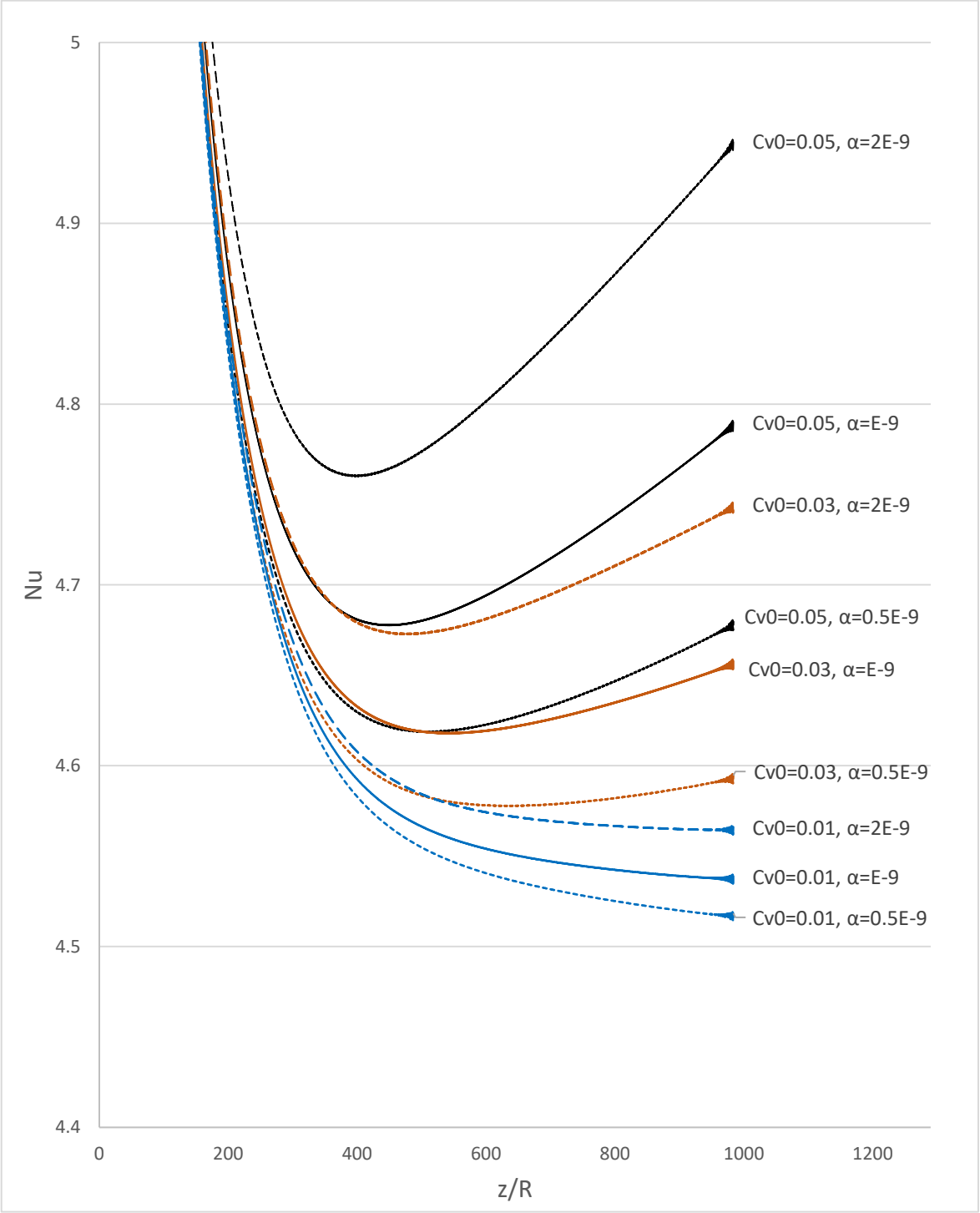


Figure 5.6. Local Nusselt number in heated section with different particle concentration and α values for Pe=2500 and $T_0$=293.15K.

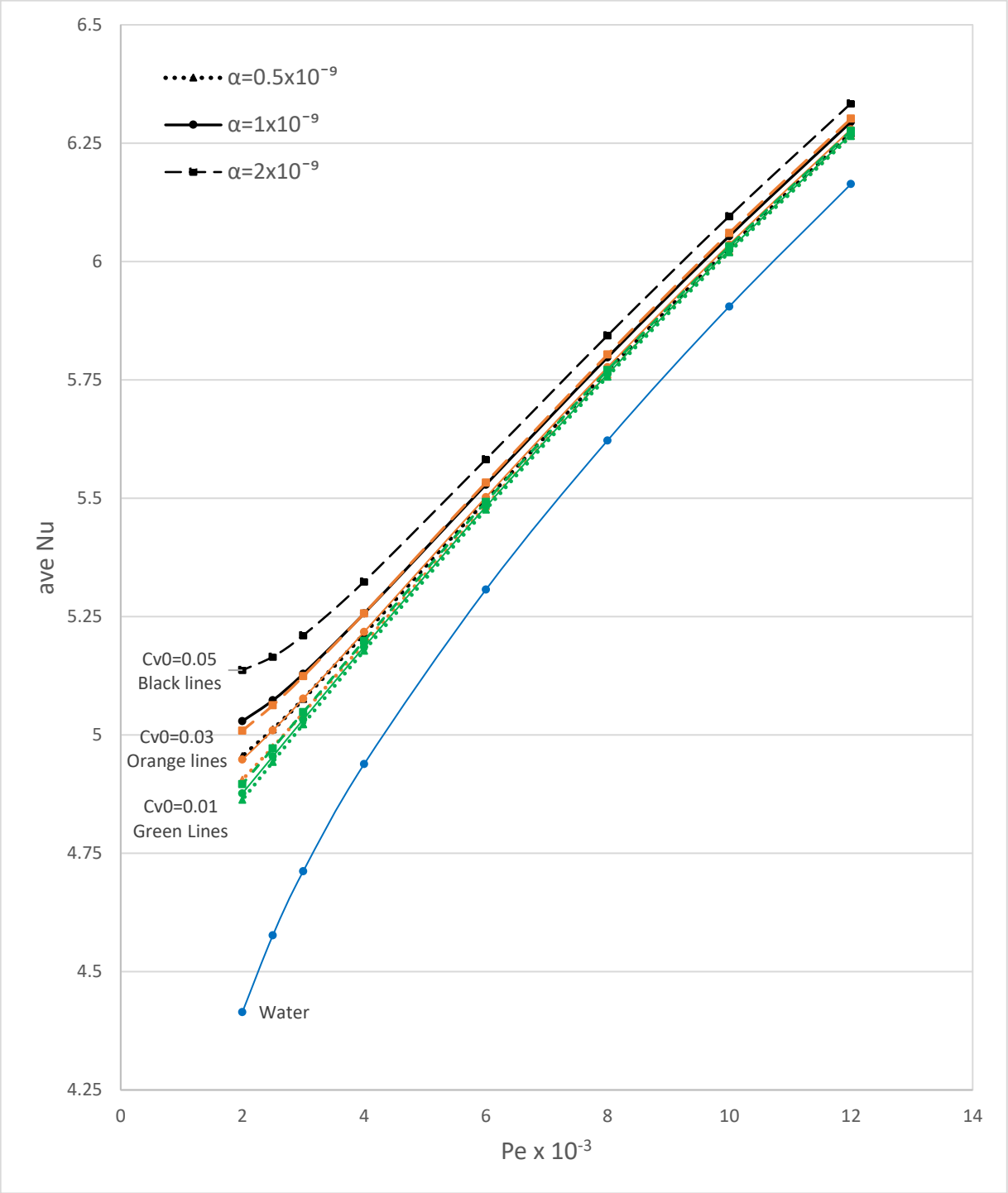


Figure 5.7. Average Nusselt number dependence on Pe number and α in heated section with different particle concentration and $T_0$=293.15K.

### 5.1.3. Alumina-Water Nanofluid Non-Homogeneous Two-Component and Single Phase Homogeneous Flow Subjected To Constant Wall Temperature

In this section, the flow and heat transfer of alumina-water nanofluid studied in is shortly reproduced for the case with wall boundaries subjected to constant temperature (T=310K) in the first half of channel. Figure 5.8 shows the temperature profiles in radial and axial directions. Temperature increases in axial direction and temperature gradient decreases in radial direction passing through the channel.

Particle migration is visible in Figure 5.9 in axial and radial directions. At the inlet of channel the temperature gradient is high (see Figure 5.8). Due to the thermophoresis effect, the particles move from walls to the center of channel and particle concentration drastically drops near the walls, leading to higher velocity in the vicinity of walls and decrease in friction factor, which is in favor of heat transfer augmentation.

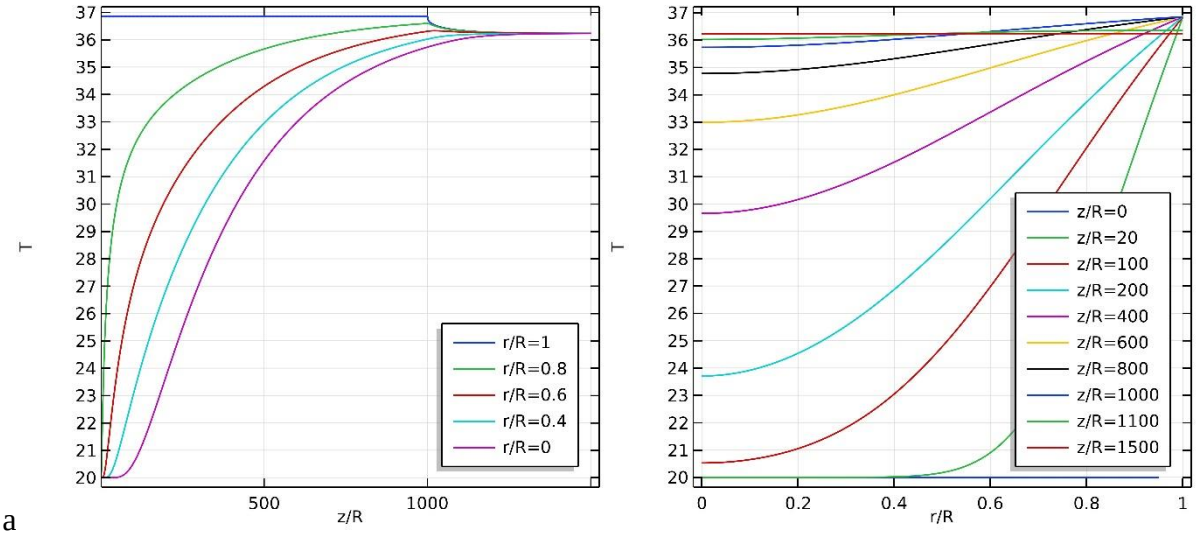


a b

Figure 5.8. Temperature profiles for sections in axial (a) and radial (b) directions of circular channel subjected to constant 310K wall temperature for $C_{v_0}$=0.05, Pe=2500.

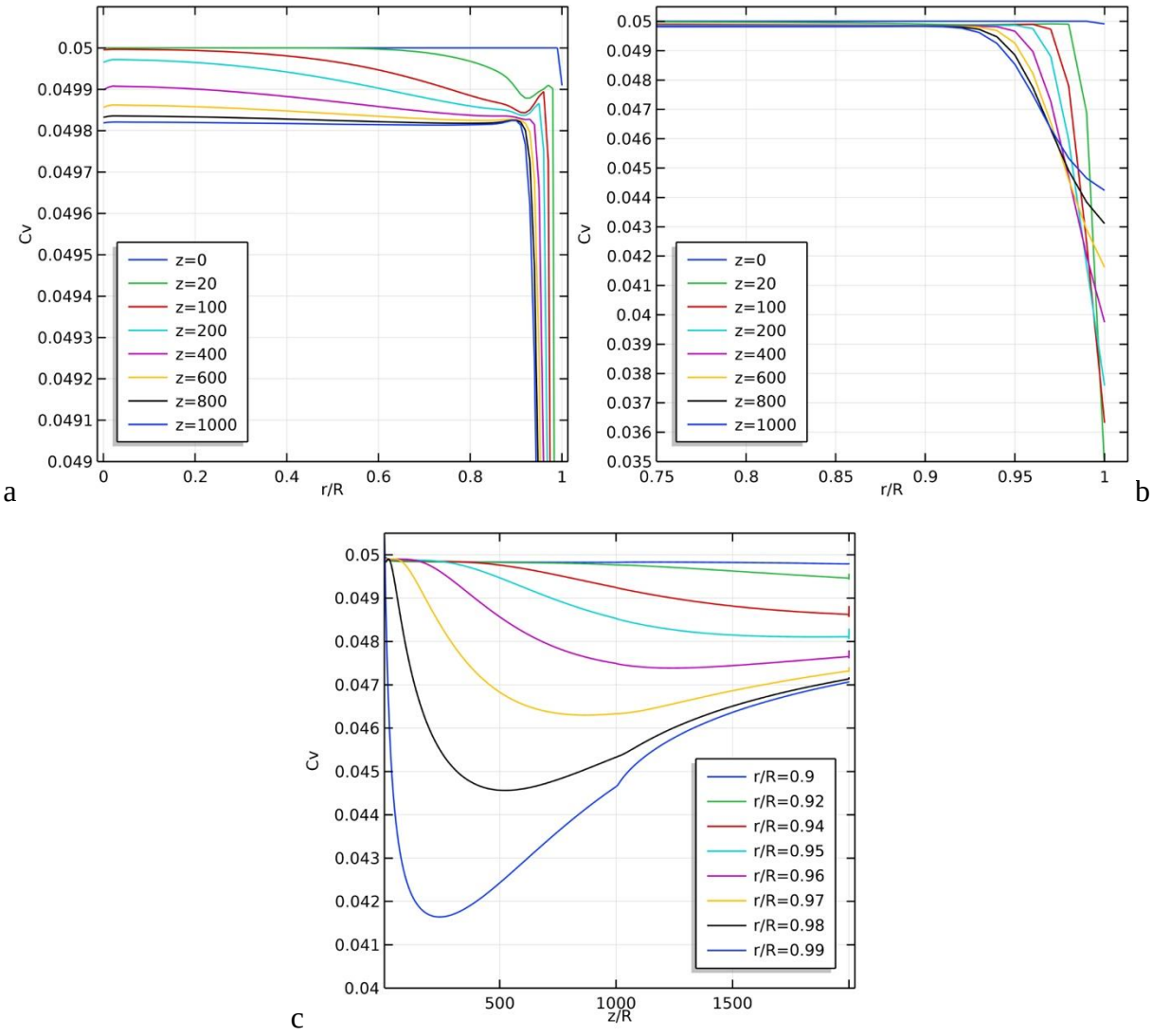


Figure 5.9. Particle concentration profiles in the sections of axial (a, b) and radial (c) directions of circular channel subjected to constant 310K wall temperature for $C_{v_0}$=0.05, Pe=2500.

The thermophoresis effect at the inlet of pipe is larger as a result of higher temperature gradient (see Figure 5.8), consequently higher particle concentration drop is visible at locations near the inlet of channel. Particle concentration rises gradually after a significant drop at heated section (see Figure 5.9). The temperature gradient decreases passing through the channel,

reduces the thermophoresis effect and can gradually give rise to the particle concentration at the walls.

Figure 5.10 and Figure 5.11 present average heat transfer coefficient and average Nusselt number respectively, where both rise at higher Pe numbers and higher inlet particle concentrations. The results of single phase homogeneous modeling show lower values for average heat transfer coefficient and Nusselt number comparing to the non-homogeneous two-component ones which stem from the incapability of homogeneous model in predicting the particle migrations from the walls to the core region.

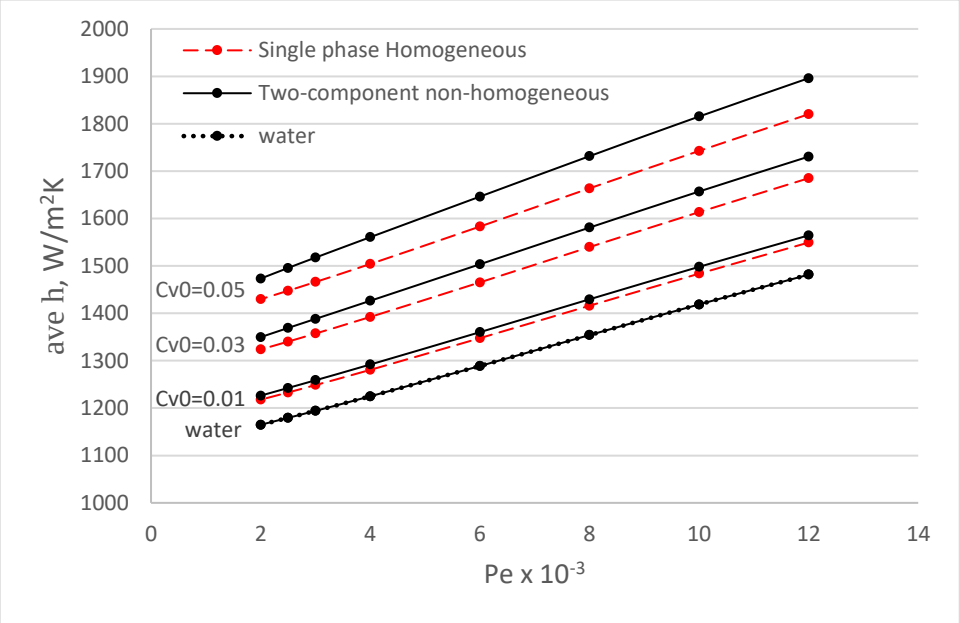


Figure 5.10. Dependence of average heat transfer coefficient results for non-homogeneous two-component, single phase homogeneous models and water on Pe number of nanofluid in a circular channel subjected to constant 310K wall temperature for $C_{v_0}$=0.05.

Heyhat and Kowsary [76] investigated flow and heat transfer of alumina-water within a circular channel subjected to constant wall temperature. They studied the effect of particle migration utilizing the Buongiorno model [55] considering the convection, Brownian motion

and thermophoresis terms. They observed non-uniform distribution of particles near the walls of pipe. They reported higher heat transfer coefficients, due to the particles move from walls toward the core region of channel, and increase in velocity and decrease in shear stress in the vicinity of walls. Results of both numerical studies on particle migration in a channel subjected to constant heat flux (see Section 4.1.2) and constant wall temperature show higher heat transfer rates for non-uniform particle distribution compared to homogenous ones.

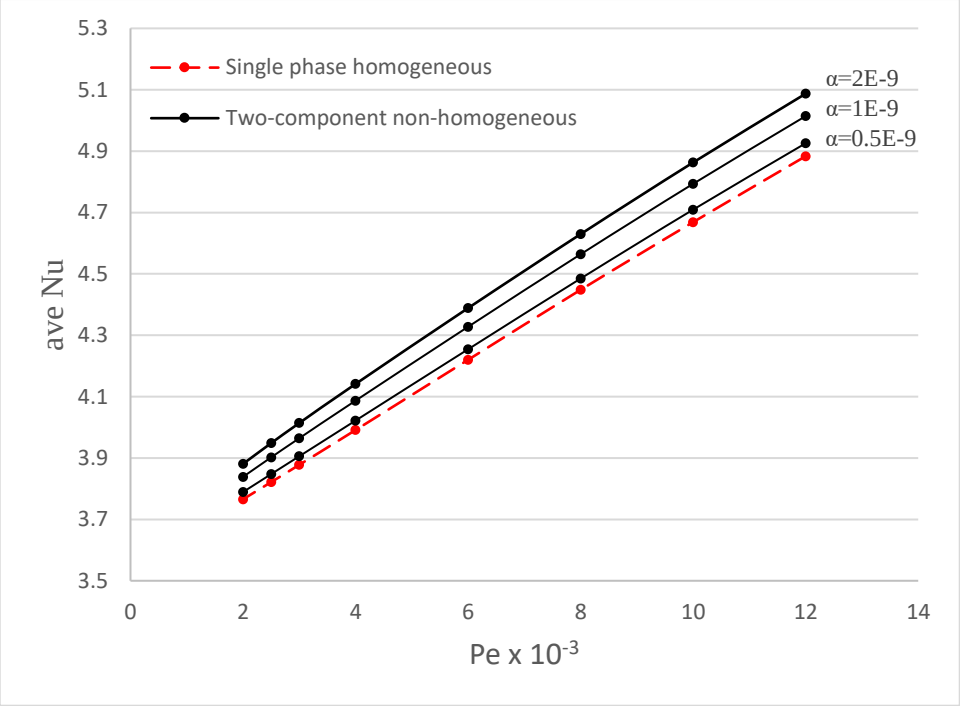


Figure 5.11. Dependence of average Nusselt number results for non-homogeneous two-component and single phase homogeneous models on Pe number of nanofluid in a circular channel subjected to constant 310K wall temperature for $C_{v_0}$=0.05.

## 5.2. Alumina-Water Flow and Heat Transfer with Properties Dependent on Particle Concentration, Size and Temperature

There have been numerous studies on the nanofluids. In numerical simulations of nanofluids flow, there have been various theoretical and numerical methods employed to obtain

the most accurate results to experimental data (see Section 1.6) [54]. Considering the pros and cons of each method [54] there is a growing body of literature in finding the most suitable method that gives the most reliable and realistic results compared to experimental results. There is still very little scientific understanding of nanofluids and their application, and performing more studies is fundamental.

In chapter 4 as test validation a two-component non-homogenous model, as well as a single phase homogeneous approach conducted on the alumina-water nanofluid flow. Convection, Brownian diffusion, and thermophoresis were taken as the key terms of nanoparticle transport equation of non-homogeneous modeling. There are many parameters affecting the terms in particle transport equation and behavior of the nanofluid flow such as temperature, particle concentration, particle size, and etc.

In the majority of studies on the nanofluid, properties have been taken as constant values, or independent on parameters that have proven significant effects. In this section, the models proposed by Masoumi *et al*. [29] for viscosity and Vajjha and Das [29] for thermal conductivity have been taken as the default models in the simulations to have more realistic predictions of these properties and study the effect of parameters affecting the nanofluid flow with a further focus on particle size.

### 5.2.1. Effect of Particle Size on Flow and Heat Transfer of Alumina-Water Nanofluid

The nature of thermophoresis effect and the parameters affecting it is still less clear. As discussed in Section 3.1.2.2. the McNab and Meisen [90] proposed model for thermophoresis coefficient has been the most used correlation in numerical studies available in the literature. Despite the importance of their model and works, there still remains a paucity of understanding of the parameters affecting the thermophoresis. Considering the cons in this model, and the model proposed by Ryzhkov and Minakov [68] has prompted this research to devote a section

to study the comparison of results obtained by utilizing the aforementioned thermophoresis coefficients and the parameters affecting them.

Figure 5.12 shows the particles size effect on the local heat transfer coefficient for $C_{v_0}$=0.05 and Pe=2500 with different thermophoresis coefficients. The heat transfer coefficient increases by decreasing the particle size. Decreasing the particle size increases the heat transfer area leading to more heat transfer. The Ryzhkov and Minakov thermophoresis coefficient [68] (black solid lines) shows higher values compared to McNab and Meisen thermophoresis coefficient [90] (red dashed lines). The homogeneous case results (green dotted lines) are identical for both thermophoresis coefficients. Considering the difference between two thermophoresis coefficients and parameters affecting as discussed in Section 3.1.2, the Ryzhkov and Minakov thermophoresis coefficient [68] shows increasing thermophoresis effect with temperature increase of flow passing throw the channel where the McNab and Meisen model [90] shows vice versa results. The increase in thermophoresis effect results higher migration of particles from wall boundaries to center of the channel, leading to decrease in viscosity and increase in velocity near walls and higher heat transfer.

Figure 5.13 demonstrates particle size effect on average heat transfer coefficient for $C_{v_0}$=0.05 and Pe=2500 and different thermophoresis coefficients. Black solid lines are Ryzhkov and Minakov thermophoresis coefficient [68] in non-homogeneous two-component model. Red Dashed lines are McNab and Meisen thermophoresis coefficient [90] in non-homogeneous two-component model and green dotted lines are single phase homogeneous model. Where the main difference is in the range of low Pe numbers. In range of low Pe numbers, the average heat transfer coefficient shows a minimum value. The observed decrease, could be attributed to the rather high temperature difference at inlet and outlet, leading to significant change in nanofluid thermophysical properties in axial and radial directions.

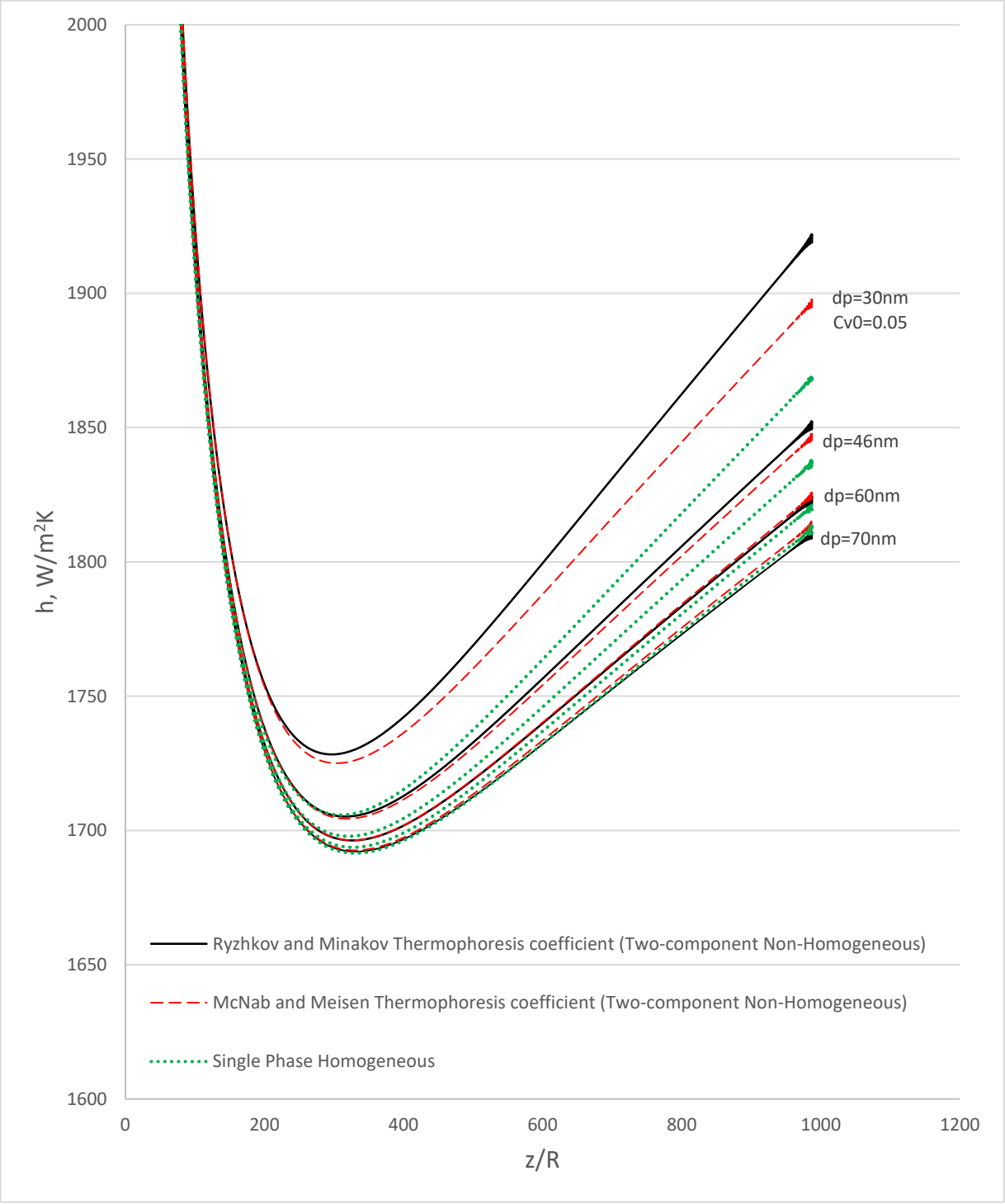


Figure 5.12. Particles size effect on local heat transfer coefficient for $C_{v_0}$=0.05, $T_0$=300K, Pe=2500 and different thermophoresis coefficients.

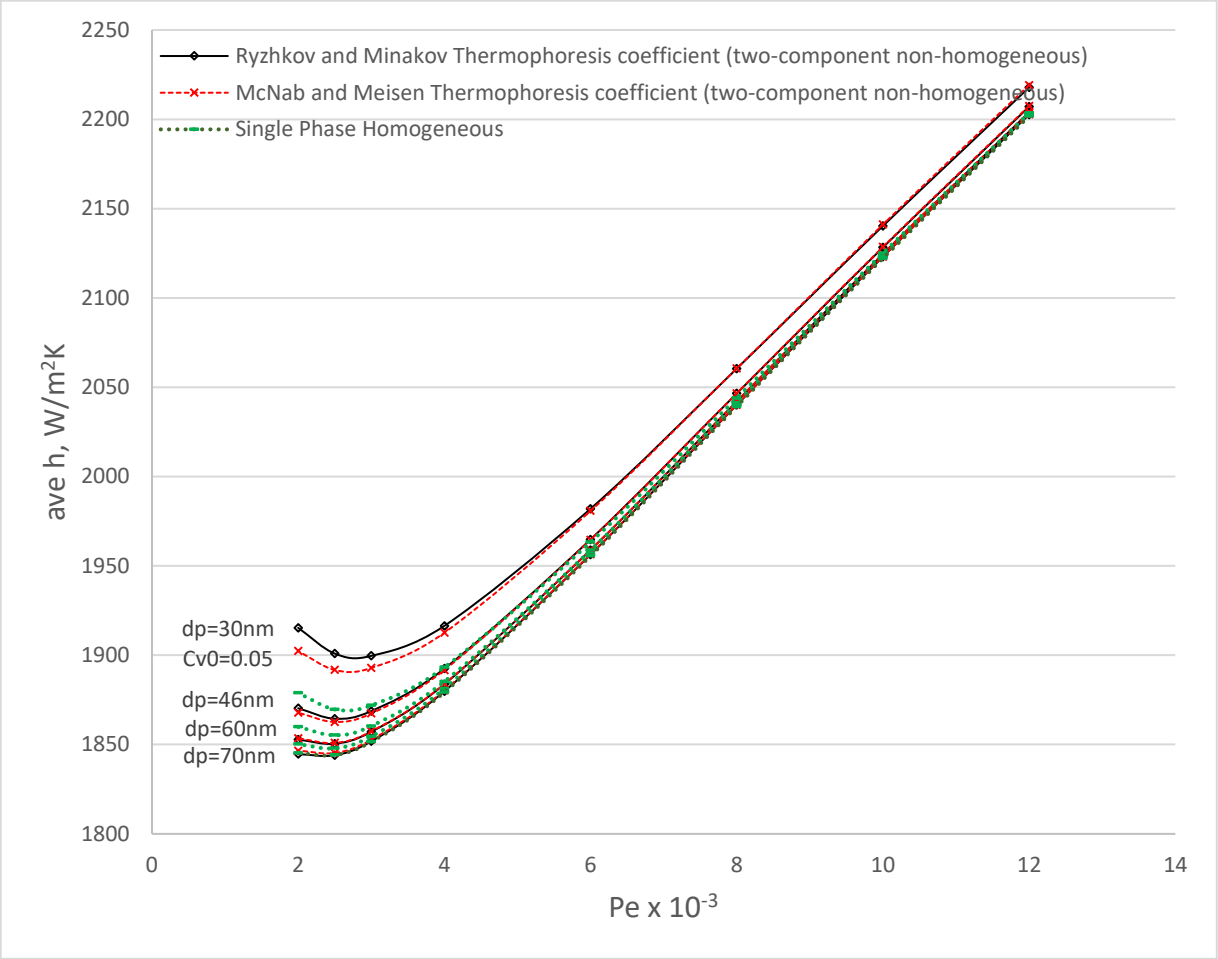


Figure 5.13. Particles size effect on average heat transfer coefficient for $C_{v_0}$=0.05, $T_0$=300K, at different Pe numbers and thermophoresis coefficients.

Figure 5.14 shows the ratio of calculated average heat transfer coefficients results on the basis of non-homogeneous two-component ($h_T$) and Single Phase Homogeneous ($h_H$) models, for $C_{v_0}$=0.05, Pe=2500 and different thermophoresis coefficients. The results show higher heat transfer coefficient values for finer particle size. Considering both thermophoresis coefficients independent of particle size, the difference is due to the change in thermophysical properties of nanofluid passing through the channel. In addition, the increase in ratio with decreasing the Pe number is a consequence of higher temperature increase with lowering the Pe number. This leads to higher thermophoresis effect. Consequently, the particles migration from wall

boundaries to center of the channel is higher. As a result, velocity increase near walls is higher because of higher viscosity and thermal conductivity decrease in wall boundaries.

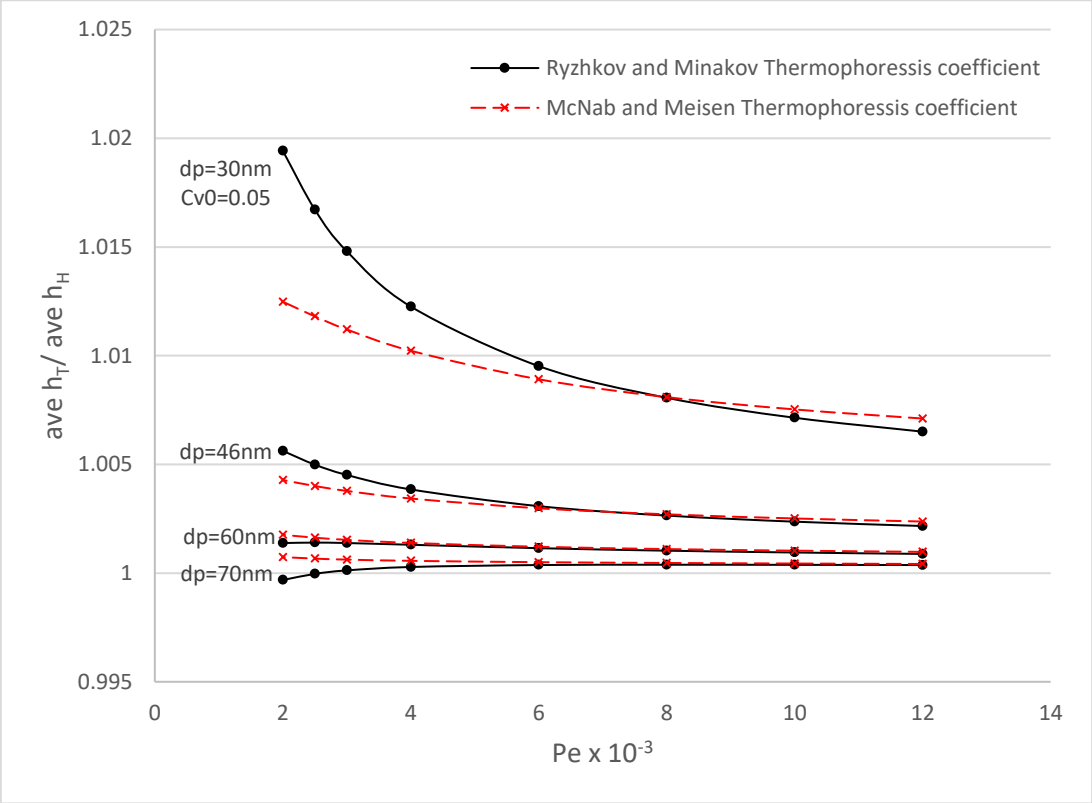


Figure 5.14. The dependence of average heat transfer coefficients ratio for calculated results with non-homogeneous two-component ($h_T$) and single phase homogeneous ($h_H$) models on Pe number, for $C_{v_0}$=0.05, $T_0$=300K, and different thermophoresis coefficients.

Figure 5.15 represents the ratio of average heat transfer coefficient results for non-homogeneous and homogeneous models, and base fluid water for various Pe numbers and particle sizes for $C_{v_0}$=0.05, $T_0$=300K. Decreasing the particle size leads to higher heat transfer coefficients. The homogeneous model highly underestimates the average heat transfer coefficient compared to non-homogeneous model. The results applying Ryzhkov and Minakov thermophoresis coefficient [68] compared to McNab and Meisen coefficient [90] shows slightly higher values.

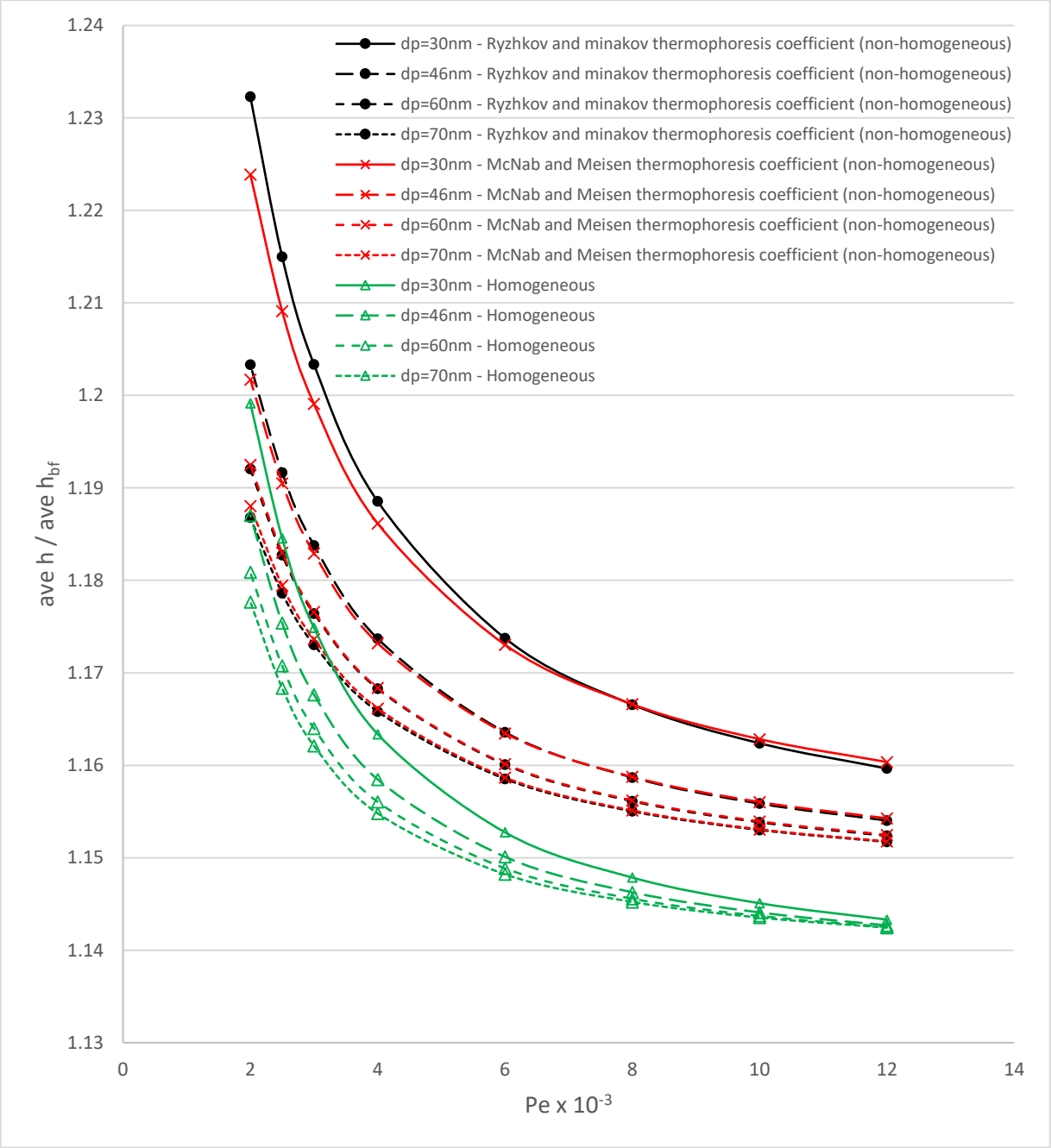


Figure 5.15. The ratio of average heat transfer coefficient results for non-homogeneous and homogeneous models, and base fluid water for various Pe numbers and particle sizes for $C_{v_0}$=0.05, $T_0$=300K.

Having same approach as heat transfer coefficient results, the local Nusselt number demonstrates similar behavior and higher values for smaller particle sizes. Figure 5.16 shows the particles size effect on local Nusselt number for $C_{v_0}$=0.05, $T_0$=300K, Pe=2500 with different thermophoresis coefficients. The dependence of average Nusselt number on Pe number is demonstrated in Figure 5.17 Where the Ryzhkov and Minakov thermophoresis coefficient [68] shows higher values compared to McNab and Meisen [90]. The homogeneous case results are identical for both thermophoresis coefficients and highly underestimated the calculated Nusselt number for different Pe number, particle concentration and sizes compared to non-homogeneous two-component ones. The difference between results becomes larger with decreasing Pe number and particle size. Homogeneous modeling underestimates the experimental results in comparison with non-homogeneous modeling due to the utilized thermophysical properties models of nanofluid and lack of capability to take into account most of the affecting terms and parameters.

The average Nusselt numbers ratio of non-homogeneous two-component and single phase homogeneous decreases with increasing the Pe number (see Figure 5.19). Figure 5.19 shows the dependence of Nusselt number ratio to Pe number in the case with $C_{v_0}$=0.05 with a glance to the effect of particle size and different thermophoresis coefficients. Decreasing particle sizes increases the ratio, and the difference between the results obtained by Ryzhkov and Minakov [68], and McNab and Meisen thermophoresis coefficients [90] becomes larger with lowering the Pe number, where in high Pe values the results are rather close. The difference is due to the definition of thermophoresis coefficients proposed by both models and the predicted particle migration near walls of the tube with lowering the Pe number. Lowering the Pe number causes higher temperature difference between inlet and outlet and the Ryzhkov and Minakov model [68] predicts higher thermophoresis effect and particle migration to tube center in high temperatures. This higher particle migration lowers the viscosity and increases the velocity in wall boundaries which leads to higher heat transfer.

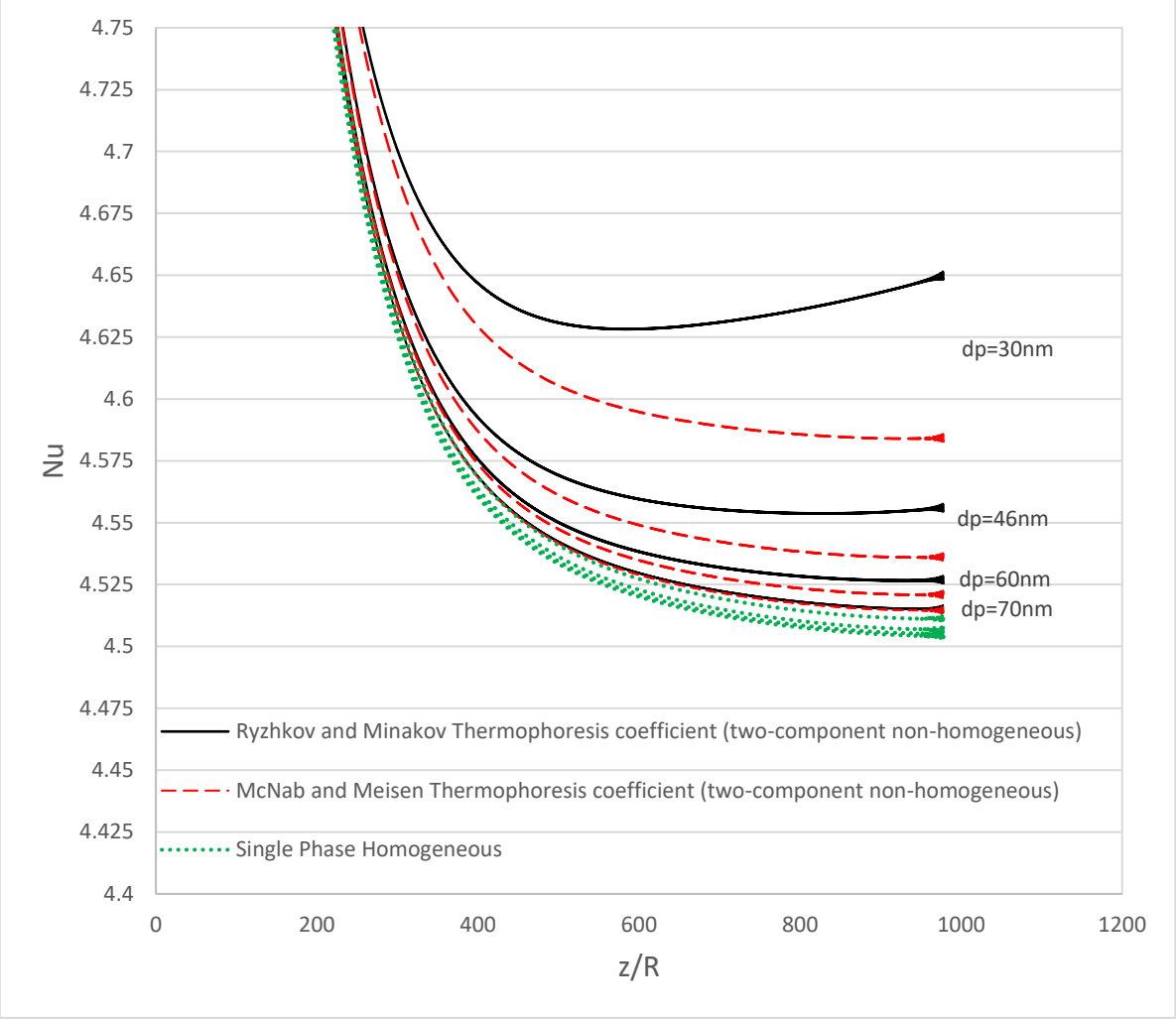


Figure 5.16. Particles size effect on local Nu number for $C_{v_0}$=0.05, $T_0$=300K, Pe=2500 and different thermophoresis coefficients.

Figure 5.18 represents the ratio of Nusselt number results for non-homogeneous and homogeneous models, and base fluid water for various particle sizes and Pe numbers for $C_{v_0}$=0.05, $T_0$=300K. The homogeneous model highly underestimates the average heat transfer coefficient compared to non-homogeneous model. Decreasing the particle size leads to higher heat transfer coefficients. In addition, the results applying Ryzhkov and Minakov thermophoresis coefficient [68] compared to McNab and Meisen coefficient [90] shows slightly higher values.

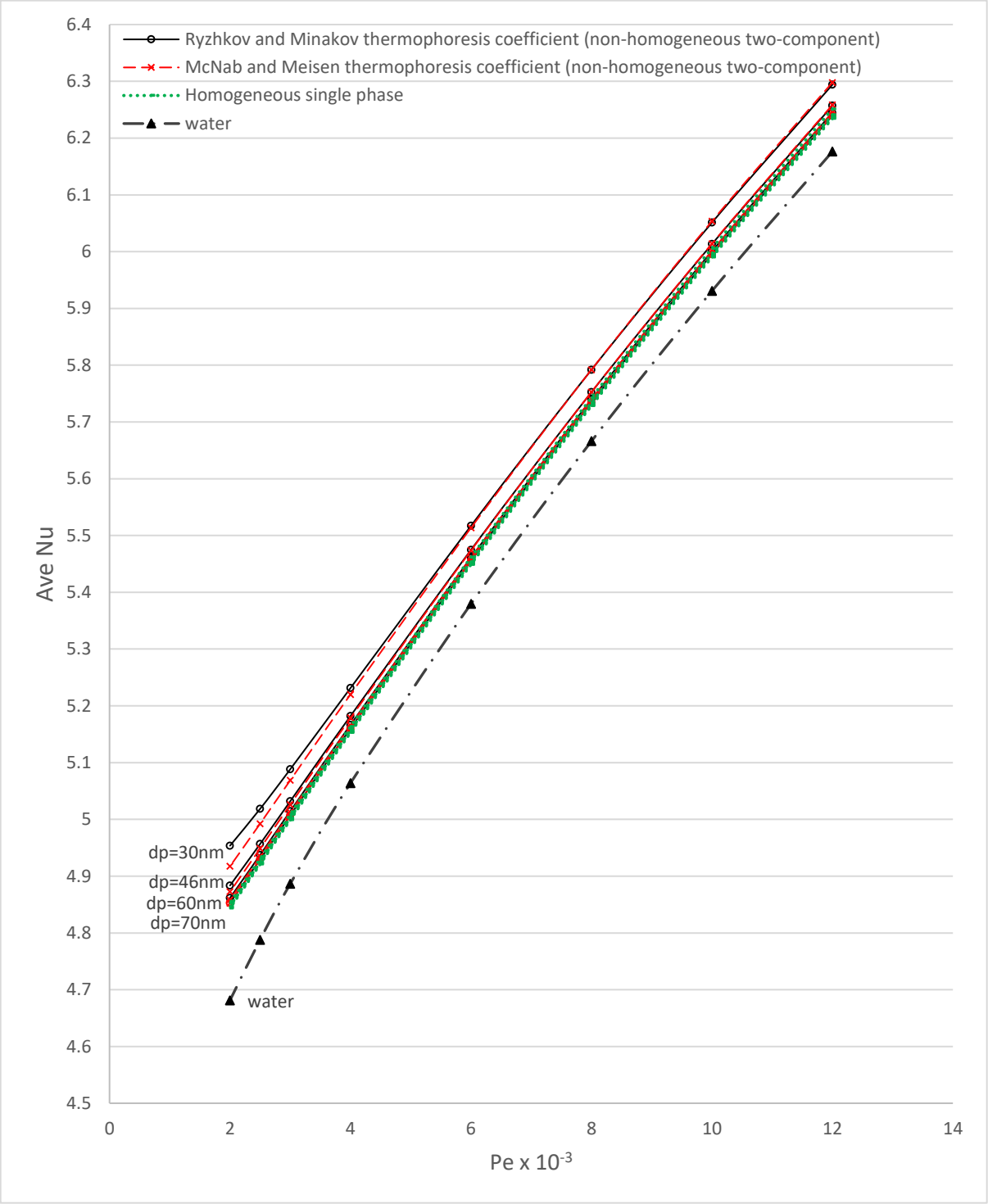


Figure 5.17. Particles size effect on average Nusselt number for $C_{v_0}$=0.05, $T_0$=300K, and different thermophoresis coefficients at different Pe numbers.

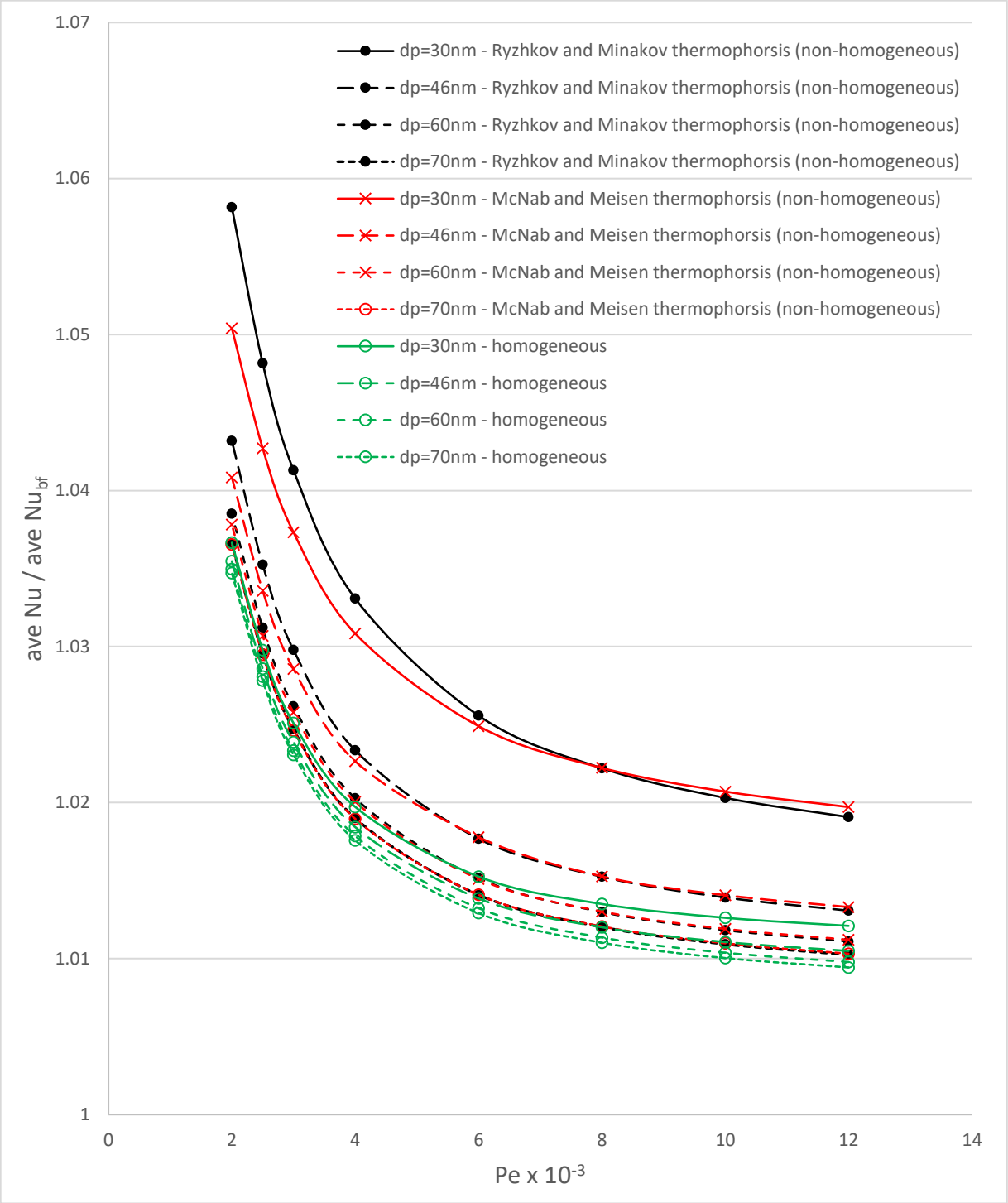


Figure 5.18. The ratio of average Nusselt numbers of results for non-homogeneous and homogeneous models, and base fluid water for various Pe numbers and particle sizes for $C_{v_0}$=0.05, $T_0$=300K.

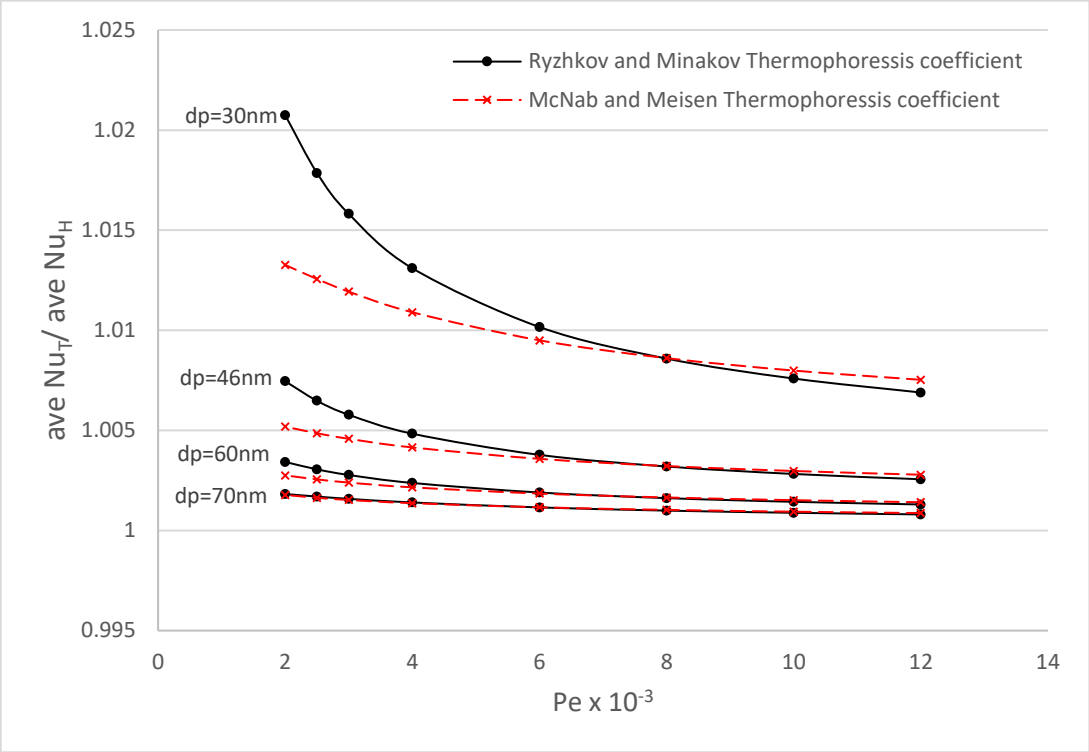


Figure 5.19. The dependence of average Nu number ratio calculated results with non-homogeneous two-component ($h_T$) and Single Phase Homogeneous ($h_H$) models to Pe number. for $C_{v_0}$=0.05, $T_0$=300K, and different thermophoresis coefficients.

The wall shear stress is presented in Figure 5.20 in the length of channel heated section. Viscosity decreases with temperature increase passing through the channel, and reduction of particles, receding from the walls. Accordingly, the wall shear stress decreases in axial direction. The results obtained with both thermophoresis models are rather close, although results with Ryzhkov and Minakov model [68] is slightly lower, due to higher particle migration from walls predicted by the model. The results show higher shear stress in homogeneous model, where is caused by incapability of model in taking account the particle reduction near walls. Increasing the particle size reduces the viscosity and reduces the wall shear stress (see Figure 5.7). The friction factor in channel axial direction is presented in Figure 5.21 for $C_{v_0}$=0.05 and Pe=2500.

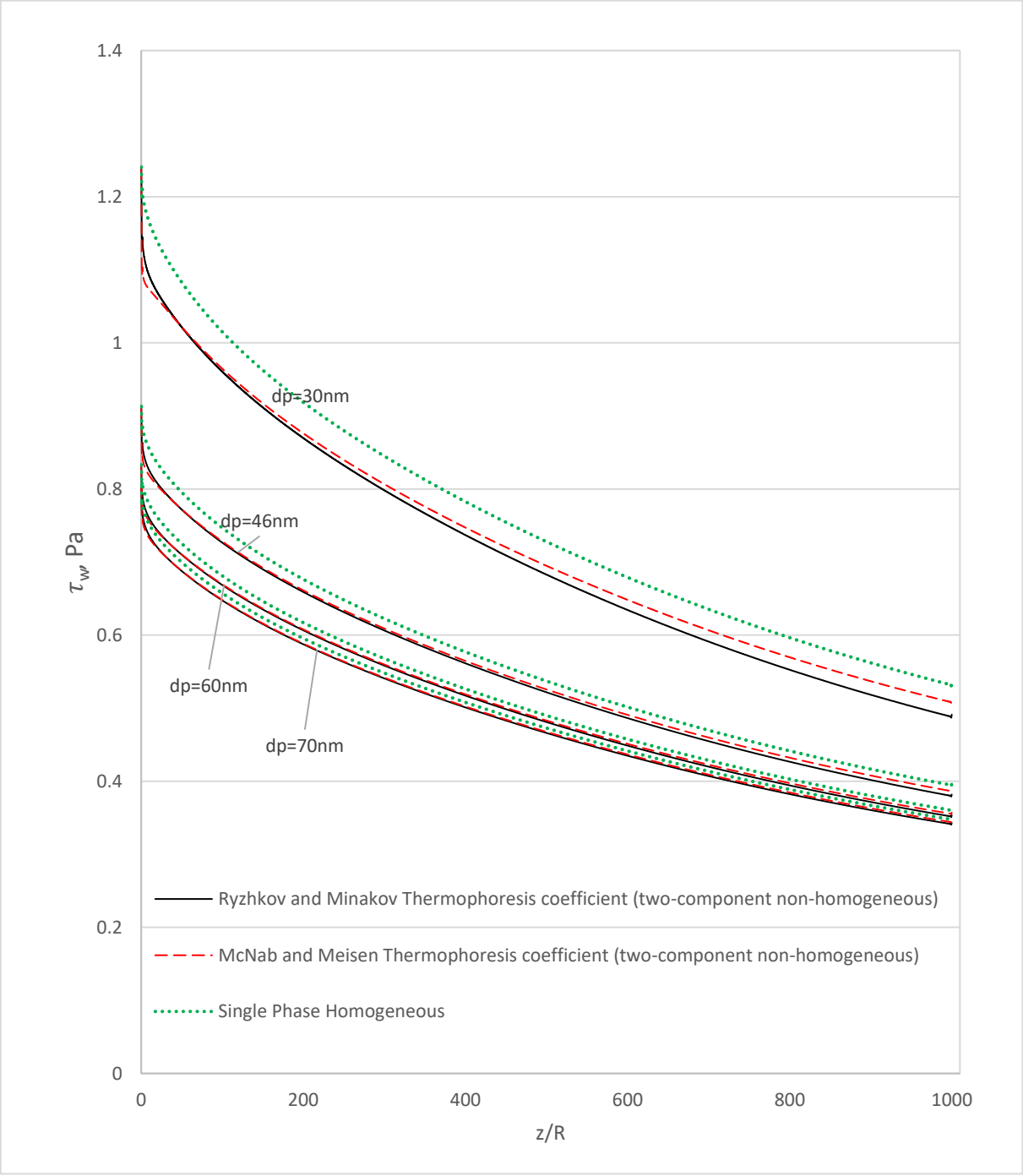


Figure 5.20. The wall shear stress results with different particle sizes, for $C_{v_0}$=0.05, $T_0$=300K, Pe=2500 and different thermophoresis coefficients.

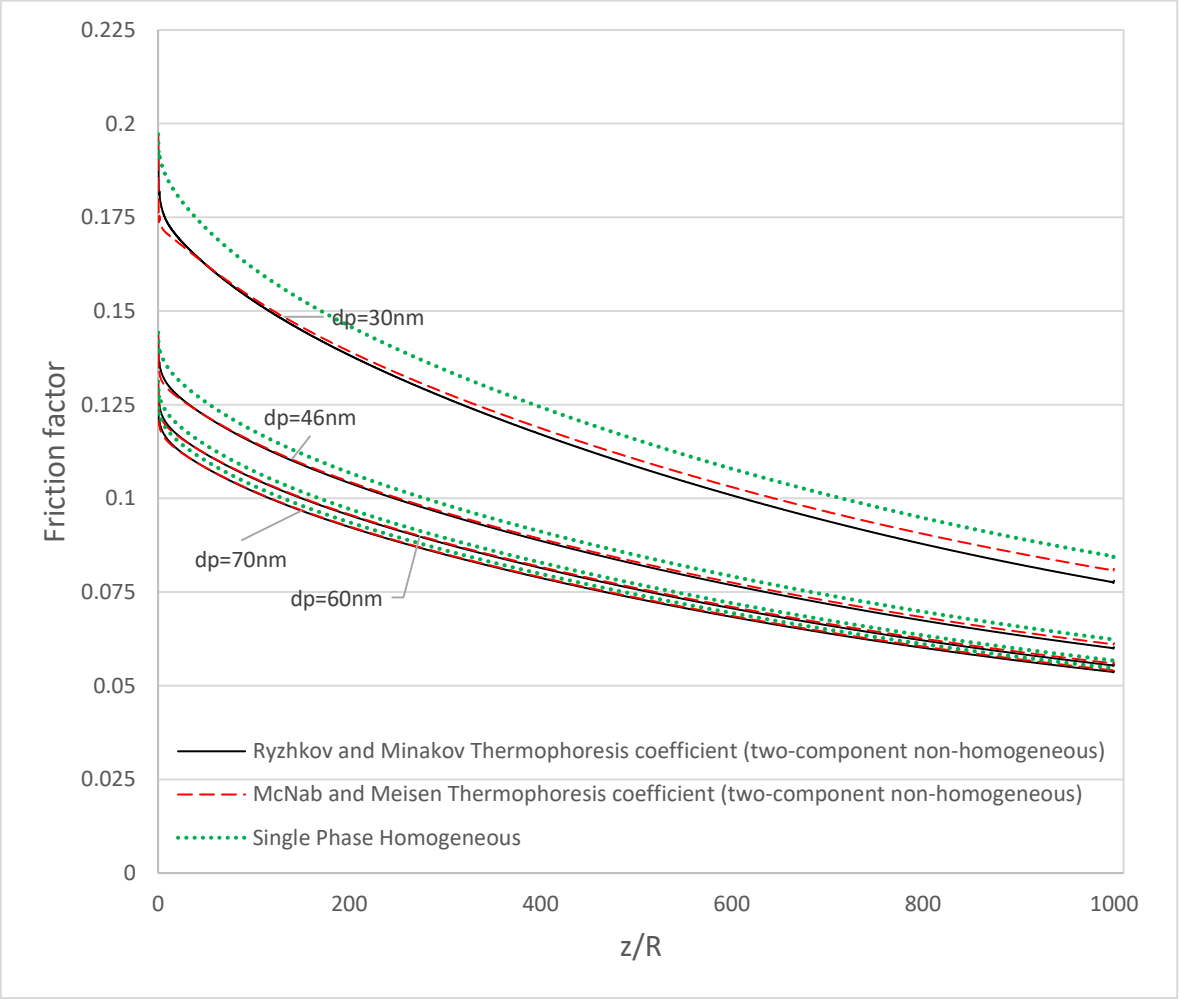


Figure 5.21. The local friction factor results with different particle sizes, for $C_{v_0}$=0.05, $T_0$=300K, Pe=2500 and different thermophoresis coefficients.

The dependence of average friction factor to Pe number for $C_{v_0}$=0.05 is presented in Figure 5.22 with different particle sizes, and the thermophoresis coefficients proposed by Ryzhkov and Minakov [68] and McNab and Meisen [90]. The average friction factor reduces with increasing the Pe number. It is important to note that calculating the average friction factor with shear stress (see Equation 3.25) and pressure drop (see Equation 3.26) produces same results.

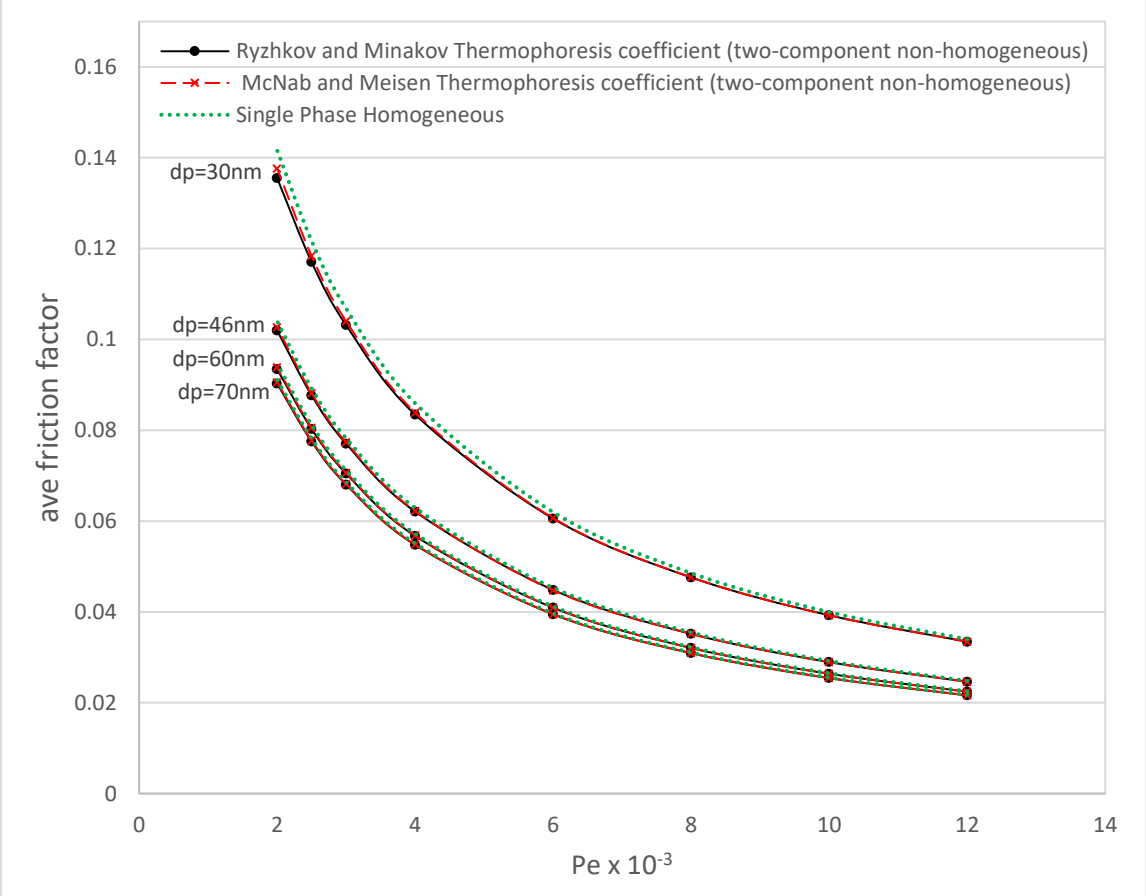


Figure 5.22. The dependence of average friction factor results on Pe number for $C_{v_0}$=0.05, $T_0$=300K, with different particle sizes, and different thermophoresis coefficients.

The dependence of PEC (performance evaluation criteria, Equation 3.27a) to Pe number with different particle sizes and both thermophoresis coefficients, for $C_{v_0}$=0.05 is represented in Figure 5.23. It can be concluded that in numerical studies, non-homogeneous modeling shows higher improvement in heat transfer with adding alumina nanoparticles to water compared to homogeneous modeling. It can also be concluded that PEC value increases with reducing the Pe number, and decreasing the particle size in fixed Pe numbers. In addition, applying the Ryzhkov and Minakov [68] thermophoresis coefficient in non-homogeneous modeling demonstrates higher PEC value compared to McNab and Meisen [90] thermophoresis coefficient.

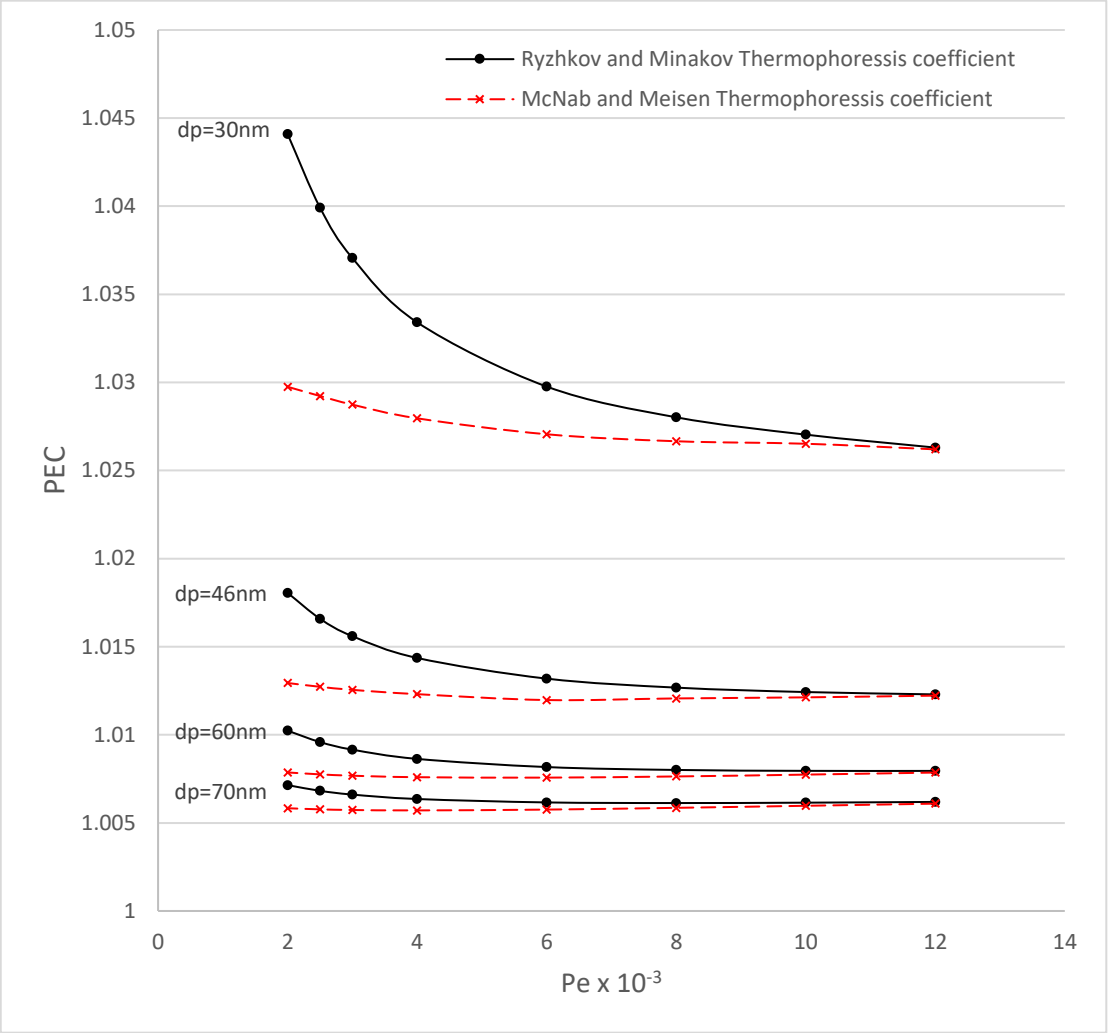


Figure 5.23. The dependence of PEC (performance evaluation criteria) on Pe number with different particle sizes, for $C_{v_0}$=0.05, $T_0$=300K, and different thermophoresis coefficients.

Figure 5.24 represents the increase in pressure drop of nanofluid with rising the Pe number and reducing particle sizes in Figure 5.24a and Figure 5.24b respectively. Decreasing particles size and increasing the particle concentration rises the nanofluid viscosity and causes higher pressure drop. The results of non-homogenous two-component model show a slightly higher pressure drop compared to homogeneous model, the particle concentration drop near walls leads to decrease in viscosity and increase in velocity.

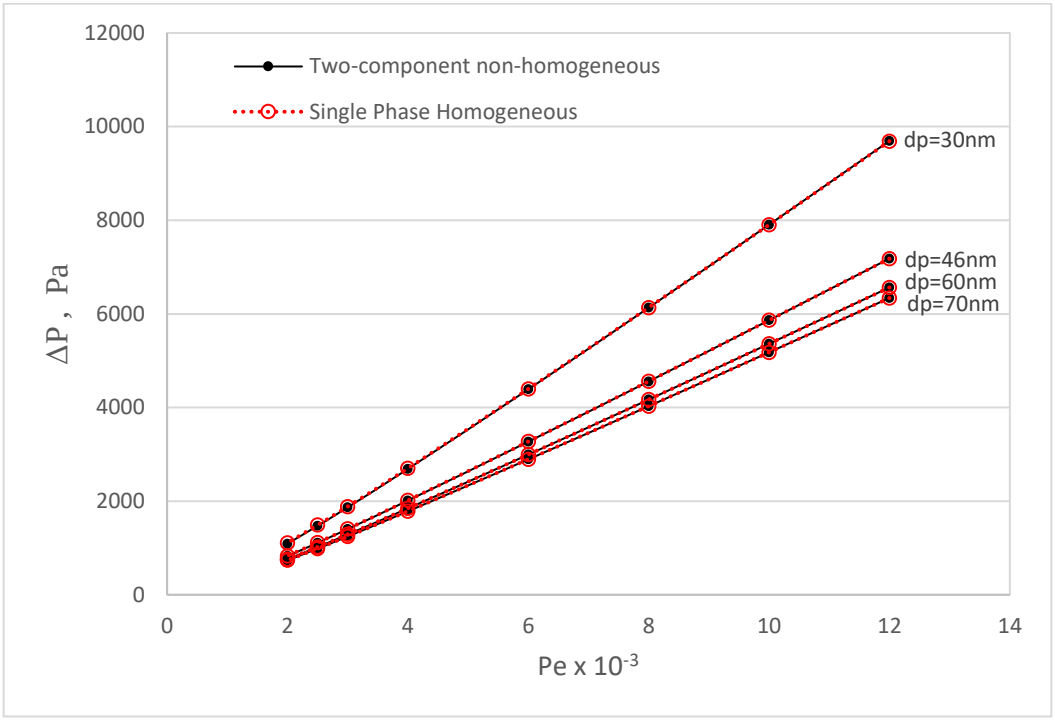


a

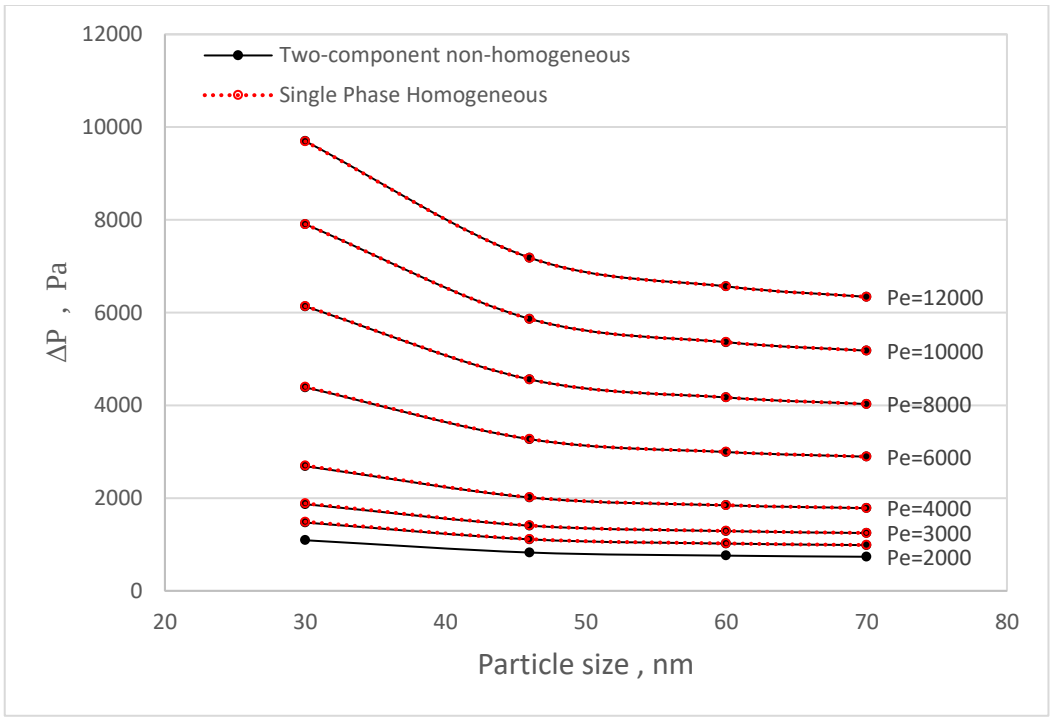


b

Figure 5.24. The dependence of pressure drop to Pe number (a) and different particle sizes (b) for $C_{v_0}$=0.05, $T_0$=300K

The ratio of non-homogeneous and homogeneous modeling pressure drops with respect to Pe number is plotted in Figure 5.25 for $C_{v_0} = 0.05$. The ratio increases with rising the Pe number, however the slop is higher with in low Pe nmbers. Despite of Non-homogeneous modeling, the homogeneous model is incapable of predictiong the particle migration. With increasing the Pe number the temperature difference between inlet and outlet is lower. There for the thermophoresis effect and particle migration becomes smaller. Consequently, with increasing the Pe number the non-homogeneous and homogeneous pressure drops come closeer and the pressure drops ratio rises.

Decreasing nanoparticle size increases the viscosity, leading to higher wall shear stress and pressure drop in fixed Pe numbers. The black solid lines and the red dashed lines in Figure 5.25 represent the ratio of non-homogeneous and homogeneous pressure drop results utilizing Ryzhkov and Minakov [68], and Mcnab and Meisen thermophoresis [90] models respectively. The temperature difference between inlet and outlet becomes larger is lower Pe number. As a result, the thermophoresis effect becomes higher, Ryzhkov and Minakov thermophoresis model [68] predicts higher particle migration with higher temperatures. higher particle migration, Lower shear stress and friction factor is a reason of higher pressure drop in obtained results utilizing the Ryzhkov and Minakov thermophoresis model [68] in comparison with Mcnab and Meisen model [90].

The dependence of PEC (Equation 3.27b) to Pe number with different particle sizes and both thermophoresis coefficients, for $C_{v_0}$=0.05 is presented in Figure 5.26. Numerical results of non-homogeneous modeling show higher enhancement in heat transfer with dispersing alumina nanoparticles to water compared to homogeneous modeling. It is revealed that PEC value rises, with decreasing the Pe number, and decreasing particle size in fixed Pe numbers. Moreover, the Ryzhkov and Minakov [68] thermophoresis coefficient in non-homogeneous modeling represents higher PEC value compared to McNab and Meisen [90] thermophoresis coefficient, especially at low Pe numbers.

Figure 5.27 demonstrated the efficiency ratio results applying ER formula (see Equation 3.28). Higher values revealed by decreasing the Pe numbers and nanoparticle size. The efficiency ratio decreases with increasing the Pe number, the temperature gradient between the inlet and outlet of channel decreases and leads to reduction thermophoresis effect. The results of non-homogeneous modeling applying the Ryzhkov and Minakov thermophoresis coefficient [68] provides higher values compared to applying McNab and Meisen thermophoresis coefficient [90], especially at lower particle sizes.

Figure 5.28 represents the Performance of non-homogeneous and homogeneous models compared to water defined as

$$ER = \frac{\overline{Nu_{\text{T and H}}}/\overline{Nu_{water}}}{\overline{\Delta P_{\text{T and H}}}/\overline{\Delta P_{water}}} \tag{10}$$

Higher performance observed with increasing the particle size and decreasing the Pe number. Applying Ryzhkov and Minakov thermophoresis coefficient [68] shows higher performance compared to McNab and Meisen thermophoresis coefficient [90]. It is important to mention increasing the particle size results in lower average Nu number (see Figure 5.18) and pressure loss (see Figure 5.24). In addition, the Brownian and thermophoresis mechanisms have effects against each other. The Brownian motion diffuses the particles, and thermophoresis effect forces particles to concentrate at a region with lower temperature gradient. Increasing the particle size reduces the Brownian motion effect (see Equation 3.6), leading to enhance in thermophoresis effect, higher particle migration from walls to core region, lower pressure loss and increase in performance in this study.

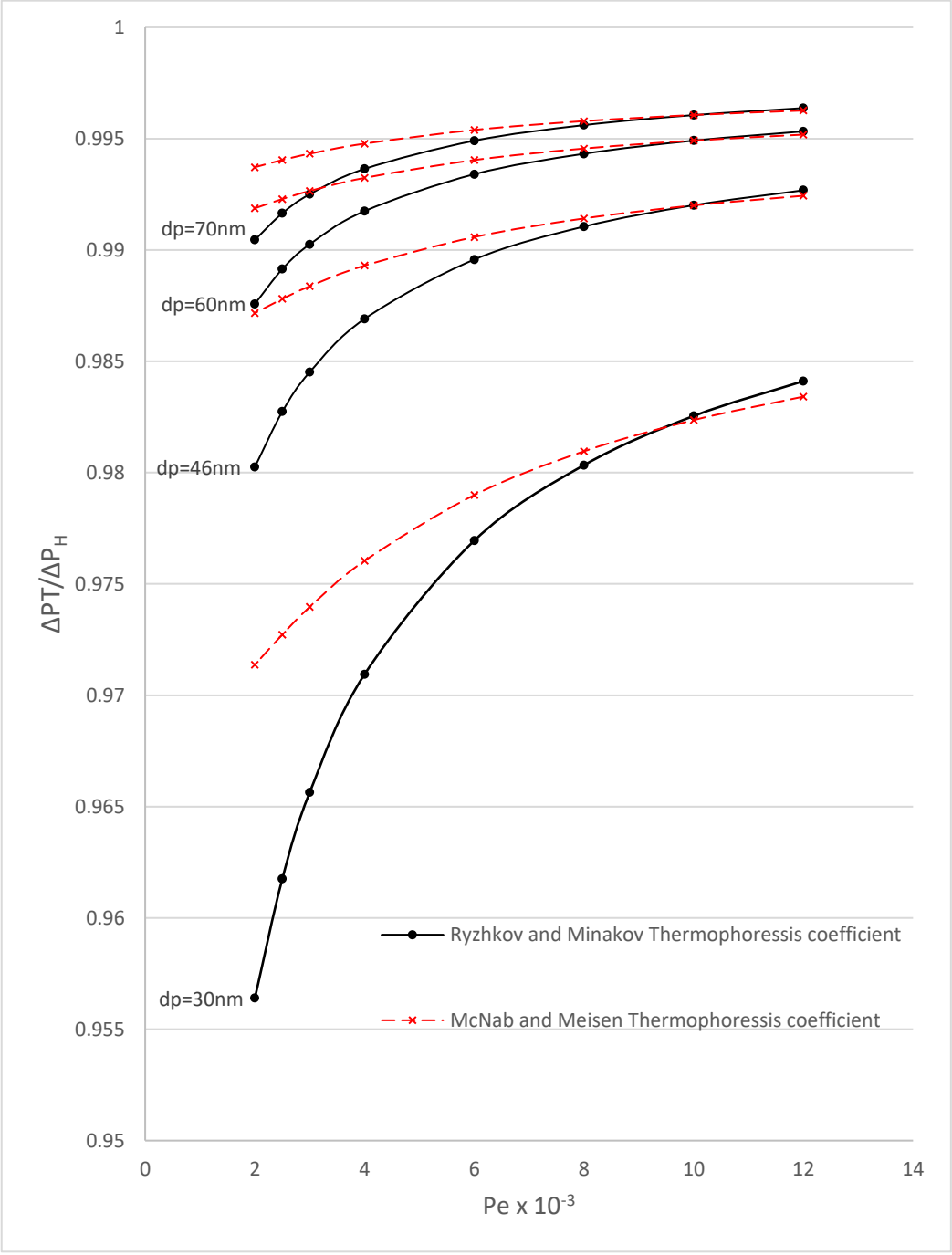


Figure 5.25. The dependence of pressure drop ratio of non-homogeneous two-component and single phase homogeneous results in heated section to Pe number for $C_{v_0}$=0.05, $T_0$=300K.

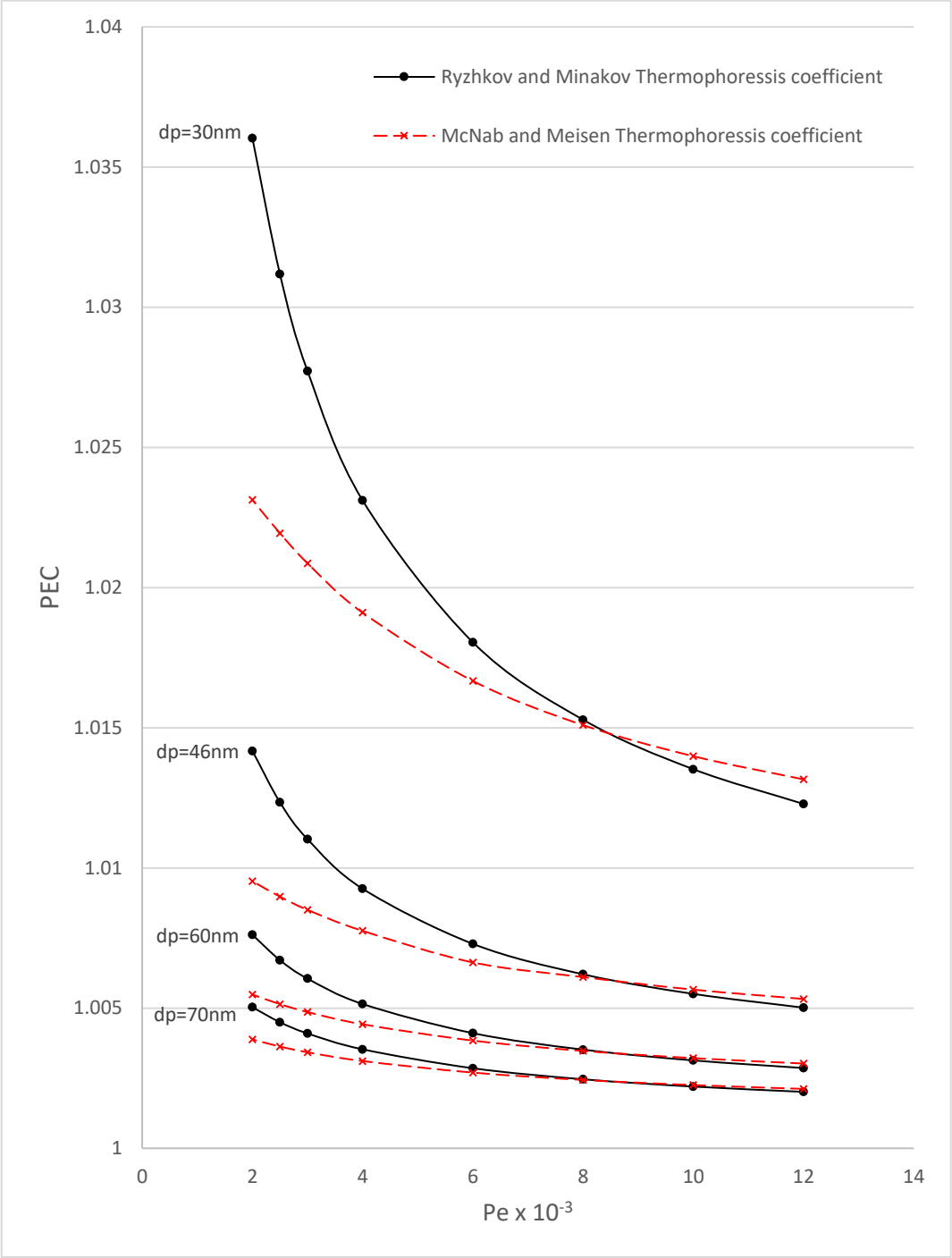


Figure 5.26. The dependence of PEC (performance efficiency criteria) to Pe number with different particle sizes, for $C_{v_0}$=0.05, $T_0$=300K, and different thermophoresis coefficients.

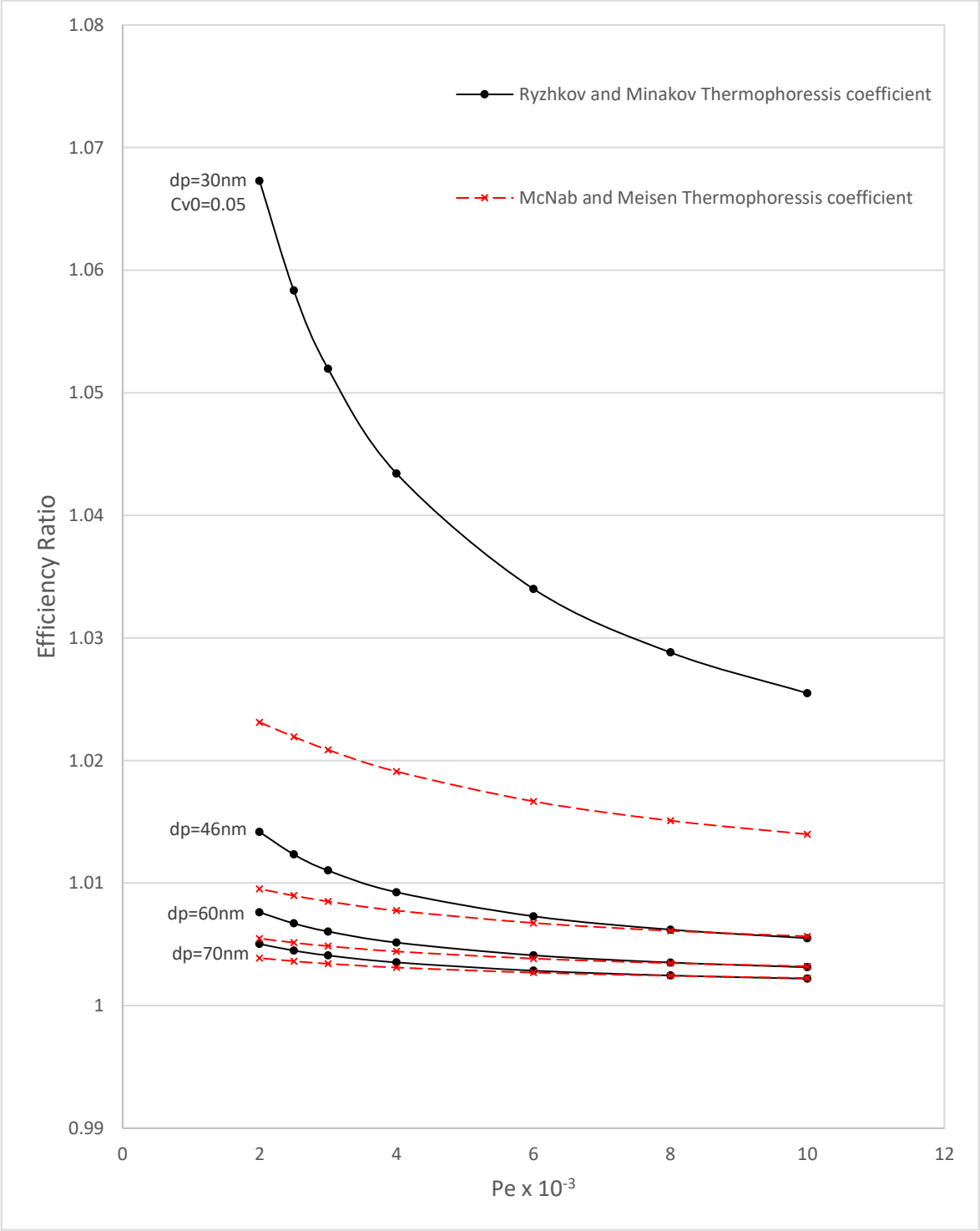


Figure 5.27. The dependence of Efficiency ratio to Pe number with different particle sizes, for $C_{v_0}$=0.05, $T_0$=300K, and different thermophoresis coefficients.

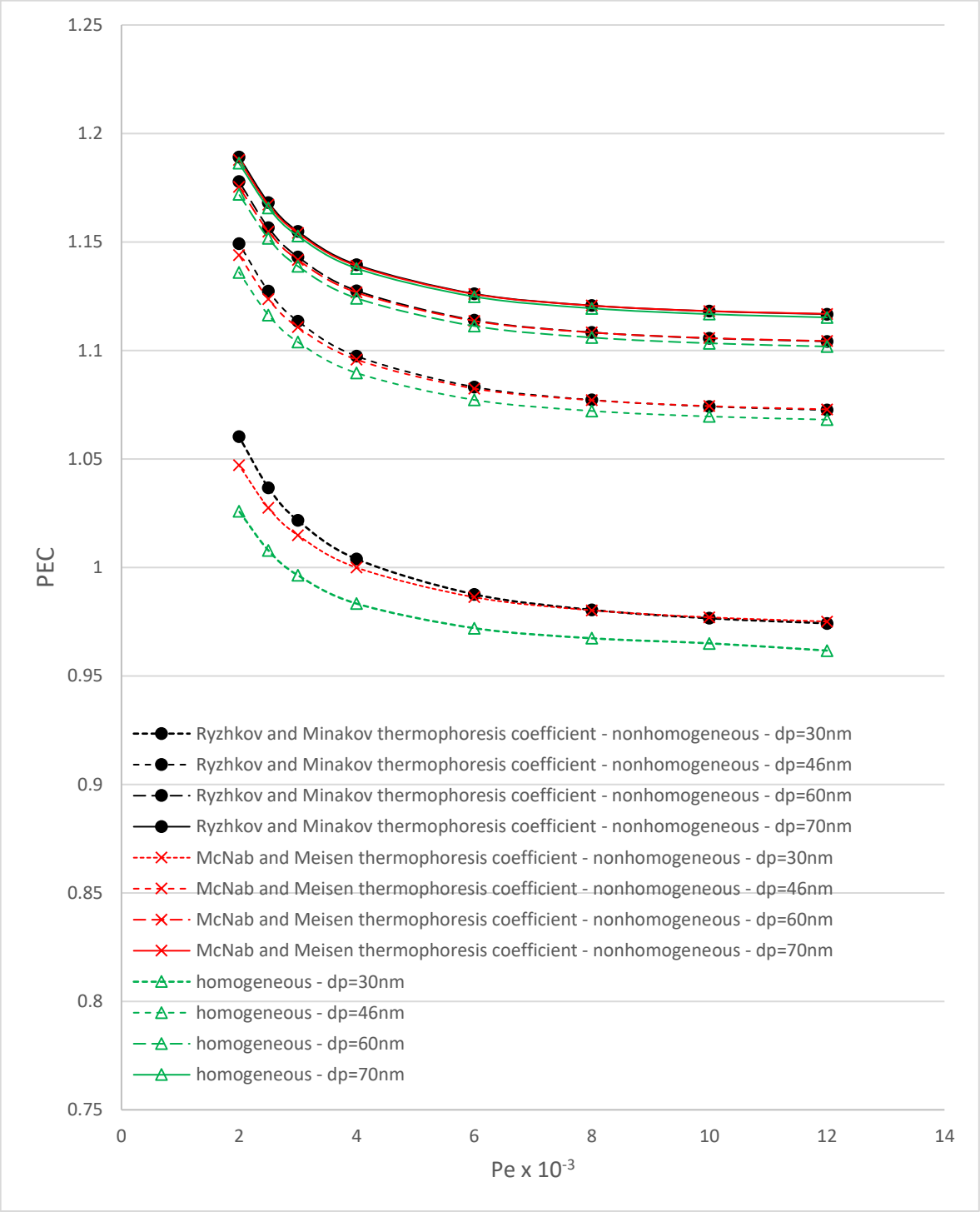


Figure 5.28. The dependence of PEC to Pe number with different particle sizes, for $C_{v_0}$=0.05, $T_0$=300K, and different thermophoresis coefficients.

### 5.2.2. Effect of Thermophoresis Strength on Alumina-Water Nanofluid

There are researches to date have tended to explain the nature of the thermophoresis effect and the parameters affecting as discussed in Section 2.6. There are many mechanisms causing thermophoretic motion (see Section 2.6) and it is a result of all aforementioned mechanisms in all real nanofluids. Thus, providing an applicable general formula for thermophoresis coefficient of all nanofluids is impossible, and experimental results are required. The proposed thermophoresis coefficient model by Ryzhkov and Minakov [68] (see Equation 3.8) allows us to have more control over predicting $D_T$ in accordance with the experimental data with introducing the parameter α, proportionality coefficient. Different values for the mentioned parameter in this section is caused by lack of experimental data for alumina-water nanofluid thermophoretic mobility. In this study, the numerical simulations are performed for $\alpha = 0$, $\alpha = 0.5 \cdot 10^{-9}$, $\alpha = 10^{-9}$ and $\alpha = 2 \cdot 10^{-9}$ to observe the effect of thermophoresis on flow and heat transfer of nanofluids. The zero value for the $\alpha$ corresponds to the case with no thermophoretic motion.

Figure 5.29 and Figure 5.31 respectively show the local heat transfer coefficient and local Nusselt number in the heated section of channel for different α values. Increasing the mobility coefficient increases thermophoresis leading to higher heat transfer. The local h results for α more than zero are almost same, and local Nu shows close results for different $\alpha$ values at same inlet particle concentrations. However, it contradicts the results obtained by Ryzhkov and Minakov [68]. The change may have caused by utilizing different viscosity and thermal conductivity models in numerical solutions, where the empirical viscosity correlation that they have used gives much higher predictions compared to theoretical values in this study. The case with $\alpha = 0$ is correspond to the result with no thermophoresis effect, where eliminates the thermophoretic motion term from the particle concentration equation. The particle concentration drop near the walls does not happen in this case. Therefore the velocity does not increase in wall boundaries, since the viscosity and thermal conductivity do not decrease at walls, and accordingly heat transfer will be lower compared to the cases where the thermophoresis still

affects the nanofluid flow. The results show about 1.1% decrease in local h and Nu with disregarding the thermophoresis term in solutions, although the results are close in this study.

The results of average heat transfer coefficient and average Nusselt number are illustrated in Figure 5.30 and Figure 5.32 respectively. The result shows higher average h and Nu with increasing the Pe number. The results are close at same Pe number for different values of α, and the case with no thermophoresis effect ($\alpha = 0$) and the difference decreases at higher Pe numbers.

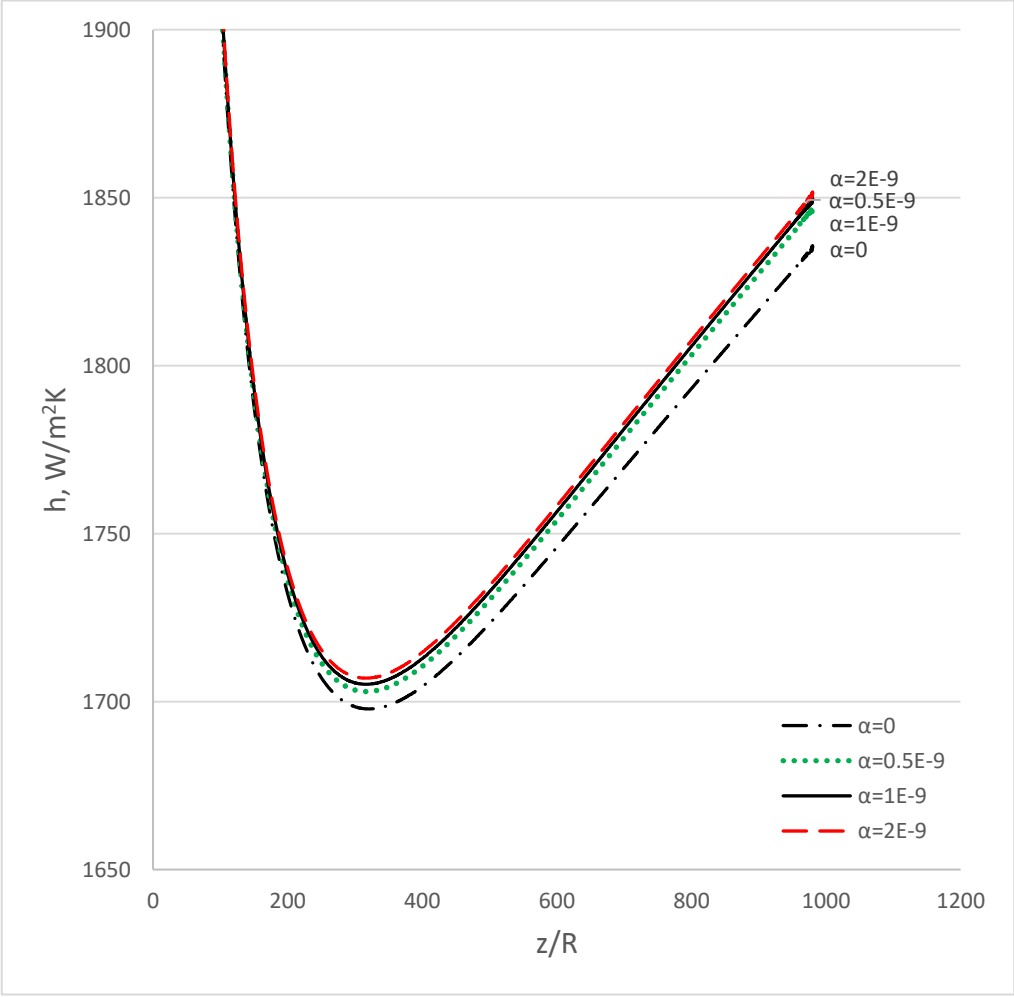


Figure 5.29. Dependence of local heat transfer coefficient in the heated section on the α (proportionality coefficient).

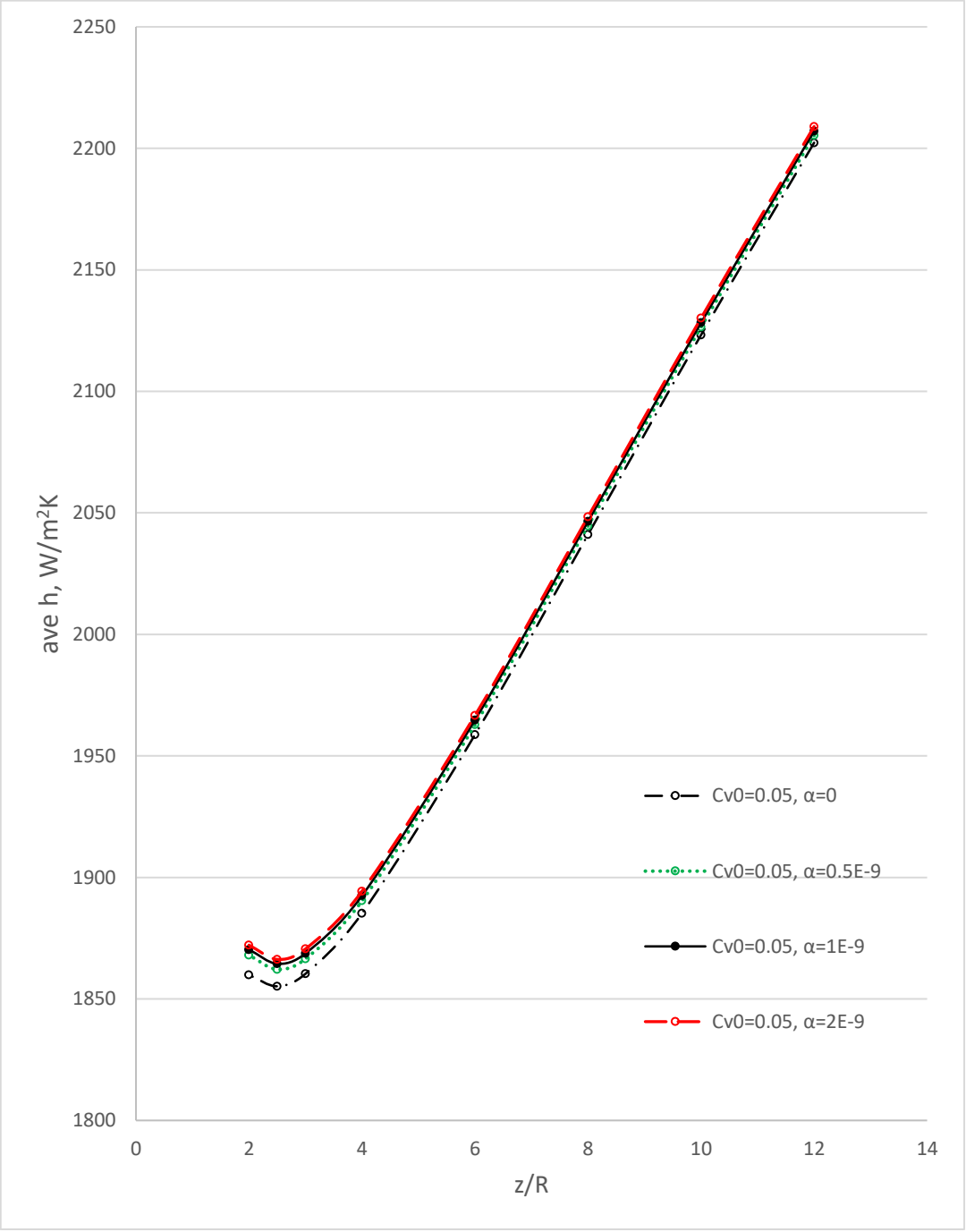


Figure 5.30. Dependence of average heat transfer coefficient on Pe number and the α, proportionality coefficient, in the heated section.

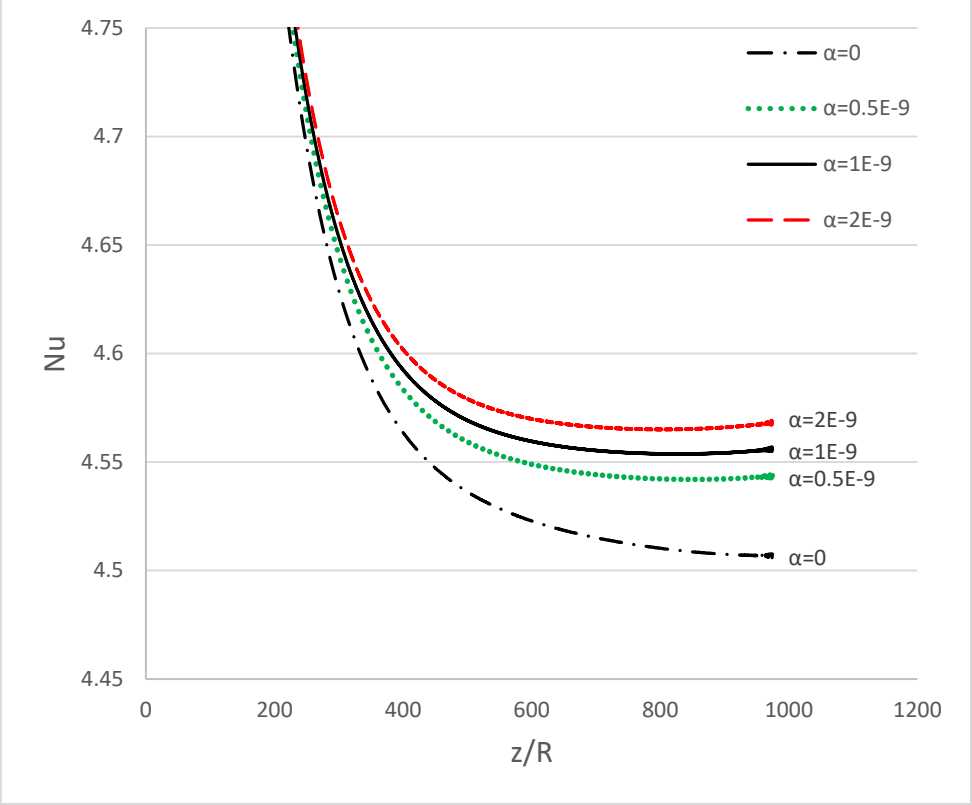


Figure 5.31. Dependence of local Nusselt number in the heated section on the α, proportionality coefficient.

It is important to note, the changes in local and average heat transfer coefficients and Nusselt numbers by applying different α values for modeling with nanofluid properties dependent on couple of parameters such as particle concentration, particle size, temperature (see Figure 5.29, Figure 5.12, Figure 5.30, Figure 5.31 and Figure 5.32), are lower compared to modeling with applying nanofluid properties only dependent on particle concentration (see Figure 5.4 and Figure 5.5, Figure 5.6 and Figure 5.7)

The ratio of Nusselt numbers for the cases with and without thermophoresis effect is demonstrated in Figure 5.33 where at maximum value shows 0.66% for the case $\alpha = 2 \times 10^{-9}$ and Pe=2000. With increasing the Pe number and decreasing the particle concentration the ratio decreases.

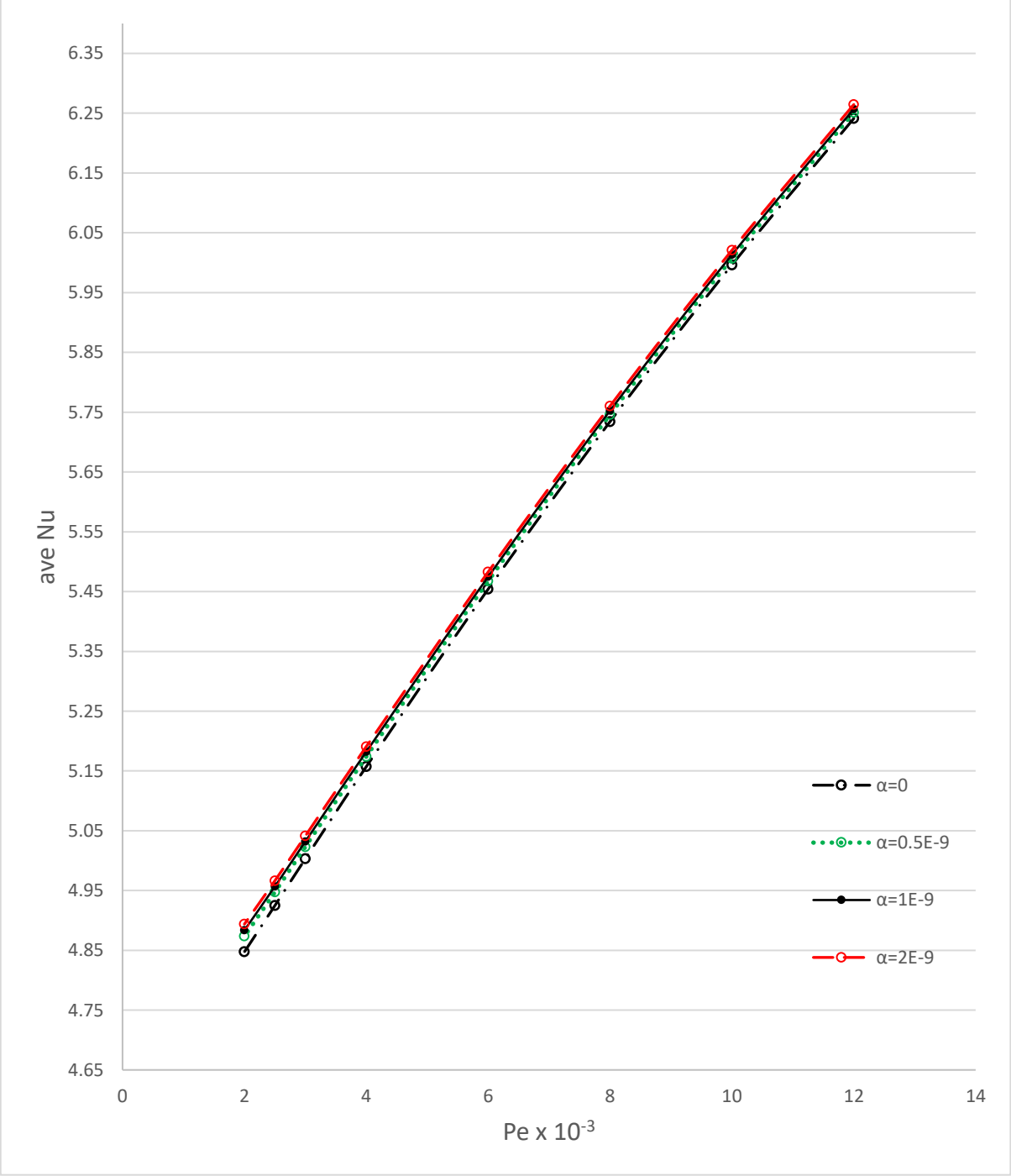


Figure 5.32. Dependence of average Nusselt number on Pe number and α (proportionality coefficient) in the heated section.

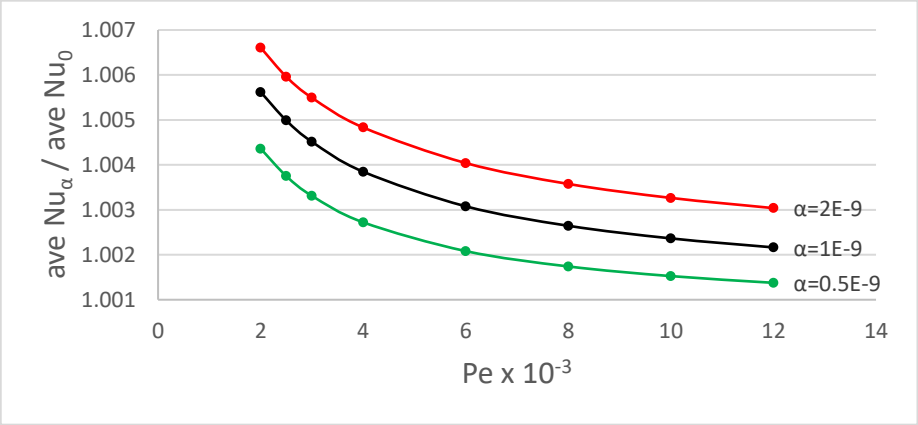


Figure 5.33. Dependence of average Nusselt number results for α (proportionality coefficient) and $\alpha = 0$ ratio, on Pe number.

The local friction factor for different $\alpha$ value cases (Figure 5.34) shows decreasing with increasing the $\alpha$. Increasing the strength of thermophoresis increases particle concentration drop near the walls leading to higher decrease in viscosity, shear stress and friction factor. Figure 5.35 presents the ratio of average friction factors with and without considering the thermophoresis. The results show higher decrease in average friction factor at higher α values compared to no thermophoresis case and in addition, the ratio of friction factors is larger at low Pe numbers which stems from higher temperature gradient between inlet and outlet of channel and thermophoresis effect.

Figure 5.36 demonstrates the performance of the nanofluid corresponding to the strength of thermophoresis and Pe number. The PEC correlation has been defined as

$$\mathrm{PEC} = \frac{\overline{Nu_\alpha}/\overline{Nu_0}}{(\overline{f_\alpha}/\overline{f_0})^{\frac{1}{3}}} \tag{11}$$

where $\overline{Nu_\alpha}$ and $\overline{f_\alpha}$ are the numerical results of the case with thermophoresis effect and $\overline{Nu_0}$ and $\overline{f_0}$ are the case without considering the thermophoresis effect. The results show higher performance rates for higher α (stronger thermophoresis effect) and lower Pe numbers.

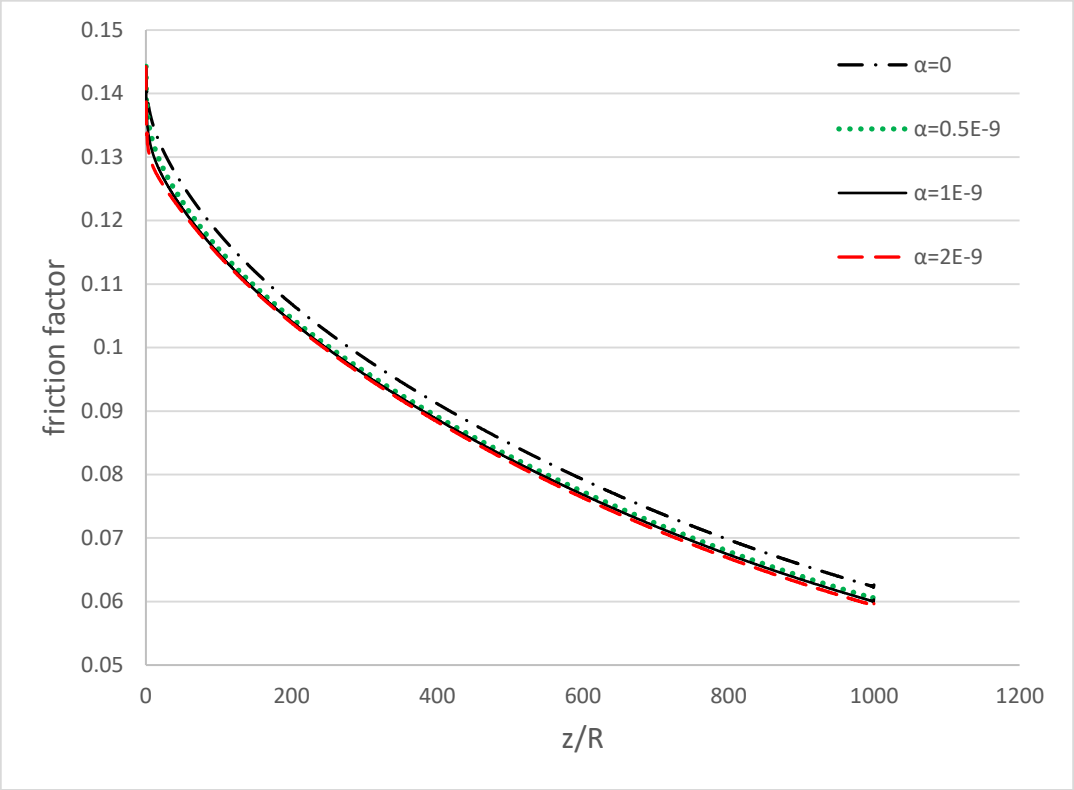


Figure 5.34. Dependence of local friction factor on α (proportionality coefficient).

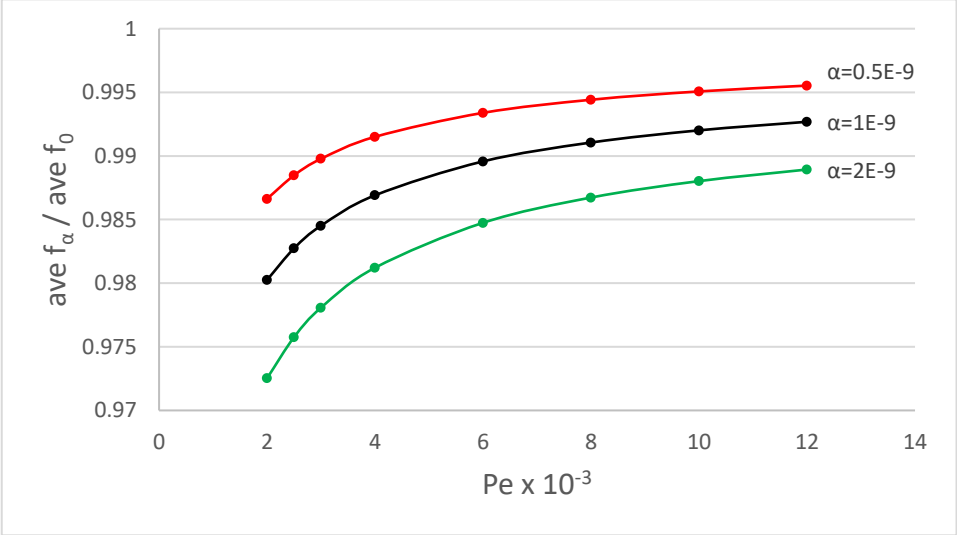


Figure 5.35. Dependence of average friction factor results for α (proportionality coefficient) and $\alpha = 0$ ratio, on Pe number.

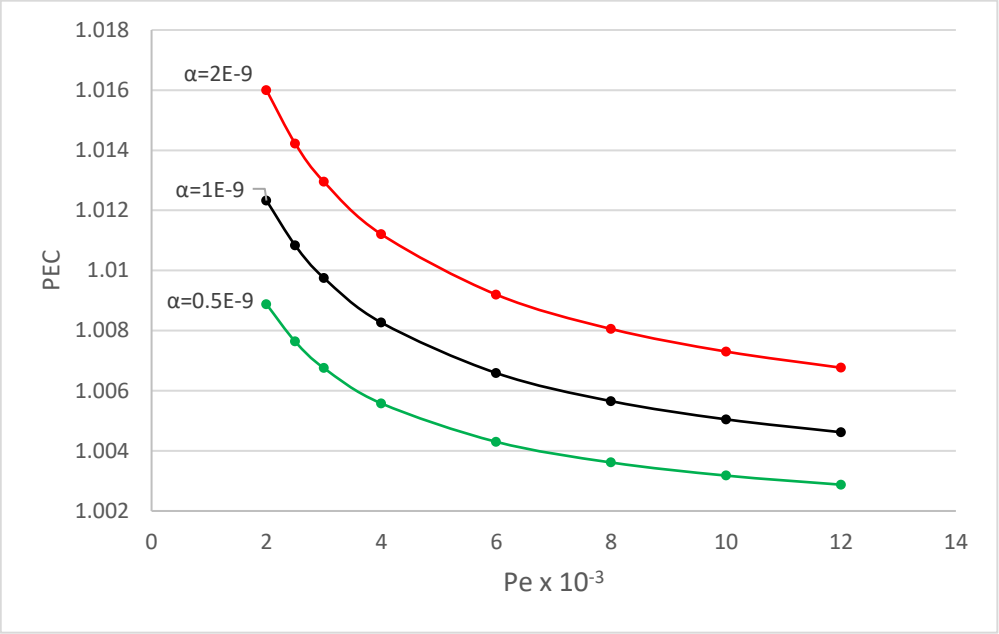


Figure 5.36. Dependence of PEC (performance efficiency criteria) results on α (proportionality) and Pe number.

Almost same pressure drop is observed in results for the cases with and without thermophoresis effect, also at higher α values (see Figure 5.37). The ER (efficiency ratio) defined as

$$ER = \frac{\overline{Nu_\alpha}/\overline{Nu_0}}{\overline{\Delta P_\alpha}/\overline{\Delta P_0}} \tag{12}$$

where $\overline{Nu_\alpha}$ and $\overline{\Delta P_\alpha}$ are average Nu number and pressure drop for the case with thermophoresis effect and $\overline{Nu_0}$ and $\overline{\Delta P_0}$ are average Nu number and pressure drop for the case with no thermophoresis effect. The results of efficiency based on ER formula (see Figure 5.38) present larger values at higher α and low Pe numbers. The efficiency ratio decreases by increasing the Pe number due to the lower temperature gradient between inlet and outlet of channel and lessening the thermophoresis effect.

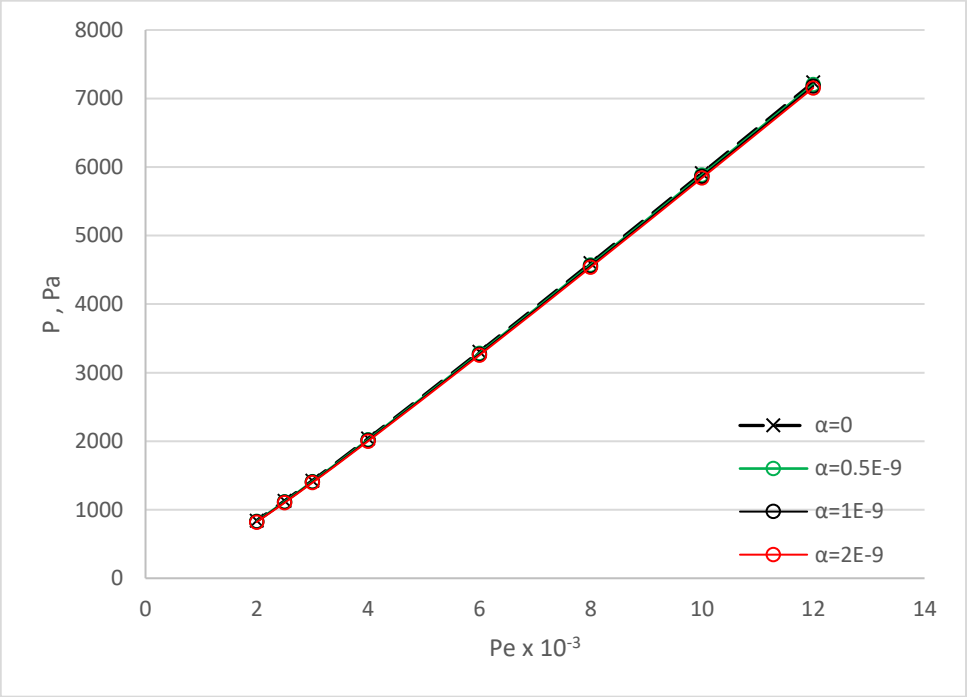


Figure 5.37. Dependence of pressure drop (performance efficiency criteria) results on α (proportionality) and Pe number.

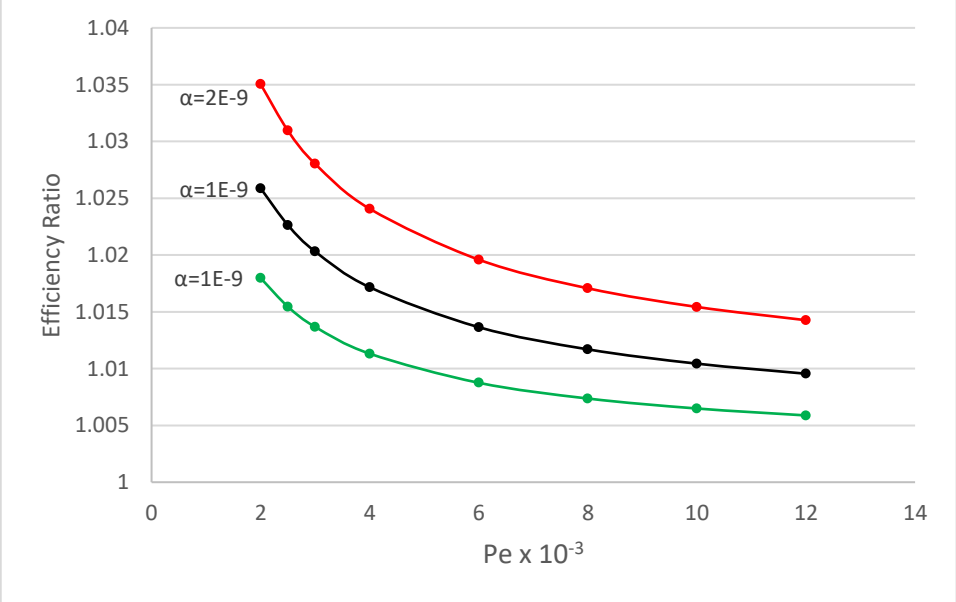


Figure 5.38. Dependence of ER (efficiency ratio) results on α (proportionality coefficient) and Pe number.

### 5.2.3. Effect of Brownian Motion and Thermophoresis

Figure 5.39 and Figure 5.40 represent the Brownian motion and thermophoresis terms of the particle transfer equation (two terms in right side of the Equation 3.4), in cross sections along the minichannel. It can be observed that the values can be taken as rather constant at core region, but the main change is near the wall boundaries which the value of both terms significantly decreases due to the high particle migration and drop in particles concentration. The values obtained for both terms are close enough to confirm Brownian and thermophoresis terms have dominant effect on nanofluids, and neither of them should be neglected.

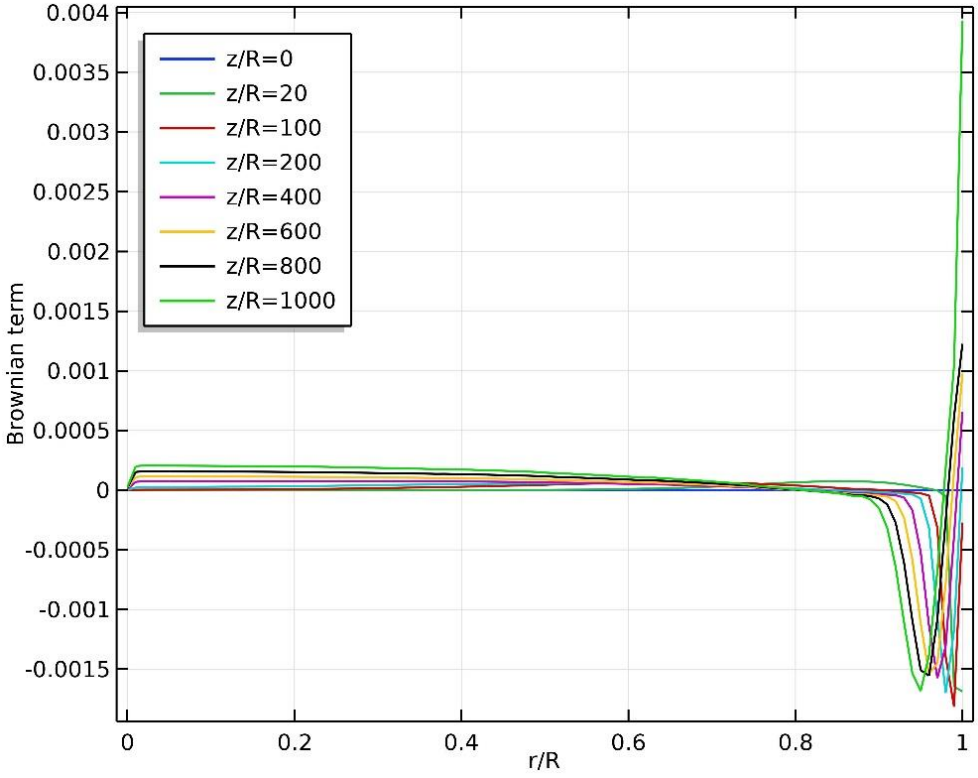


Figure 5.39. Brownian term values at cross sections in axial direction. Results of alumina-water nanofluid with Pe=2500, $C_{v_0}$=0.05 and $T_0$=300K

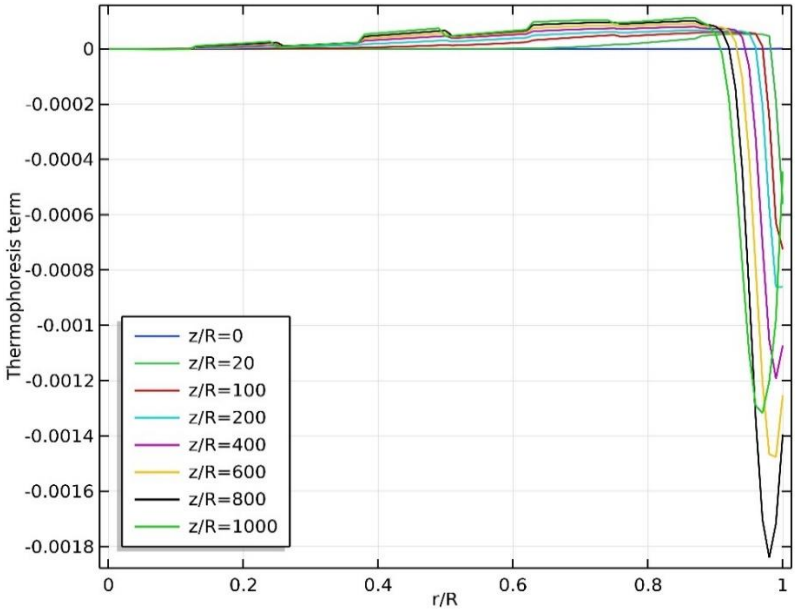


Figure 5.40. Thermophoresis term values at cross sections in axial direction. Results of alumina-water nanofluid with Pe=2500, $C_{v_0}$=0.05 and $T_0$=300K

Bahiraei *et al*. [65] studied the $TiO_2$-water nanofluid particle migration considering the thermophoresis in a circular channel experimentally and numerically. They performed a scale analysis on the terms of particle concentration equation and claimed the thermophoresis can have higher effect on particle migration and should not be ignored. They performed the numerical study utilizing a thermal dispersion model. They ignored thermophoresis in a case to observe its effect, and reported more uniform particle concentration profiles and the thermophoresis term effect is more significant at higher particle concentrations.

## 5.3. Effect of Thermophoresis Strength on CuO-Water Nanofluid with Properties Dependent on Particle Concentration, Size and Temperature

As discussed in Section 2.6 the thermophoresis coefficient model proposed by Ryzhkov and Minakov [68] is an empirical formula (see Equation 3.8). The proportionality coefficient (α parameter) should be defined in accordance with experimental data and theoretical studies. Unfortunately, there is no experimental data available on $Al_2O_3$ -water and $CuO$ -water nanofluids thermophoresis mobility. The α parameter predicted as $10^{-9}$ for alumina-water

nanofluid. In this section, we numerically study copper oxide nanoparticles dispersed in water based fluid to estimate the α parameter change for different materials, applying the Masoumi *et al.* [29] viscosity model and Vajjha and Das [29] thermal conductivity model.

Considering the McNab and Meisen thermophoresis coefficient [90] as the most common formula, the results with different α values for CuO-water nanofluid are compared with it. Figure 5.41 and Figure 5.42 are the local heat transfer coefficient and the ratio of average heat transfer coefficient results, modeling with Ryzhkov and Minakov [68], and McNab and Meisen thermophoresis [90] formulas, respectively, at $C_{v_0}$=0.05 and Pe=2500. The results show higher heat transfer coefficient at higher α values corresponding to stronger thermophoresis effect, where numerical result with the $\alpha = 0.75 \cdot 10^{-9}$ gives rather close average heat transfer coefficient to the result with McNab and Meisen thermophoresis [90] formula.

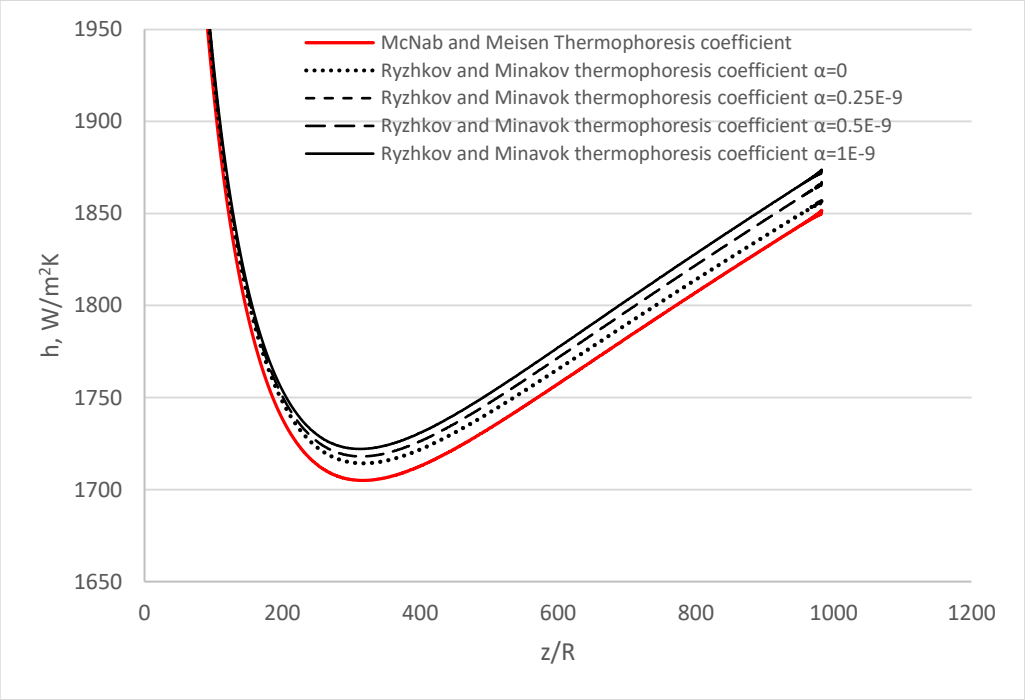


Figure 5.41. The local heat transfer coefficient of CuO-water nanofluid for $C_{v_0}$=0.05 and Pe=2500 with various α values of Ryzhkov and Minakov thermophoresis coefficient [68], and McNab and Meisen thermophoresis coefficient [90].

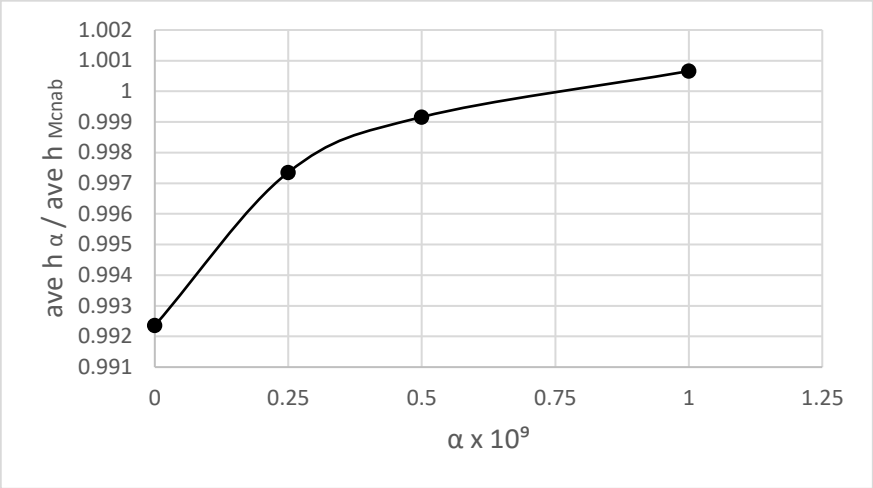


Figure 5.42. The dependence of ratio of heat transfer coefficient of results with Ryzhkov and Minakov [68], and McNab and Meisen thermophoresis coefficient [90] on α for CuO-water nanofluid. $C_{v_0}$=0.05 and Pe=2500.

Figure 5.44 and Figure 5.44 provide the local Nu and ratio of average Nu results for modeling with Ryzhkov and Minakov [68], and McNab and Meisen thermophoresis coefficients [90]. Similar to the heat transfer coefficient the thermophoresis effect rises with increasing the α value. $\alpha = 0.68 \cdot 10^{-9}$ gives same result as numerical modeling with McNab and Meisen thermophoresis [90] formula for average Nu number.

Figure 5.45 provides the friction factor ratio of numerical results with utilizing the Ryzhkov and Minakov [68], and McNab and Meisen thermophoresis [90] models. Increasing thermophoresis effect means higher particle migration, decreases in thermal conductivity and lower friction factor near the walls, as well as increase in average heat transfer coefficient (see Figure 5.42) and average Nu number (see Figure 5.44). In overall, it can be concluded that the performance of CuO-water nanofluid (see Figure 5.46) improves with rising the α parameter (thermophoresis effect), and in this study, the numerical result of $\alpha = 0.62 \cdot 10^{-9}$ shows same performance as modeling the CuO-water nanofluid with the McNab and Meisen thermophoresis coefficient [90]. This confirms the Ryzkvov and Minakov thermophoresis coefficient [68] is an empirical formula and experimental studies should be performed on the nanofluids to find the α parameter that should be employed for each one.

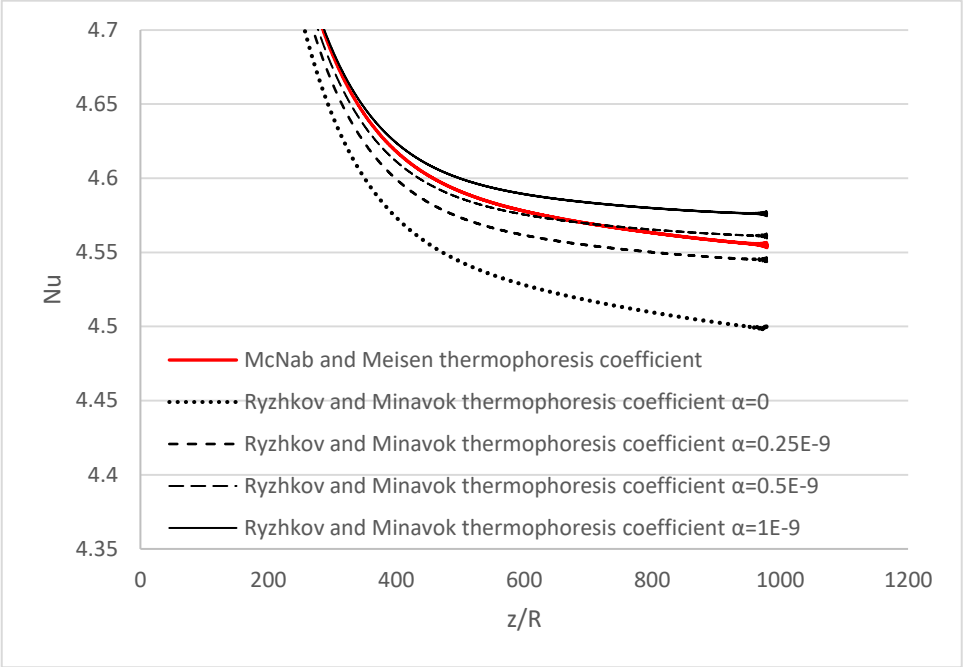


Figure 5.43. The local Nu of CuO-water nanofluid for $C_{v_0}$=0.05 and Pe=2500 with various α values of Ryzkov and Minakov thermophoresis coefficient [68], and McNab and Meisen thermophoresis coefficient [90].

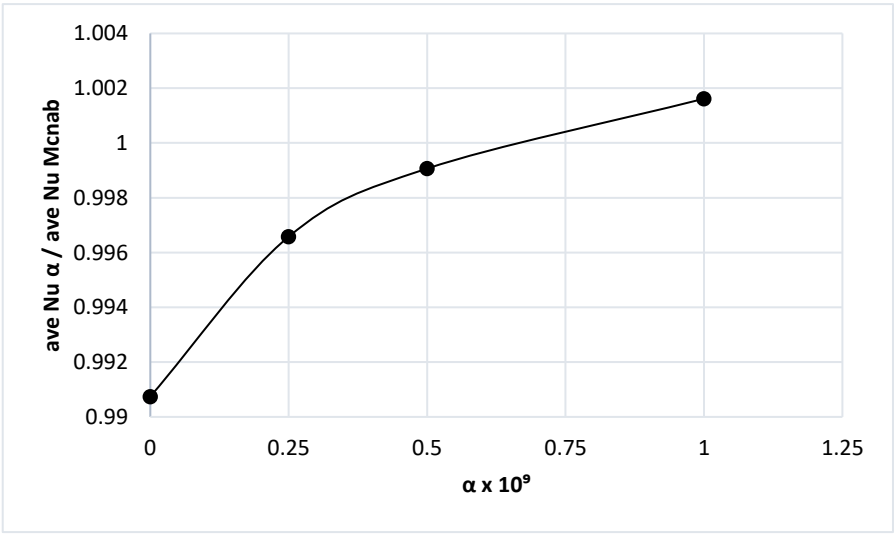


Figure 5.44. The α effect on average Nu ratio of results with Ryzhkov and Minakov [68], and McNab and Meisen thermophoresis coefficient [90] for CuO-water nanofluid. $C_{v_0}$=0.05 and Pe=2500.

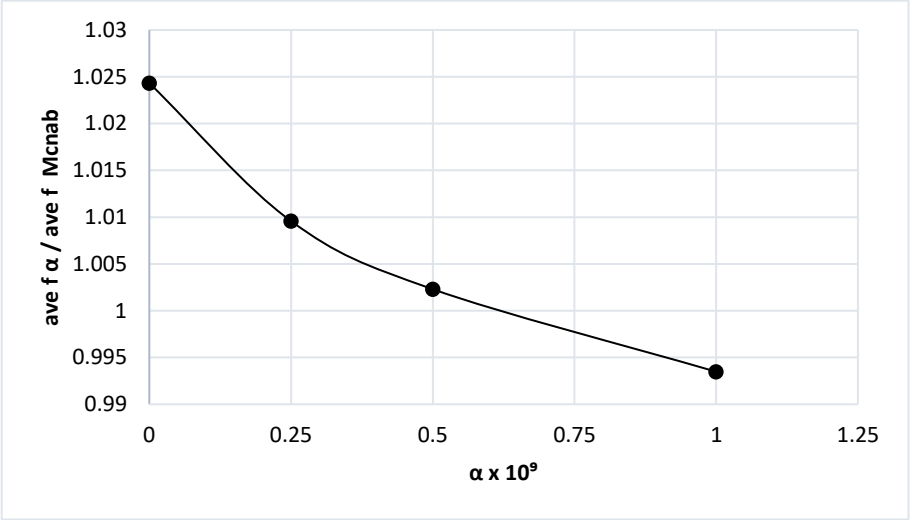


Figure 5.45. The effect of α on average friction factor ratio of results with Ryzhkov and Minakov [68], and McNab and Meisen thermophoresis coefficients [90] for CuO-water nanofluid. $C_{v_0}$=0.05 and Pe=2500.

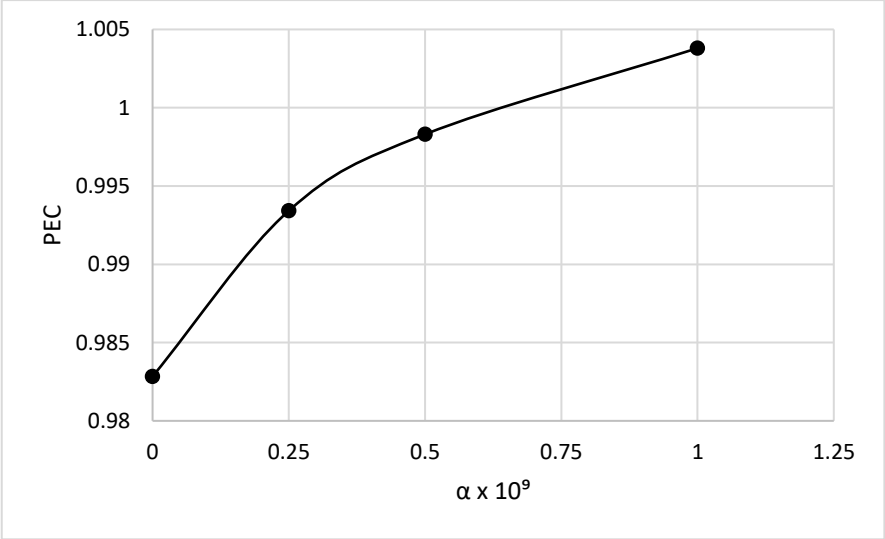


Figure 5.46. The effect of α on PEC for CuO-water nanofluid. $C_{v_0}$=0.05 and Pe=2500.

# 6. CONCLUSION AND FUTURE WORKS

In this study convective laminar flow and heat transfer of alumina-water nanofluid inside a circular minichannel subjected to constant heat flux and wall temperature has been investigated. The aim of the thesis was to examine the difference of results obtained by two-component non-homogeneous and single phase homogeneous nanofluid modeling. Therefore, the model proposed by Buongiorno [55] was utilized including the convective, thermophoresis and Brownian motion, as the key terms. To have more accurate results, the base fluid and particle properties are considered as dependent on temperature. The viscosity and thermal conductivity models used for nanofluid properties are dependent on parameters such as particle size, temperature and particle concentration. More restricted study of the same problem for minichannel subjected to a constant wall temperature was conducted as well. The second aim of this study was to investigate the thermophoresis effect on the particle migration and its alterations on the flow, heat transfer and performance of nanofluid. A new thermophoresis coefficient proposed by Ryzhkov and Minakov [68] was exploited, as well as the most commonly used model, presented by McNab and Meisen [90]. In addition, the proportionality coefficient introduced by Ryzhkov and Minakov [68] was examined for alumina-water and CuO-water nanofluids to study the strength of the thermophoresis effect in nanofluids.

The results of this research support the idea that thermophoresis effect forces particles to migrate from walls to the core region of channel due to the temperature gradient, and produces a non-uniformity near the walls while the particle concentration on the core region is almost same. This particle concentration drop reduces viscosity and hence velocity rises in the vicinity of the wall and for keeping mass flow rate constant, velocity profile flattens at the center of channel. Moreover, shear stress and friction factor decrease on the walls. The aforementioned reasons lead to higher heat transfer coefficient, Nusselt number, lower friction factor, and pressure drop. Overall higher heat transfer enhancement is observed in non-homogeneous modeling compared to homogeneous. Even if the accuracy of homogeneous modeling increase by utilizing the more reliable nanofluid properties, and variable depending on the parameters

affecting, still homogeneous modeling is not able to predict the high particle concentration drop near the walls. Non-homogeneous modeling gives close result to the experimental findings.

Decreasing the particle size yields higher heat transfer coefficient and Nusselt number. The nanofluid shows higher performance and efficiency rates at lower Pe number although decrease in particle size increases the friction factor and pressure drop. In addition, in comparison of numerical results between non-homogeneous and homogeneous modeling, utilizing the Ryzhkov and Minakov [68] thermophoresis coefficient shows higher performance and efficiency compared to the McNab and Meisen [90]. The results of numerical studies on non-homogeneous model presented higher performance compared to the base fluid with increasing the particle size and decreasing the Pe number.

The results on the strength of thermophoresis by alteration of α parameter show higher heat transfer coefficient and Nusselt number, and lower friction factor by increasing the thermophoresis effect. The performance increases at low Pe numbers and decreases with increasing the Pe number. Also, results of alumina-water and CuO-water nanofluids confirms the α parameter is highly dependent on the empirical data and more experiments are required to calculate the parameter value corresponding to each nanofluid.

This information can be used to develop targeted studies aimed at the underestimation of experimental data with numerical results. There have been studies such as Moreira *et al*. [66] claiming that the thermophoresis is not adequate for explaining the high difference between obtained experimental and numerical data. They studied the convective enhancement of alumina-water in a 1.1 mm diameter cylindrical tube. They studied different particle sizes $d_p$=20-30 nm and 40-60 nm and different particle concentrations (0.001%, 0.01%, and 0.1%), and reported 8% enhancement in maximum Nusselt number in fully developed region. However, they concluded that there might be another not identified mechanism/s that affect heat transfer and heat flux in some way has apparently a link to enhancing mechanism/s which leads to a belief that it is associated with thermophoresis, nanoparticle concentration gradient, Brownian motion, also orbiting and rotating of particles.

Although, Moreira *et al*. and numerous other studies [66][68][54] account the self-diffusion term as negligible, Metzer *et al*. [110] study show that there may be a mechanism related to self-diffusion that can explain the difference between the experimental and numerical results and predict the heat transfer augmentation as obtained in experimental data. Batchelor *et al*. [111] reported that spherical particles rotate at rates imposed locally by flow in Stokes flow.

In overall conclusion, further investigation and experimentation into nanofluids are strongly recommended. Works are needed to fully understand the implications and applications of nanofluids.

# REFERENCES


1. D. Wen, G. Lin, S. Vafaei, and K. Zhang, “Review of nanofluids for heat transfer applications,” *Particuology*, vol. 7, no. 2, pp. 141–150, Apr. 2009.

2. L. Léal *et al.*, “An overview of heat transfer enhancement methods and new perspectives: Focus on active methods using electroactive materials,” *Int. J. Heat Mass Transf.*, vol. 61, pp. 505–524, Jun. 2013.

3. M. Sheikholeslami, M. Gorji-Bandpy, and D. D. Ganji, “Review of heat transfer enhancement methods: Focus on passive methods using swirl flow devices,” *Renew. Sustain. Energy Rev.*, vol. 49, pp. 444–469, Sep. 2015.

4. D. K. Devendiran and V. A. Amirtham, “A review on preparation, characterization, properties and applications of nanofluids,” *Renew. Sustain. Energy Rev.*, vol. 60, pp. 21–40, 2016.

5. Y. Li, J. Zhou, S. Tung, E. Schneider, and S. Xi, “A review on development of nanofluid preparation and characterization,” *Powder Technol.*, vol. 196, no. 2, pp. 89–101, 2009.

6. P. Singh, “heat transfer characteristics of propylene glycol/water based magnesium oxide nanofluid flowing through straight tubes and helical coils,” *J. Therm. Eng.*, vol. 4, no. 1, pp. 1737–1755, Dec. 2017.

7. J. Maxwell, *A treatise on electricity and magnetism*. Clarendon press, 1881.

8. J. J. Taha-Tijerina, “Thermal Transport and Challenges on Nanofluids Performance,” in *Microfluidics and Nanofluidics*, InTech, 2018.

9. S. U. S. Choi and J. A. Eastman, “Enhancing thermal conductivity of fluids with nanoparticles,” *1995 Int. Mech. Eng. Congr. Exhib. San Fr. CA (United States), 12-17 Nov 1995*, Oct. 1995.

10. S. U. S. Choi, Z. G. Zhang, W. Yu, F. E. Lockwood, and E. A. Grulke, “Anomalous thermal conductivity enhancement in nanotube suspensions,” *Appl. Phys. Lett.*, vol. 79, no. 14, pp. 2252–2254, Oct. 2001.

11. S. K. Das and Wiley InterScience (Online service), *Nanofluids : science and technology*. Wiley-Interscience, 2008.

12. X. Wang, X. Xu, and S. U. S. Choi, “Thermal Conductivity of Nanoparticle - Fluid Mixture,” *J. Thermophys. Heat Transf.*, vol. 13, no. 4, pp. 474–480, Oct. 1999.

13. S. Lee, S. U.-S. Choi, S. Li, and J. A. Eastman, “Measuring Thermal Conductivity of Fluids Containing Oxide Nanoparticles,” *J. Heat Transfer*, vol. 121, no. 2, p. 280, May 1999.

14. S. K. Das, N. Putra, P. Thiesen, and W. Roetzel, “Temperature Dependence of Thermal Conductivity Enhancement for Nanofluids,” *J. Heat Transfer*, vol. 125, no. 4, p. 567, 2003.

15. J.-Y. Jung, H.-S. Oh, and H.-Y. Kwak, “Forced Convective Heat Transfer of Nanofluids in Microchannels,” in *Heat Transfer, Volume 3*, 2006, vol. 2006, pp. 327–332.

16. K. B. Anoop, T. Sundararajan, and S. K. Das, “Effect of particle size on the convective heat transfer in nanofluid in the developing region,” *Int. J. Heat Mass Transf.*, vol. 52, no. 9–10, pp. 2189–2195, Apr. 2009.

17. D. Wen and Y. Ding, “Experimental investigation into convective heat transfer of nanofluids at the entrance region under laminar flow conditions,” *Int. J. Heat Mass*

*Transf.*, vol. 47, no. 24, pp. 5181–5188, Nov. 2004.

18. A. Einstein and R. (Reinhold) Fürth, *Investigations on the theory of Brownian movement*. Dover Publications, 1956.

19. H. C. Brinkman, "The Viscosity of Concentrated Suspensions and Solutions," *J. Chem. Phys.*, vol. 20, no. 4, pp. 571–571, Apr. 1952.

20. I. M. Krieger and T. J. Dougherty, "A Mechanism for Non-Newtonian Flow in Suspensions of Rigid Spheres," *Trans. Soc. Rheol.*, vol. 3, no. 1, pp. 137–152, Mar. 1959.

21. T. S. Lundgren, "Slow flow through stationary random beds and suspensions of spheres," *J. Fluid Mech.*, vol. 51, no. 02, p. 273, Jan. 1972.

22. G. K. Batchelor, "The effect of Brownian motion on the bulk stress in a suspension of spherical particles," *J. Fluid Mech.*, vol. 83, no. 01, p. 97, Nov. 1977.

23. A. L. Graham, "On the viscosity of suspensions of solid spheres," *Appl. Sci. Res.*, vol. 37, no. 3–4, pp. 275–286, 1981.

24. C. T. Nguyen *et al.*, "Temperature and particle-size dependent viscosity data for water-based nanofluids – Hysteresis phenomenon," *Int. J. Heat Fluid Flow*, vol. 28, no. 6, pp. 1492–1506, Dec. 2007.

25. T. Kitano, T. Kataoka, and T. Shirota, "An empirical equation of the relative viscosity of polymer melts filled with various inorganic fillers," *Rheol. Acta*, vol. 20, no. 2, pp. 207–209, Mar. 1981.

26. J. Bicerano, J. F. Douglas, And D. A. Brune, "Model for the Viscosity of Particle Dispersions," *J. Macromol. Sci. Part C Polym. Rev.*, vol. 39, no. 4, pp. 561–642, Sep.

1999.

27. E. Abu-Nada, “Effects of variable viscosity and thermal conductivity of Al 2 O 3-water nanofluid on heat transfer enhancement in natural convection,” *Int. J. HEAT FLUID FLOW*.

28. C. T. Nguyen *et al.*, “Temperature and particle-size dependent viscosity data for water-based nanofluids – Hysteresis phenomenon,” *Int. J. Heat Fluid Flow*, vol. 28, no. 6, pp. 1492–1506, Dec. 2007.

29. N. Masoumi, N. Sohrabi, and a Behzadmehr, “A new model for calculating the effective viscosity of nanofluids,” *J. Phys. D. Appl. Phys.*, vol. 42, no. 5, p. 055501, 2009.

30. Satish G. Kandlikar, S. Garimella, D. (Professor) Li, S. Colin, and M. R. KIng, *Heat transfer and fluid flow in minichannels and microchannels*. Butterworth-Heinemann, 2013.

31. Satish G. Kandlikar, *Heat transfer and fluid flow in minichannels and microchannels*. Elsevier, 2006.

32. M. G. Khan and A. Fartaj, “A review on microchannel heat exchangers and potential applications,” *Int. J. Energy Res.*, vol. 35, no. 7, pp. 553–582, Jun. 2011.

33. C.-C. Wang, Y.-R. Jeng, J.-J. Chien, and Y.-J. Chang, “Frictional performance of highly viscous fluid in minichannels,” *Appl. Therm. Eng.*, vol. 24, no. 14–15, pp. 2243–2250, Oct. 2004.

34. B. C. Pak and Y. I. Cho, “hydrodynamic and heat transfer study of dispersed fluids with submicron metallic oxide particles,” *Exp. Heat Transf.*, vol. 11, no. 2, pp. 151–170, Apr. 1998.

35. Q. Li and Y. Xuan, “Convective heat transfer and flow characteristics of Cu-water nanofluid,” *Sci. China Ser. E Technolgical Sci.*, vol. 45, no. 4, pp. 408–416.

36. W. Duangthongsuk and S. Wongwises, “An experimental study on the heat transfer performance and pressure drop of TiO2-water nanofluids flowing under a turbulent flow regime,” *Int. J. Heat Mass Transf.*, vol. 53, no. 1–3, pp. 334–344, Jan. 2010.

37. S. Lee and S. U-S Choi, “Application of Metallic Materials in Advanced Engineering Systems,” 1996.

38. W. Y. Lai, P. E. Phelan, S. Vinod, and R. Prasher, “Convective heat transfer for water-based alumina nanofluids in a single 1.02-mm tube,” in *2008 11th Intersociety Conference on Thermal and Thermomechanical Phenomena in Electronic Systems*, 2008, pp. 970–978.

39. J. Wu, J. Zhao, J. Lei, and B. Liu, “Effectiveness of nanofluid on improving the performance of microchannel heat sink,” 2016.

40. M. Corcione, “Empirical correlating equations for predicting the effective thermal conductivity and dynamic viscosity of nanofluids,” *Energy Convers. Manag.*, vol. 52, no. 1, pp. 789–793, Jan. 2011.

41. C. T. Nguyen *et al.*, “Temperature and particle-size dependent viscosity data for water-based nanofluids – Hysteresis phenomenon,” *Int. J. Heat Fluid Flow*, vol. 28, no. 6, pp. 1492–1506, Dec. 2007.

42. A. Koşar, “Effect of substrate thickness and material on heat transfer in microchannel heat sinks,” *Int. J. Therm. Sci.*, vol. 49, no. 4, pp. 635–642, Apr. 2010.

43. P.-S. Lee, S. V. Garimella, and D. Liu, “Investigation of heat transfer in rectangular

microchannels," *Int. J. Heat Mass Transf.*, vol. 48, no. 9, pp. 1688–1704, Apr. 2005.

44. J. Koo and C. Kleinstreuer, "Laminar nanofluid flow in microheat-sinks," *Int. J. Heat Mass Transf.*, vol. 48, no. 13, pp. 2652–2661, Jun. 2005.

45. H.-C. Chiu, J.-H. Jang, H.-W. Yeh, and M.-S. Wu, "The heat transfer characteristics of liquid cooling heatsink containing microchannels," *Int. J. Heat Mass Transf.*, vol. 54, no. 1–3, pp. 34–42, Jan. 2011.

46. W. Escher *et al.*, "on the cooling of electronics with nanofluids," *J. Heat Transfer*, vol. 133, no. 5, p. 051401, 2011.

47. A. Ijam and R. Saidur, "Nanofluid as a coolant for electronic devices (cooling of electronic devices)," *Appl. Therm. Eng.*, vol. 32, pp. 76–82, Jan. 2012.

48. H. A. Mohammed, P. Gunnasegaran, and N. H. Shuaib, "Influence of channel shape on the thermal and hydraulic performance of microchannel heat sink," *Int. Commun. Heat Mass Transf.*, vol. 38, no. 4, pp. 474–480, Apr. 2011.

49. D. Lelea, *International journal of heat and mass transfer.* Pergamon Press, 2011.

50. G. Xia, L. Chai, H. Wang, M. Zhou, and Z. Cui, "Optimum thermal design of microchannel heat sink with triangular reentrant cavities," *Appl. Therm. Eng.*, vol. 31, no. 6–7, pp. 1208–1219, May 2011.

51. A. Ijam, R. Saidur, and P. Ganesan, "Cooling of minichannel heat sink using nanofluids," *Int. Commun. Heat Mass Transf.*, vol. 39, no. 8, pp. 1188–1194, Oct. 2012.

52. H. Zhang, S. Shao, H. Xu, and C. Tian, "Heat transfer and flow features of Al2O3–water nanofluids flowing through a circular microchannel – Experimental results and

correlations," *Appl. Therm. Eng.*, vol. 61, no. 2, pp. 86–92, Nov. 2013.

53. M. R. Sohel, R. Saidur, M. F. M. Sabri, M. Kamalisarvestani, M. M. Elias, and A. Ijam, "Investigating the heat transfer performance and thermophysical properties of nanofluids in a circular micro-channel," *Int. Commun. Heat Mass Transf.*, vol. 42, pp. 75–81, Mar. 2013.

54. S. M. Vanaki, P. Ganesan, and H. A. Mohammed, "Numerical study of convective heat transfer of nanofluids: A review," *Renew. Sustain. Energy Rev.*, vol. 54, pp. 1212–1239, Feb. 2016.

55. J. Buongiorno, "Convective Transport in Nanofluids," *J. Heat Transfer*, vol. 128, no. 3, p. 240, Mar. 2006.

56. K. S. Hwang, S. P. Jang, and S. U. S. Choi, "Flow and convective heat transfer characteristics of water-based Al2O3 nanofluids in fully developed laminar flow regime," *Int. J. Heat Mass Transf.*, vol. 52, no. 1–2, pp. 193–199, Jan. 2009.

57. F. Hedayati, A. Malvandi, M. H. Kaffash, and D. D. Ganji, "Fully developed forced convection of alumina/water nanofluid inside microchannels with asymmetric heating," *Powder Technol.*, vol. 269, pp. 520–531, Jan. 2015.

58. F. Hedayati and G. Domairry, "Effects of nanoparticle migration and asymmetric heating on mixed convection of TiO2–H2O nanofluid inside a vertical microchannel," *Powder Technol.*, vol. 272, pp. 250–259, Mar. 2015.

59. A. Malvandi and D. D. Ganji, "Magnetic field effect on nanoparticles migration and heat transfer of water/alumina nanofluid in a channel," *J. Magn. Magn. Mater.*, vol. 362, pp. 172–179, Aug. 2014.

60. A. Malvandi and D. D. Ganji, “Brownian motion and thermophoresis effects on slip flow of alumina/water nanofluid inside a circular microchannel in the presence of a magnetic field,” *Int. J. Therm. Sci.*, vol. 84, pp. 196–206, Oct. 2014.

61. C. Yang, W. Li, Y. Sano, M. Mochizuki, and A. Nakayama, “On the Anomalous Convective Heat Transfer Enhancement in Nanofluids: A Theoretical Answer to the Nanofluids Controversy,” *J. Heat Transfer*, vol. 135, no. 5, p. 054504, Apr. 2013.

62. C. Yang, W. Li, and A. Nakayama, “Convective heat transfer of nanofluids in a concentric annulus,” *Int. J. Therm. Sci.*, vol. 71, pp. 249–257, Sep. 2013.

63. F. Garoosi, L. Jahanshaloo, and S. Garoosi, “Numerical simulation of mixed convection of the nanofluid in heat exchangers using a Buongiorno model,” *Powder Technol.*, vol. 269, pp. 296–311, Jan. 2015.

64. P. Fariñas Alvariño, J. M. Sáiz Jabardo, A. Arce, and M. I. Lamas Galdo, “A numerical investigation of laminar flow of a water/alumina nanofluid,” *Int. J. Heat Mass Transf.*, vol. 59, pp. 423–432, Apr. 2013.

65. M. Bahiraei and S. M. Hosseinalipour, “Particle migration in nanofluids considering thermophoresis and its effect on convective heat transfer,” *Thermochim. Acta*, vol. 574, pp. 47–54, Dec. 2013.

66. T. A. Moreira, P. Fariñas Alvariño, L. Cabezas-Gómez, and G. Ribatski, “Experimental and numerical study of slightly loaded water alumina nanofluids in the developing region of a 1.1 mm in diameter pipe and convective enhancement evaluation,” *Int. J. Heat Mass Transf.*, vol. 115, pp. 317–335, Dec. 2017.

67. M. M. Heyhat and F. Kowsary, “Effect of Particle Migration on Flow and Convective Heat Transfer of Nanofluids Flowing Through a Circular Pipe,” *J. Heat Transfer*, vol.

132, no. 6, p. 062401, Jun. 2010.

68. I. I. Ryzhkov and A. V. Minakov, “The effect of nanoparticle diffusion and thermophoresis on convective heat transfer of nanofluid in a circular tube,” *Int. J. Heat Mass Transf.*, vol. 77, pp. 956–969, Oct. 2014.

69. F. Hedayati and G. Domairry, “Nanoparticle migration effects on fully developed forced convection of TiO2–water nanofluid in a parallel plate microchannel,” *Particuology*, vol. 24, pp. 96–107, Feb. 2016.

70. W. Yu *et al.*, “Heat transfer to a silicon carbide/water nanofluid,” *Int. J. Heat Mass Transf.*, vol. 52, no. 15–16, pp. 3606–3612, Jul. 2009.

71. A. Malvandi, S. A. Moshizi, E. G. Soltani, and D. D. Ganji, “Modified Buongiorno’s model for fully developed mixed convection flow of nanofluids in a vertical annular pipe,” *Comput. Fluids*, vol. 89, pp. 124–132, Jan. 2014.

72. A. Malvandi and D. D. Ganji, “Effects of nanoparticle migration on hydromagnetic mixed convection of alumina/water nanofluid in vertical channels with asymmetric heating,” *Phys. E Low-dimensional Syst. Nanostructures*, vol. 66, pp. 181–196, Feb. 2015.

73. A. Malvandi, S. A. Moshizi, and D. D. Ganji, “Effect of magnetic fields on heat convection inside a concentric annulus filled with Al2O3–water nanofluid,” *Adv. Powder Technol.*, vol. 25, no. 6, pp. 1817–1824, Nov. 2014.

74. A. Malvandi, S. A. Moshizi, and D. D. Ganji, “Two-component heterogeneous mixed convection of alumina/water nanofluid in microchannels with heat source/sink,” *Adv. Powder Technol.*, vol. 27, no. 1, pp. 245–254, Jan. 2016.

75. A. Malvandi, S. A. Moshizi, and D. D. Ganji, “Effects of temperature-dependent thermophysical properties on nanoparticle migration at mixed convection of nanofluids in vertical microchannels,” *Powder Technol.*, vol. 303, no. 303, pp. 7–19, Dec. 2016.

76. M. M. Heyhat and F. Kowsary, “Effect of Particle Migration on Flow and Convective Heat Transfer of Nanofluids Flowing Through a Circular Pipe,” *J. Heat Transfer*, vol. 132, no. 6, p. 062401, Jun. 2010.

77. Y. Ding and D. Wen, “Particle migration in a flow of nanoparticle suspensions,” *Powder Technol.*, vol. 149, no. 2–3, pp. 84–92, Jan. 2005.

78. Y. Xuan and W. Roetzel, “Conceptions for heat transfer correlation of nanofluids,” *Int. J. Heat Mass Transf.*, vol. 43, no. 19, pp. 3701–3707, Oct. 2000.

79. M. Sheikholeslami and D. D. Ganji, “Nanofluid convective heat transfer using semi analytical and numerical approaches: A review,” *J. Taiwan Inst. Chem. Eng.*, vol. 65, no. 65, pp. 43–77, Aug. 2016.

80. P. J. L. and and W. G. Mallard, “The NIST Chemistry WebBook: A Chemical Data Resource on the Internet†,” 2001.

81. R. Morrell and National Physical Laboratory (Great Britain), *Handbook of properties of technical and engineering ceramics*. H.M.S.O, 1985.

82. M. Sharifpur, S. Yousefi, and J. P. Meyer, “A new model for density of nanofluids including nanolayer,” *Int. Commun. Heat Mass Transf.*, vol. 78, pp. 168–174, 2016.

83. S.-Q. Zhou and R. Ni, “Measurement of the specific heat capacity of water-based Al2O3 nanofluid,” *Appl. Phys. Lett.*, vol. 92, no. 9, p. 093123, Mar. 2008.

84. W. Williams, J. Buongiorno, and L.-W. Hu, “Experimental Investigation of Turbulent Convective Heat Transfer and Pressure Loss of Alumina/Water and Zirconia/Water Nanoparticle Colloids (Nanofluids) in Horizontal Tubes,” *J. Heat Transfer*, vol. 130, no. 4, p. 042412, Apr. 2008.

85. C. Kleinstreuer and J. Koo, “Computational Analysis of Wall Roughness Effects for Liquid Flow in Micro-Conduits,” *J. Fluids Eng.*, vol. 126, no. 1, p. 1, Jan. 2004.

86. J. Koo, “Computational Nanofluid Flow and Heat Transfer Analyses Applied to Micro-systems,” Jun. 2005.

87. J. Li, “Computational Analysis of Nanofluid Flow in Microchannels with Applications to Micro-heat Sinks and Bio-MEMS,” Dec. 2008.

88. R. S. Vajjha and D. K. Das, “Experimental determination of thermal conductivity of three nanofluids and development of new correlations,” *Int. J. Heat Mass Transf.*, vol. 52, no. 21–22, pp. 4675–4682, Oct. 2009.

89. A. Einstein, “A New Determination of Molecular Dimensions,” Ann. Phys. 19, 1906.

90. G. . McNab and A. Meisen, “Thermophoresis in liquids,” *J. Colloid Interface Sci.*, vol. 44, no. 2, pp. 339–346, Aug. 1973.

91. A. Würger, “Thermal non-equilibrium transport in colloids,” *Reports Prog. Phys.*, vol. 73, no. 12, p. 126601, Dec. 2010.

92. M. Braibanti, D. Vigolo, and R. Piazza, “Does Thermophoretic Mobility Depend on Particle Size?,” *Phys. Rev. Lett.*, vol. 100, no. 10, p. 108303, Mar. 2008.

93. G. Galliero and S. Volz, “Thermodiffusion in model nanofluids by molecular dynamics

simulations," *J. Chem. Phys.*, vol. 128, no. 6, p. 064505, Feb. 2008.

94. S. Iacopini, R. Rusconi, and R. Piazza, "The "macromolecular tourist": Universal temperature dependence of thermal diffusion in aqueous colloidal suspensions," *Eur. Phys. J. E*, vol. 19, no. 1, pp. 59–67, Jan. 2006.

95. R. Piazza and A. Parola, "Thermophoresis in colloidal suspensions," *J. Phys. Condens. Matter*, vol. 20, no. 15, p. 153102, Apr. 2008.

96. J. H. Lienhard and J. H. Lienhard, *A heat transfer textbook*. Dover Publications, 2011.

97. R. K. (Ramesh K. . Shah and A. L. (Alexander L. London, *Laminar flow forced convection in ducts : a source book for compact heat exchanger analytical data*. Academic Press, 1978.

98. F. M. White, *Fluid mechanics*. McGraw Hill, 2011.

99. Y. A. Çengel and A. J. (Afshin J. Ghajar, *Heat and mass transfer : fundamentals & applications*.

100. R. L. Webb, "Performance evaluation criteria for use of enhanced heat transfer surfaces in heat exchanger design," *Int. J. Heat Mass Transf.*, vol. 24, no. 4, pp. 715–726, Apr. 1981.

101. R. Karwa, C. Sharma, and N. Karwa, "Performance Evaluation Criterion at Equal Pumping Power for Enhanced Performance Heat Transfer Surfaces," *J. Sol. Energy*, vol. 2013, pp. 1–9, Jun. 2013.

102. O. Manca, S. Nardini, and D. Ricci, "A numerical study of nanofluid forced convection in ribbed channels," *Appl. Therm. Eng.*, vol. 37, pp. 280–292, May 2012.

103. L. Chai, G. Xia, M. Zhou, J. Li, and J. Qi, “Optimum thermal design of interrupted microchannel heat sink with rectangular ribs in the transverse microchambers,” *Appl. Therm. Eng.*, vol. 51, no. 1–2, pp. 880–889, Mar. 2013.

104. R. O. Sayyar and M. Saghafian, “Numerical simulation of convective heat transfer of nonhomogeneous nanofluid using Buongiorno model,” *Heat Mass Transf.*, vol. 53, no. 8, pp. 2627–2636, Aug. 2017.

105. A. Behnampour *et al.*, “Analysis of heat transfer and nanofluid fluid flow in microchannels with trapezoidal, rectangular and triangular shaped ribs,” *Phys. E Low-dimensional Syst. Nanostructures*, vol. 91, pp. 15–31, Jul. 2017.

106. M. Khoshvaght-Aliabadi and M. Sahamiyan, “Performance of nanofluid flow in corrugated minichannels heat sink (CMCHS),” *Energy Convers. Manag.*, vol. 108, pp. 297–308, Jan. 2016.

107. J. Zhang, Y. Diao, Y. Zhao, and Y. Zhang, “Experimental study of TiO2–water nanofluid flow and heat transfer characteristics in a multiport minichannel flat tube,” *Int. J. Heat Mass Transf.*, vol. 79, pp. 628–638, Dec. 2014.

108. A. Mohammed Adham, N. Mohd-Ghazali, R. Ahmad, A. Mohammed Adham, N. Mohd-Ghazali, and R. Ahmad, *Renewable & sustainable energy reviews.*, vol. 21, no. C. Elsevier Science, 1997.

109. J. Buongiorno, “A Non-Homogeneous Equilibrium Model for Convective Transport in Flowing Nanofluids,” pp. 599–607, 2009.

110. B. Metzger, O. Rahli, and X. Yin, “Heat transfer across sheared suspensions: role of the shear-induced diffusion,” *J. Fluid Mech.*, vol. 724, pp. 527–552, Jun. 2013.

111. G. K. Batchelor and J. T. Green, “The hydrodynamic interaction of two small freely-moving spheres in a linear flow field,” *J. Fluid Mech.*, vol. 56, no. 2, pp. 375–400, Nov. 1972.